# Astroparticle Physics 2023/24

1. Historical introduction - basic properties of cosmic rays
2. Hadronic interactions and accelerator data
3. Cascade equations
4. Electromagnetic cascades
5. Extensive air showers
6. Detectors for extensive air showers
7. High-energy cosmic rays and the knee in the energy spectrum of cosmic rays
8. Radio detection of extensive air showers
9. Acceleration, Astrophysical accelerators and beam dumps
10. Extragalactic propagation of cosmic rays
11. Ultra-high-energy energy cosmic rays
12. Astrophysical gamma rays and neutrinos
13. Neutrino astronomy
14. Gamma-ray astronomy

# lecture 7
# High energy cosmic rays and the knee in the energy spectrum
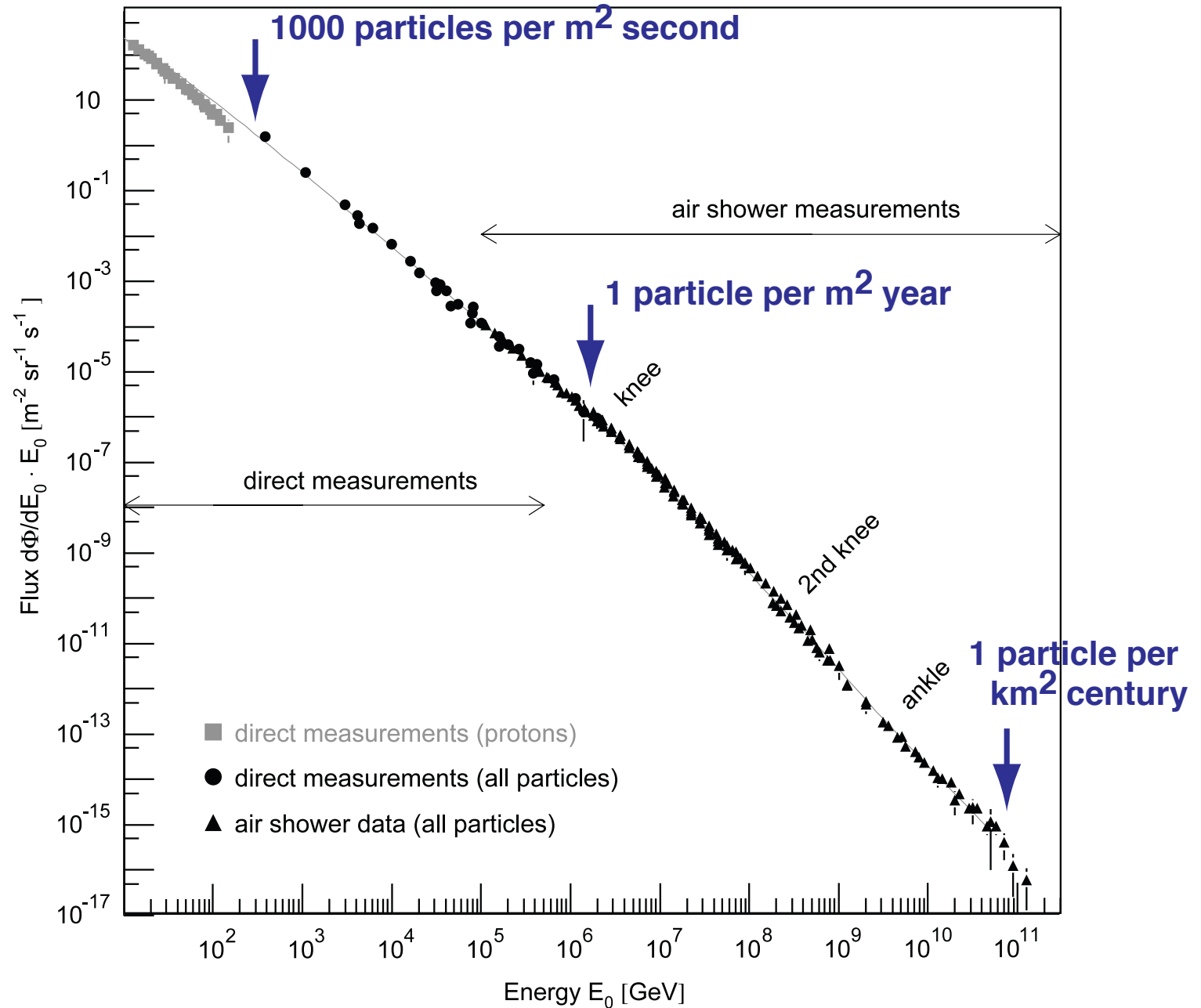## *Gaisser chapter 17*

Fig. 1.　All-particle energy spectrum of cosmic rays as measured directly with detectors above the atmosphere and with air shower detectors. At low energies, the flux of primary protons is shown.

# Energy spectrum of cosmic rays

**energy density**

$$\rho_E = \frac{4\pi}{c} \int \frac{E}{\beta} \frac{dN}{dE} dE \approx 1 \; \frac{\text{eV}}{\text{cm}^3}$$
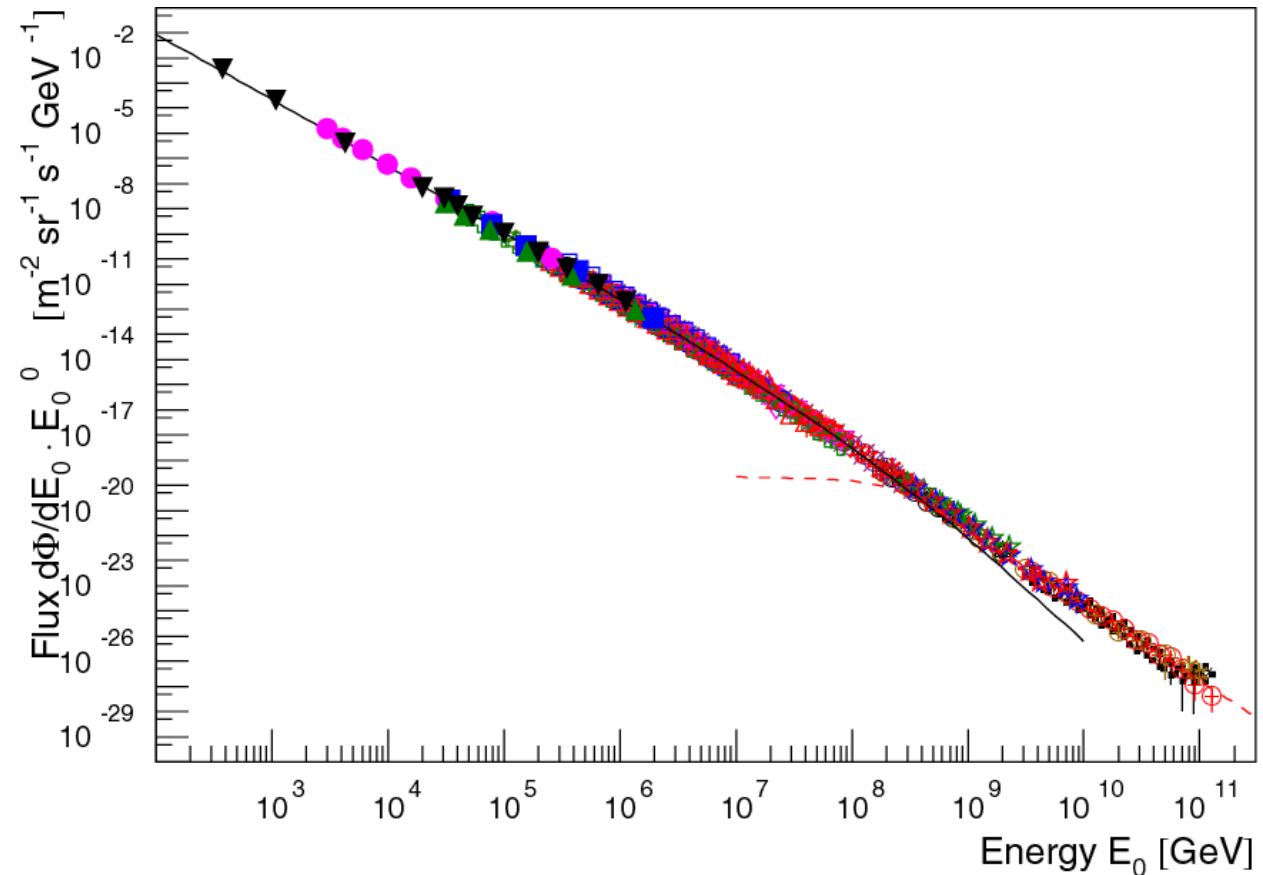
**for comparison:**

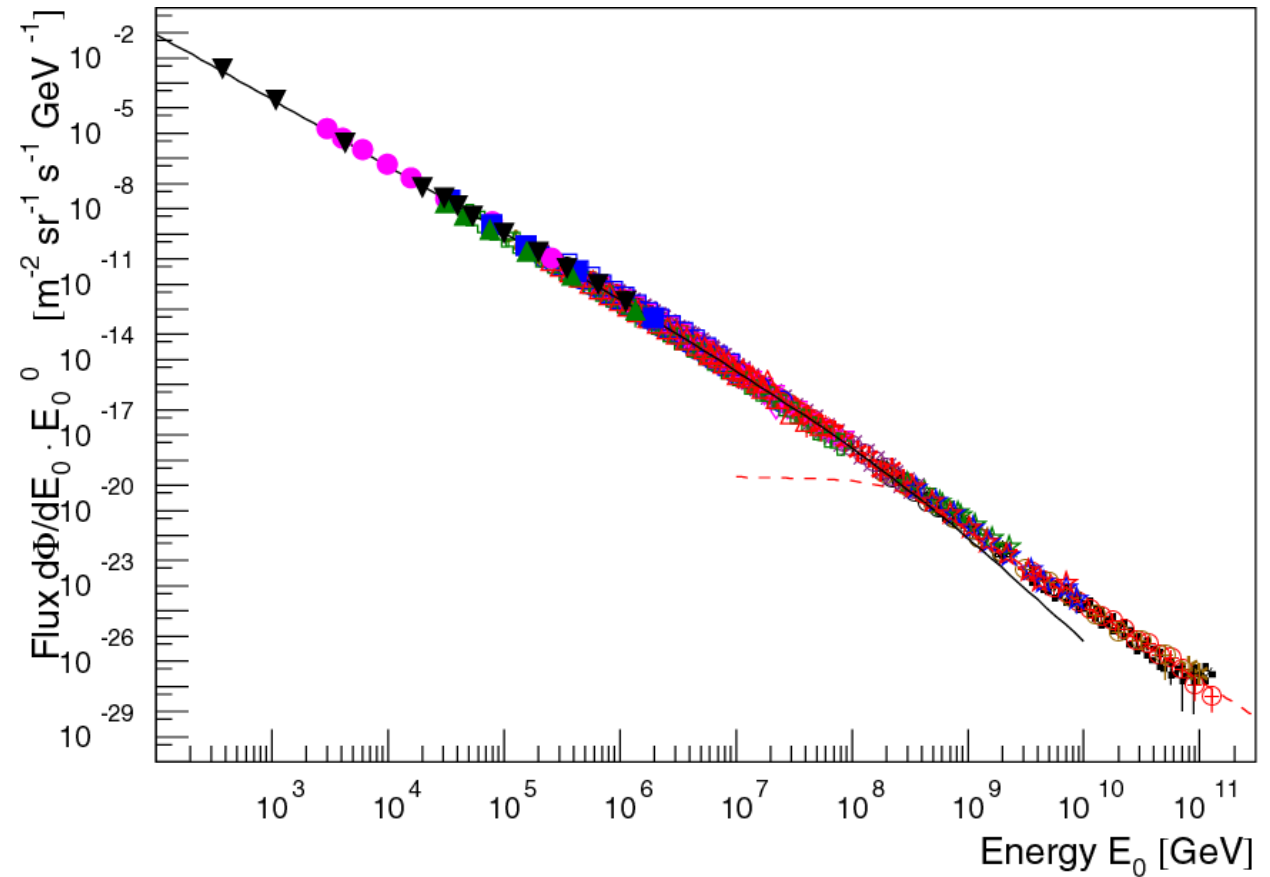$$\rho_B = \frac{B^2}{2\mu_0} \approx 0.25 \; \text{eV/cm}^3$$

$$\rho_{SL} \approx 0.3 \; \text{eV/cm}^3$$

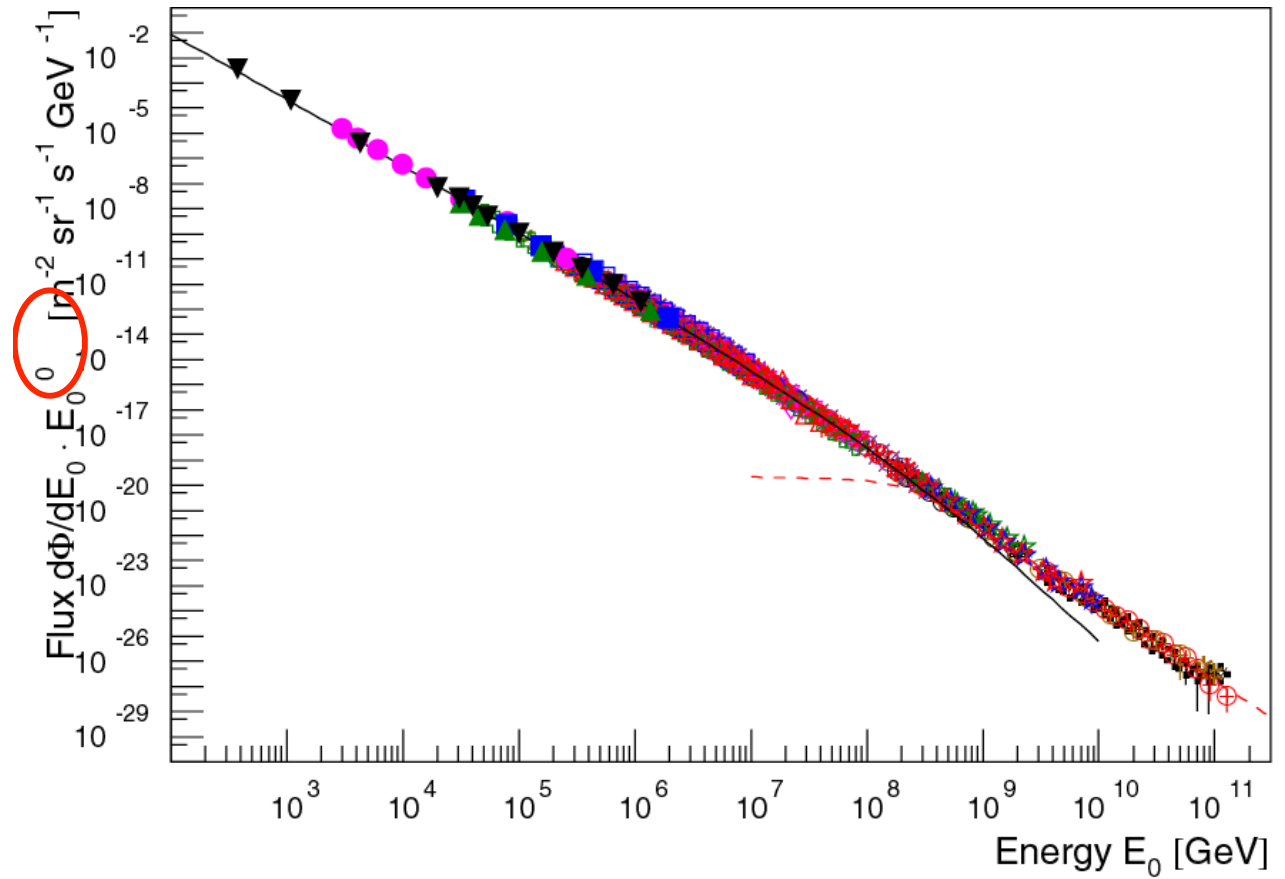$$\rho_{IR} \approx 0.4 \; \text{eV/cm}^3$$
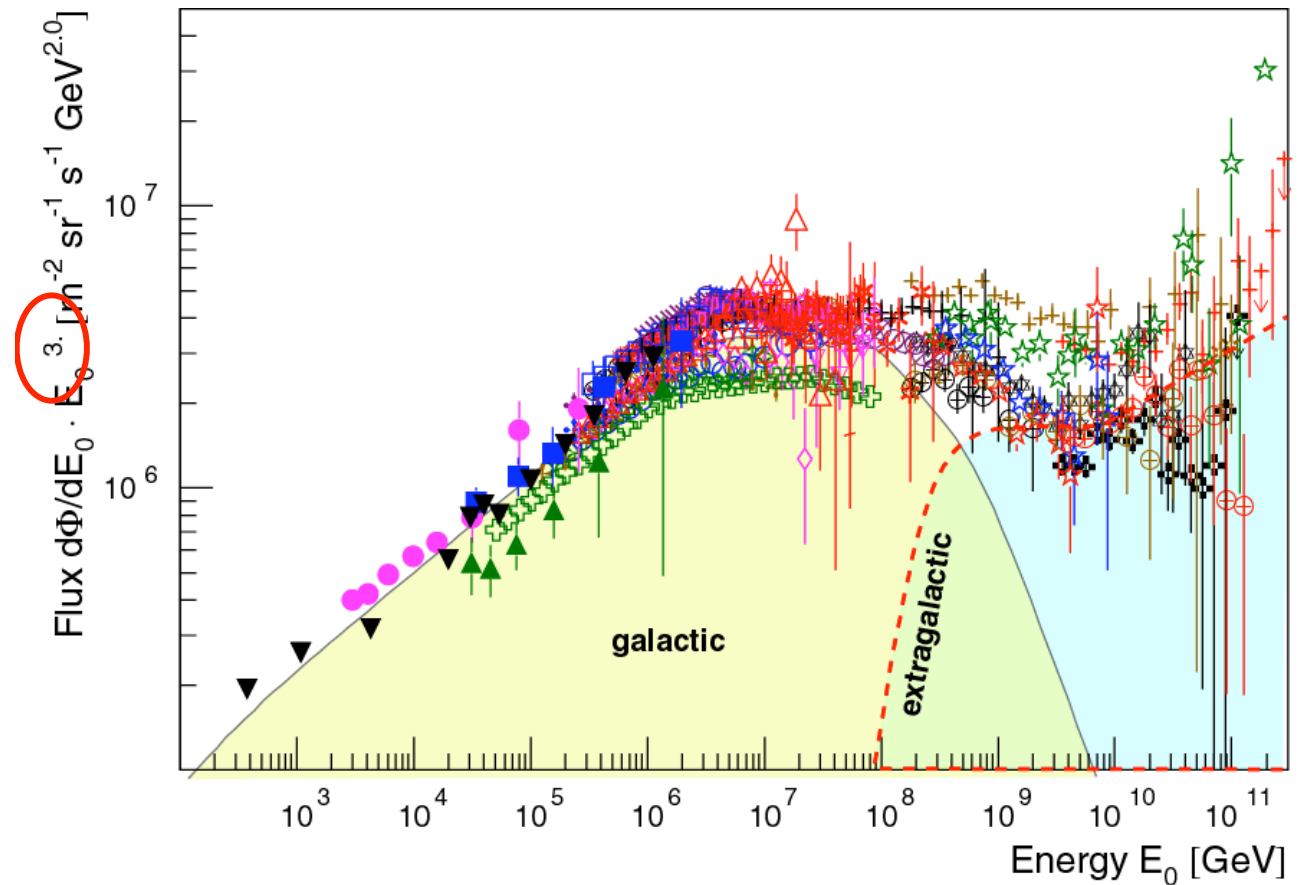
$$\rho_{3K} \approx 0.25 \; \text{eV/cm}^3$$

# Energy spectrum of cosmic rays

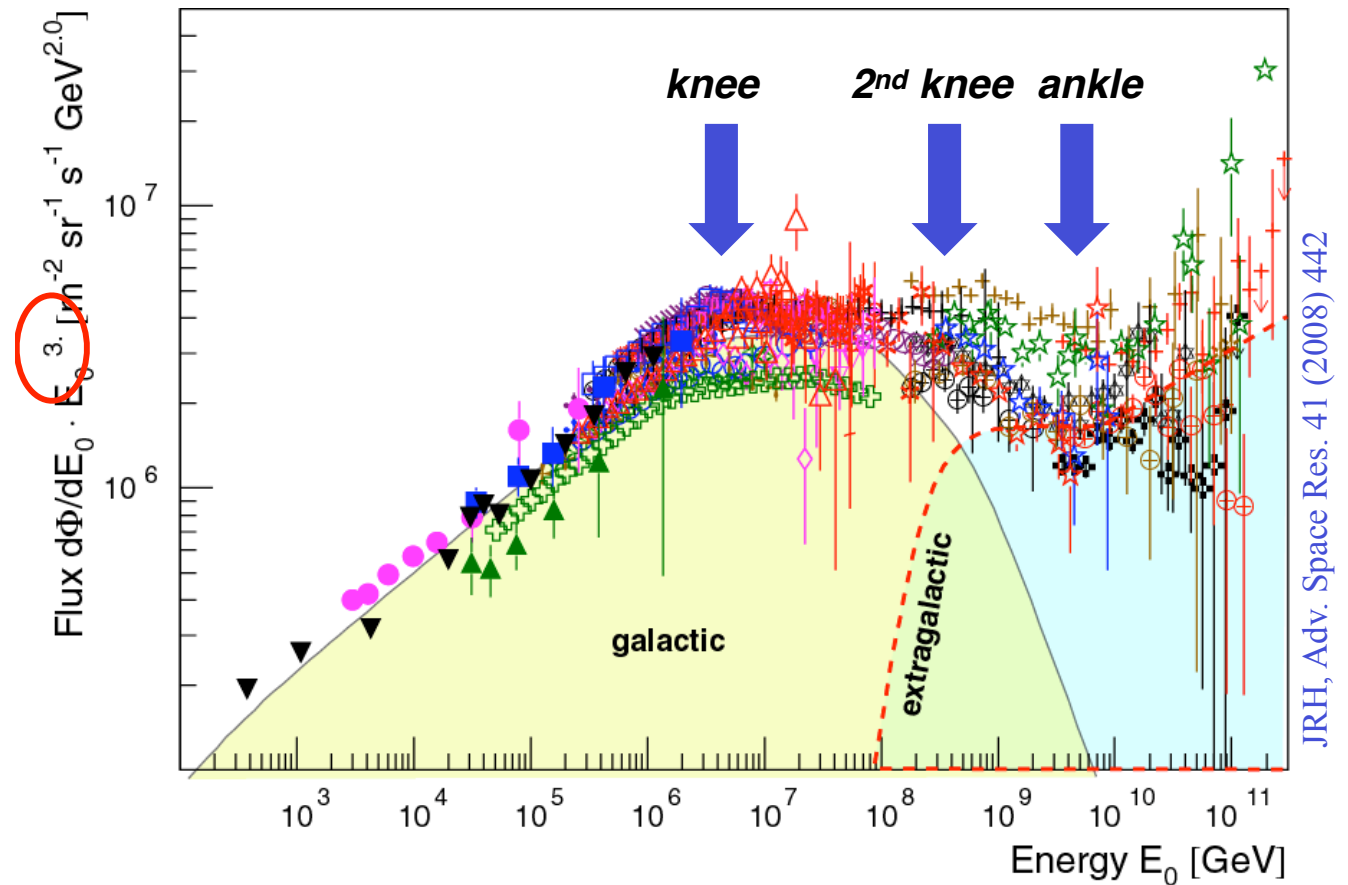# Energy spectrum of cosmic rays

# Energy spectrum of cosmic rays

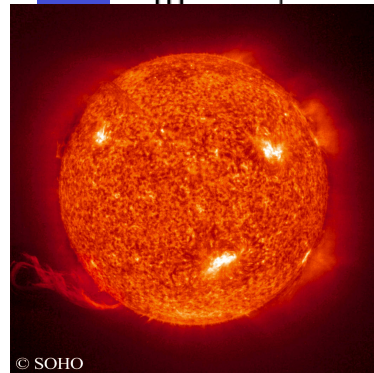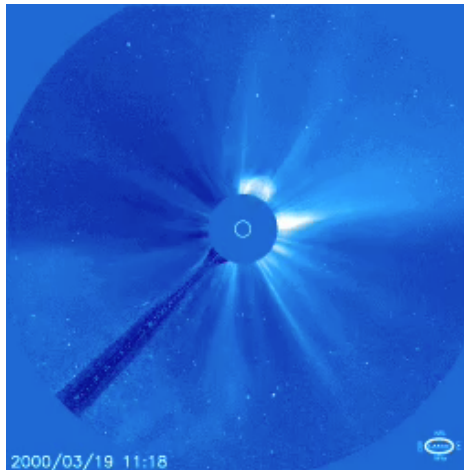# Energy spectrum of cosmic rays

# Energy spectrum of cosmic rays
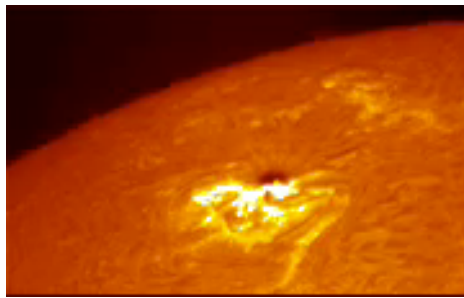
**Solar flares**

solar particles



knee  2nd knee  ankle

galactic

extragalactic

$E_0 \cdot E_0^{3.0}$ [m$^{-2}$ sr$^{-1}$ s$^{-1}$ GeV$^{2.0}$]

$10^7$

Energy $E_0$ [GeV]

$10^3$  $10^4$  $10^5$  $10^6$  $10^7$  $10^8$  $10^9$  $10^{10}$  $10^{11}$

JRH, Adv. Space Res. 41 (2008) 442

2000/03/19 11:18

© SOHO

# Energy spectrum of cosmic rays

## Solar flares



© SOHO

solar particles

$E_0 \cdot E_0^{3.0}$ [m$^{-2}$ sr$^{-1}$ s$^{-1}$ GeV$^{2.0}$]

knee   2$^{nd}$ knee   ankle

$10^7$

galactic

extragalactic

JRH, Adv. Space Res. 41 (2008) 442

$10^3$   $10^4$   $10^5$   $10^6$   $10^7$   $10^8$   $10^9$   $10^{10}$   $10^{11}$

Energy E$_0$ [GeV]

2000/03/19 11:18

# Energy spectrum of cosmic rays



galactic cosmic rays

solar particles

knee   2nd knee   ankle

$E_0 \cdot E_0^{3.0}$ [m$^{-2}$ sr$^{-1}$ s$^{-1}$ GeV$^{2.0}$]

$10^7$

galactic

extragalactic

$10^3$   $10^4$   $10^5$   $10^6$   $10^7$   $10^8$   $10^9$   $10^{10}$   $10^{11}$

Energy $E_0$ [GeV]

Kepler's Supernova Remnant
SN 1604
Chandra X-ray Observatory
Hubble Space Telescope
Spitzer Space Telescope

SST MIPS 24μm
HST 658nm Hα
CXO 0.3-1.4keV
CXO 4-6keV

3.8 light-years
1.2 parsecs 60"

© SOHO

JRH, Adv. Space Res. 41 (2008) 442
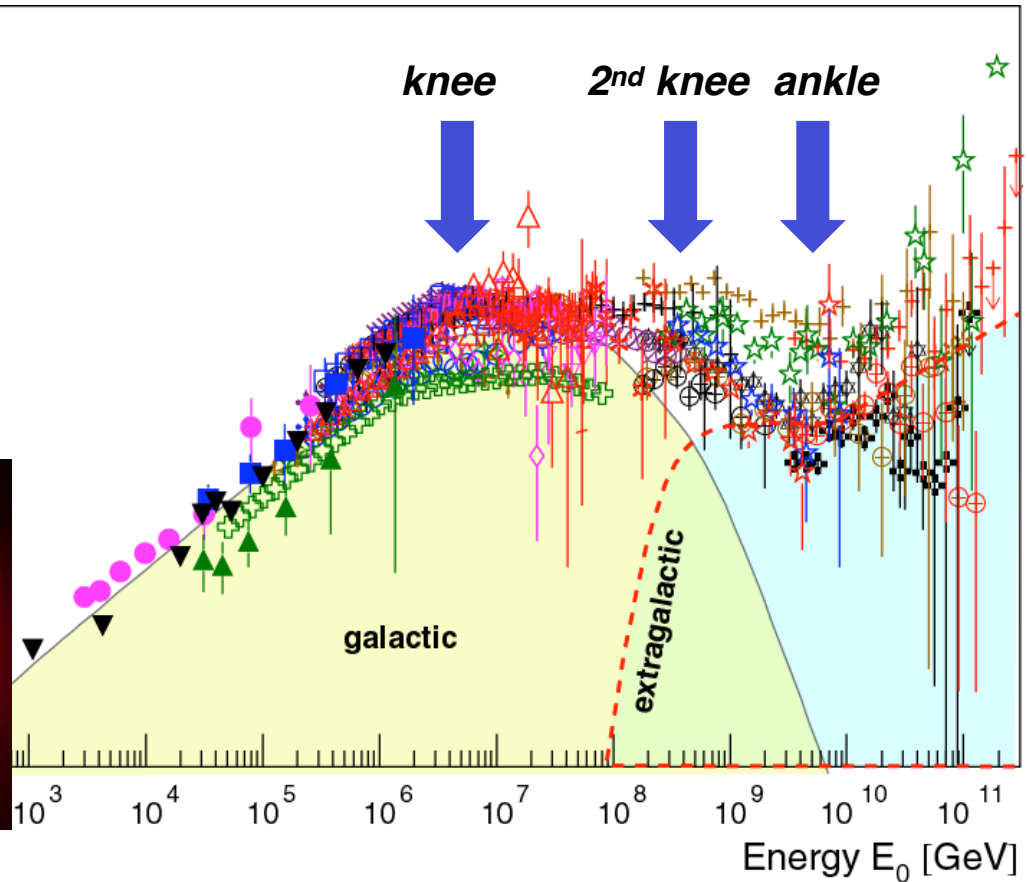
# Energy spectrum of cosmic rays
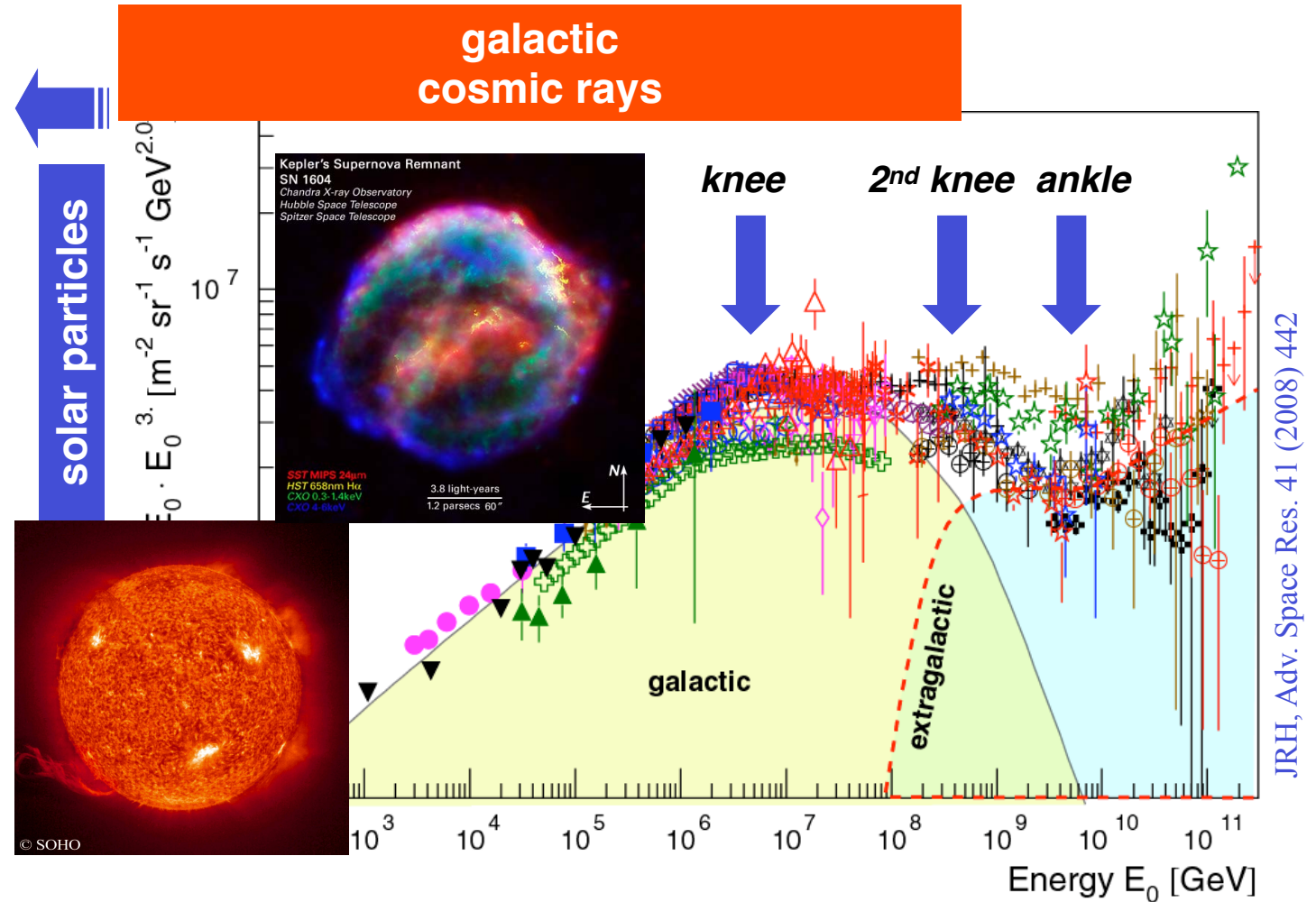
# Energy spectrum of cosmic rays
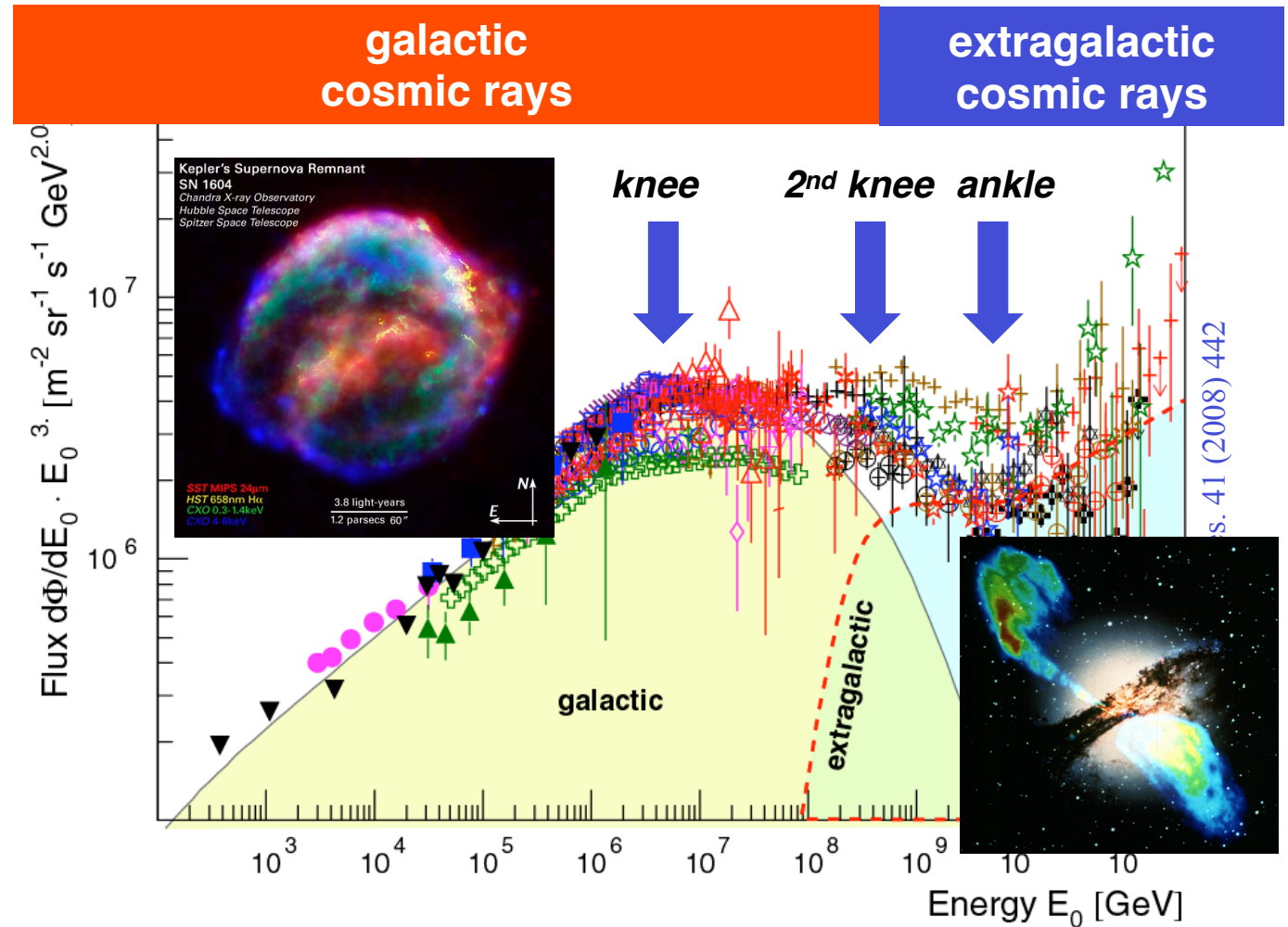
# Energy spectrum of cosmic rays

**Radius of particle in magnetic field**

$$r = \frac{p}{ZeB}$$

$$r[pc] = 1.08 * \frac{E\ [PeV]}{B\ [\mu G]}$$



galactic cosmic rays

extragalactic cosmic rays
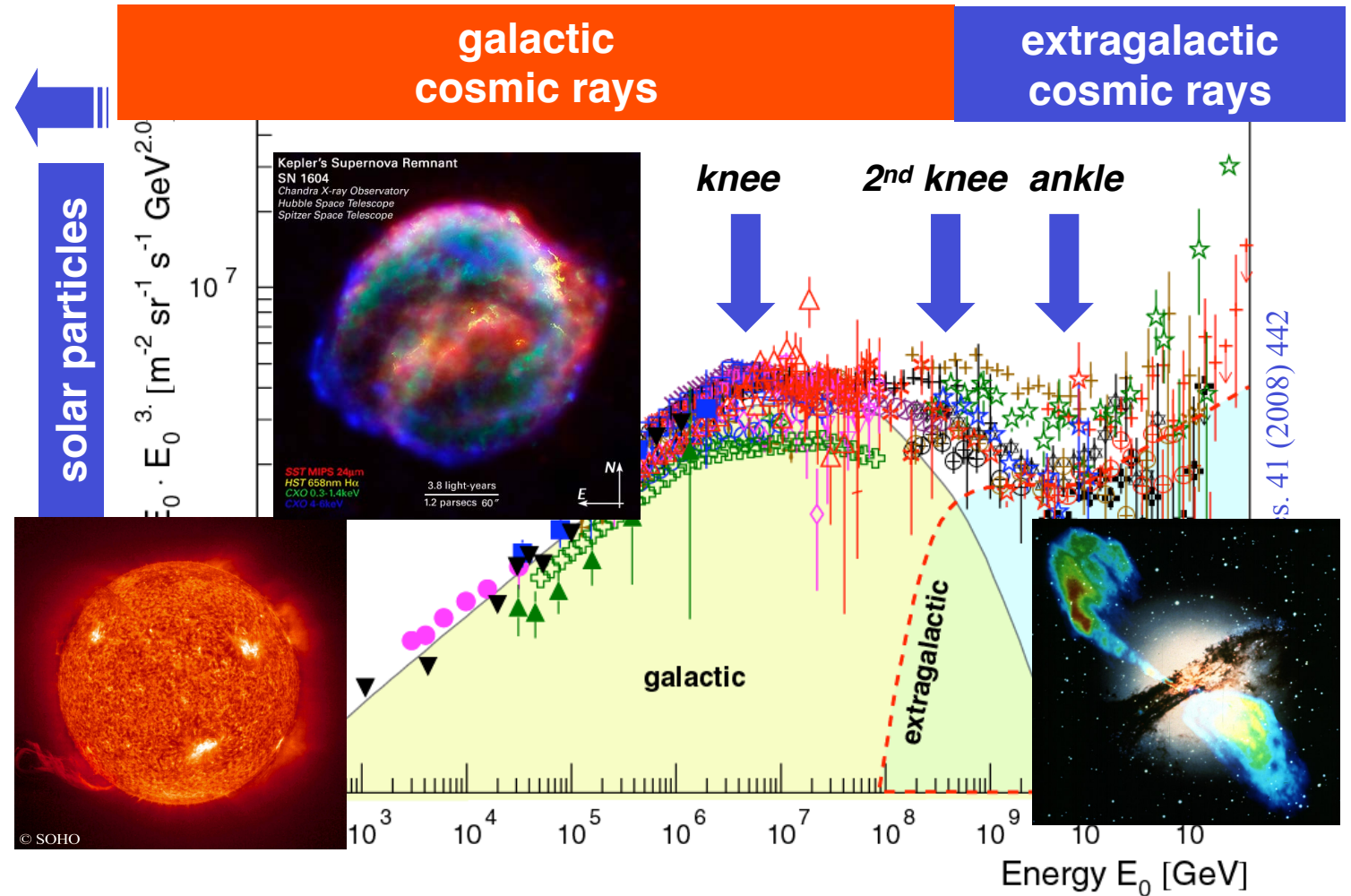
knee    2nd knee    ankle

galactic

extragalactic

Flux $d\Phi/dE_0 \cdot E_0^{3.0}$ [$m^{-2}$ $sr^{-1}$ $s^{-1}$ $GeV^{2.0}$]

Energy $E_0$ [GeV]

r=    0.04 pc    3.6 pc    360 pc    36 kpc

# Extensive air showers – Mass

## Simple Heitler model of (hadronic) showers

**Primary mass:**

- **Average depth of shower maximum $X_{max}$**

$$\boxed{X_{max}^{A} \sim \ln \frac{E_0}{A}}$$

$$X_{max}^{A} = X_{max}^{p} - X_0 \ln A$$

$$X_{max}^{Fe} = X_{max}^{p} - 150 \, \text{g/cm}^2$$

- **$N_e$-$N_\mu$ ratio**

$$\frac{N_e}{N_\mu} \approx 35.1 \left( \frac{E_0}{A \, \text{PeV}} \right)^{0.15} \quad \textbf{or}$$

$$\lg \left( \frac{N_e}{N_\mu} \right) = C - 0.065 \ln A$$



**11 $\lambda_i$**

**30 $X_0$**

**hadronic**

**electromagnetic**          **muonic**

**shower components**

**JRH, Mod. Phys. Lett. A 22 (2007) 1533**          **JRH, Nucl. Instr. and Meth. A 588 (2008) 181**          **J. Matthews, Astropart. Phys. 22 (2005) 387**

# Extensive air showers – Mass

## Simple Heitler model of (hadronic) showers

**Primary mass:**

- **Average depth of shower maximum $X_{max}$**
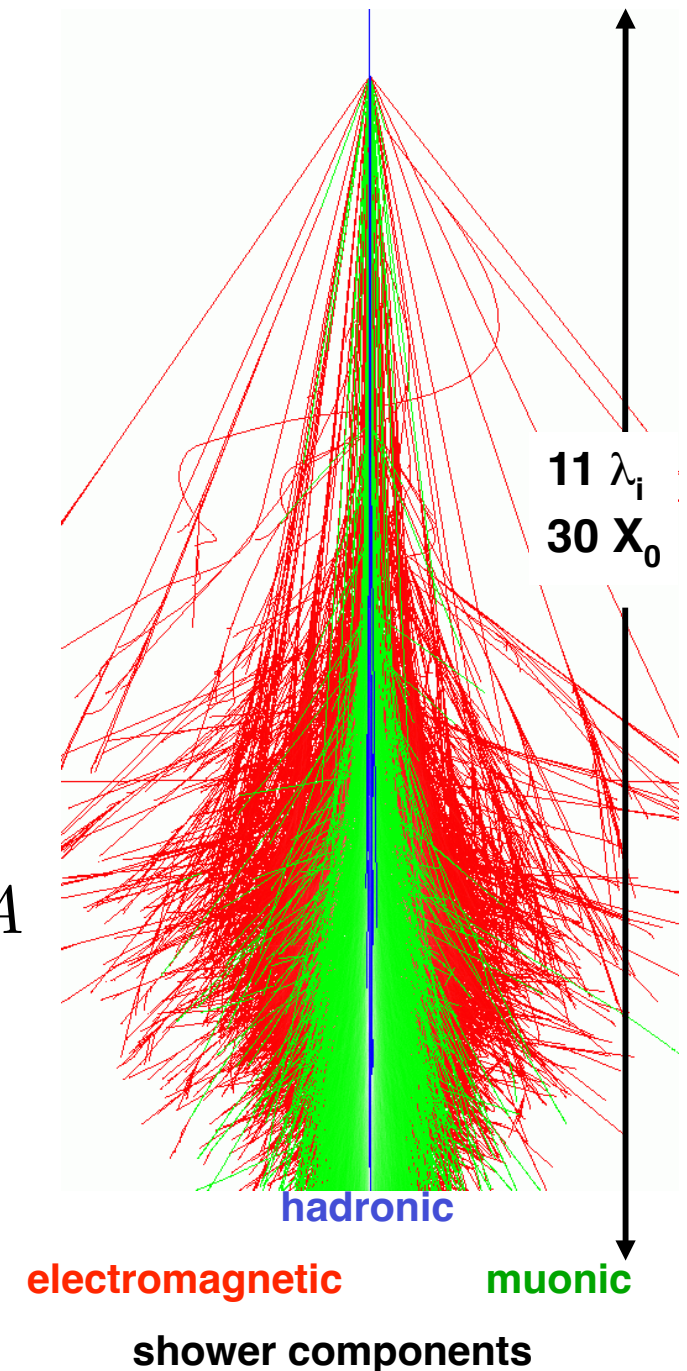
$$X^A_{max} \sim \ln \frac{E_0}{A}$$

$$X^A_{max} = X^p_{max} - X_0 \ln A$$

$$X^{Fe}_{max} = X^p_{max} - 150\,\mathrm{g/cm^2}$$

- **$N_e$-$N_\mu$ ratio**

$$\frac{N_e}{N_\mu} \approx 35.1 \left( \frac{E_0}{A\,\mathrm{PeV}} \right)^{0.15}$$  **or**
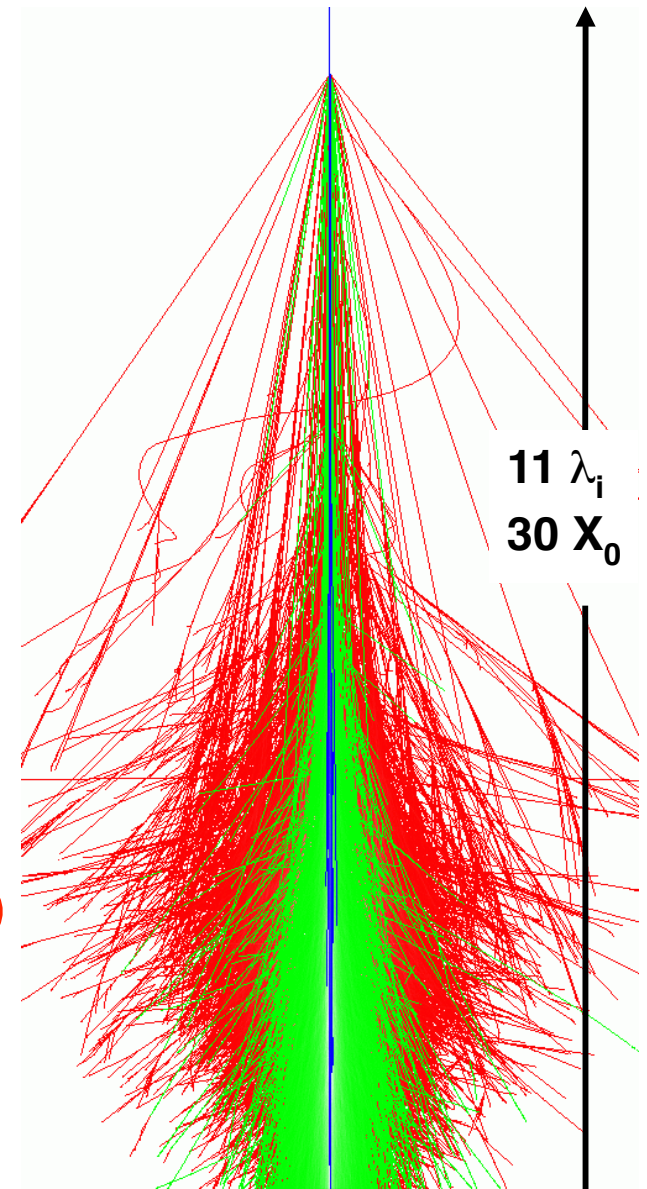
$$\lg \left( \frac{N_e}{N_\mu} \right) = C - 0.065 \ln A$$

**ΔlnA ~ 1**
**→Δ $X_{max}$ ~ 36 g/cm²**
**→Δ ($N_e/N_\mu$) ~ 16%**

$$\Delta \ln A \approx 0.8$$

**in „best" experiments**

**11 $\lambda_i$**
**30 $X_0$**

**hadronic**

**electromagnetic**     **muonic**

**shower components**

**JRH, Mod. Phys. Lett. A 22 (2007) 1533**          **JRH, Nucl. Instr. and Meth. A 588 (2008) 181**          **J. Matthews, Astropart. Phys. 22 (2005) 387**

# The KASCADE Array
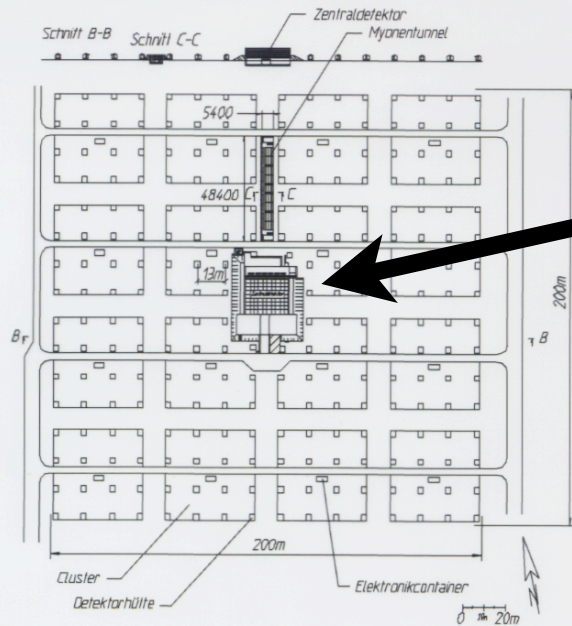


**200 m**

**200 m**

❑ Array

252 stations with

❑ e/γ detectors: 4 cm liquid scintillator ($\approx 3.1\ m^2$)

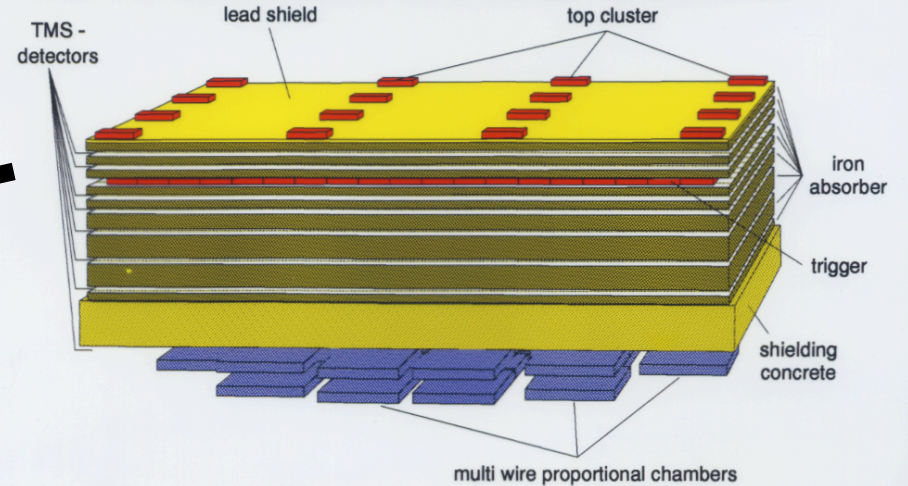❑ muon detectors: 3 cm plastic scintillator ($\approx 3.2\ m^2$)

   shield 10 cm Pb + 4 cm Fe ➜ 20 $X_0$

➟ $E_\mu > 300$ MeV

→ measurement of particle densities and arrival times

# The KASCADE Central Detector



4 different detector systems:

❑ Top array 32 × 0.45 $m^2$ scintillation counters (14 $m^2$)

❑ Trigger layer 456 × 0.45 $m^2$ scintillation counters (206 $m^2$)

❑ 32 Multiwire proportional chambers (2 × 150 $m^2$) $E_\mu > 2$ GeV

❑ Iron sampling calorimeter (16 × 20 $m^2$)

   8 active layers ➜ 10 000 liquid ionisation chambers

   40 000 electronic channels

   separation of individual hadrons by a fine segmentation

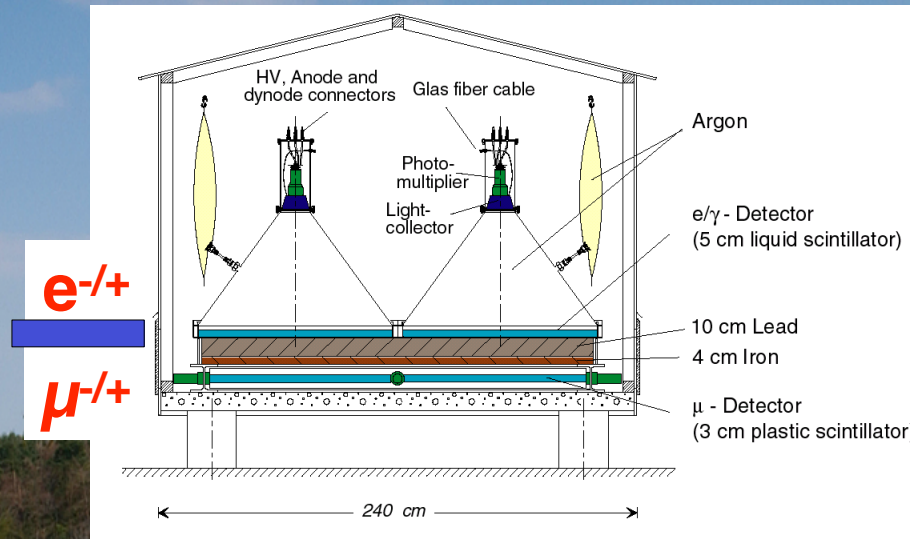   depth $\approx 11\ \lambda_i$ ➜ hadrons up to 10 TeV 95% contained

# KArlsruhe Shower Core and Array DEtector

**Simultaneous measurement of**
**electromagnetic,**
**muonic,**
**hadronic**
**shower components**

200 m

200 m

# KArlsruhe Shower Core and Array DEtector

**Simultaneous measurement of**
**electromagnetic,**
**muonic,**
**hadronic**
**shower components**

e⁻/⁺

μ⁻/⁺

HV, Anode and dynode connectors

Glas fiber cable

Argon

Photo-multiplier

Light-collector

e/γ - Detector
(5 cm liquid scintillator)

10 cm Lead

4 cm Iron

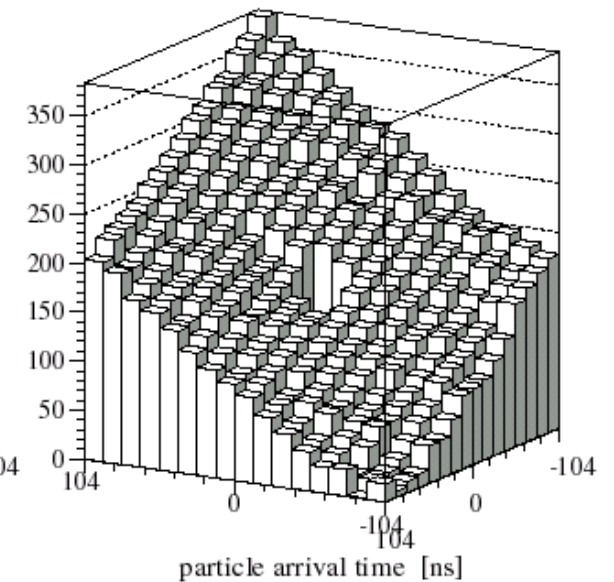μ - Detector
(3 cm plastic scintillator)

240 cm

200 m

200 m

# Event reconstruction in the scintillator array
## electromagnetic component

| shower core | $\Delta r = 2.5 - 5.5$ m |
|---|---|
| shower direction | $\Delta\alpha = 0.5° - 1.2°$ |
| shower size | $\Delta N_e/N_e = 6 - 12$ % |



e/γ-Detectors, Run 1, Event 71089, 96-03-05 22:07:48.956078

energy deposit [MeV/m²]

particle arrival time [ns]

energy deposit [MeV/m²]

particle arrival time [ns]

KASCADE
GRANDE Array

37 detector stations

370 m² e/γ:
scintillation counter

KASCADE

200 m x 200 m

700 m

700 m

G. Navarra et al., Nucl Instr & Meth A 518 (2004) 207
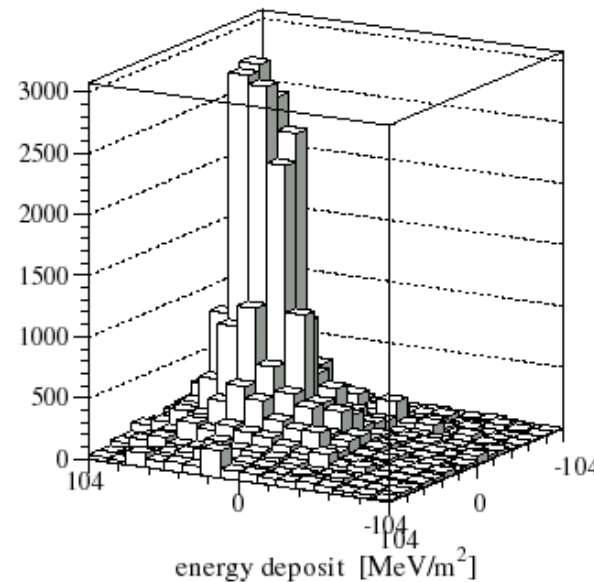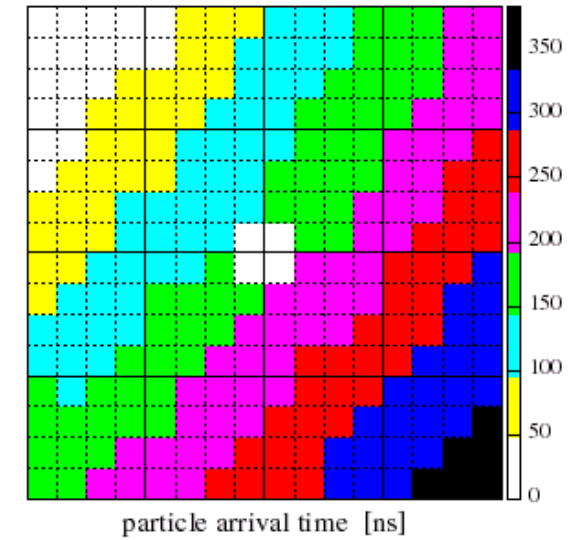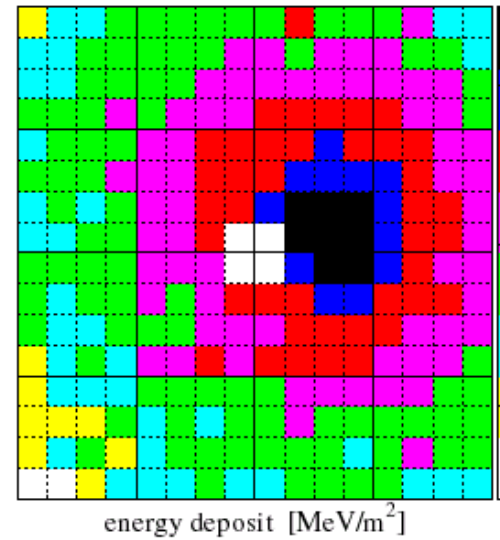
**KASCADE GRANDE Array**

37 detector stations

370 m² e/$\gamma$: scintillation counter

**KASCADE**

200 m x 200 m
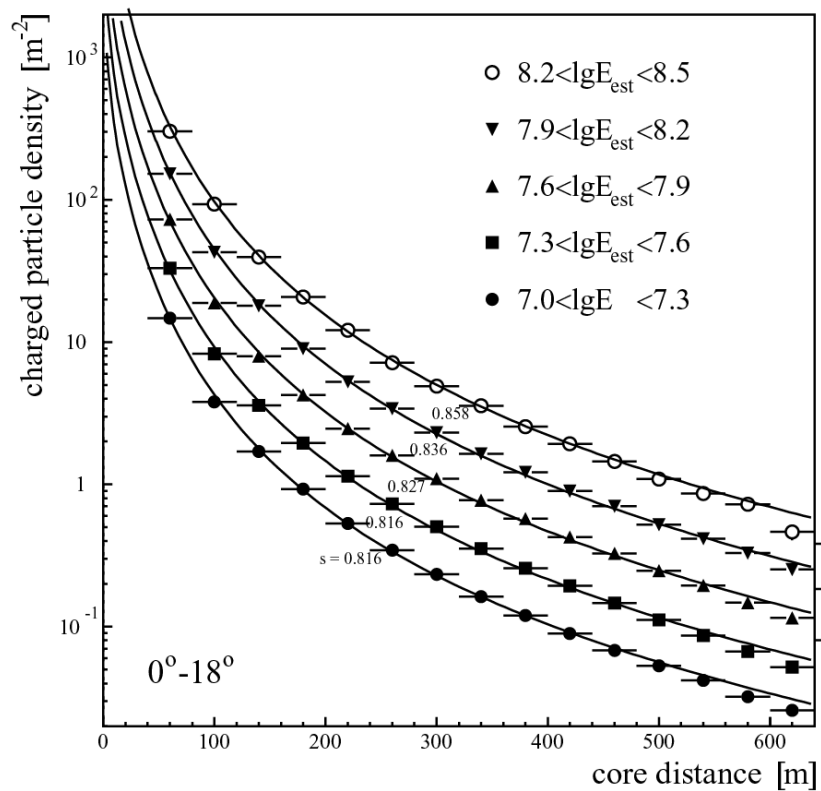
700 m

700 m

G. Navarra et al., Nucl Instr & Meth A 518 (2004) 207

# KASCADE-Grande – Lateral distributions

## Electromagnetic component



## Muons



R. Glasstetter et al., Proc. 29th ICRC, Pune 6 (2005) 293
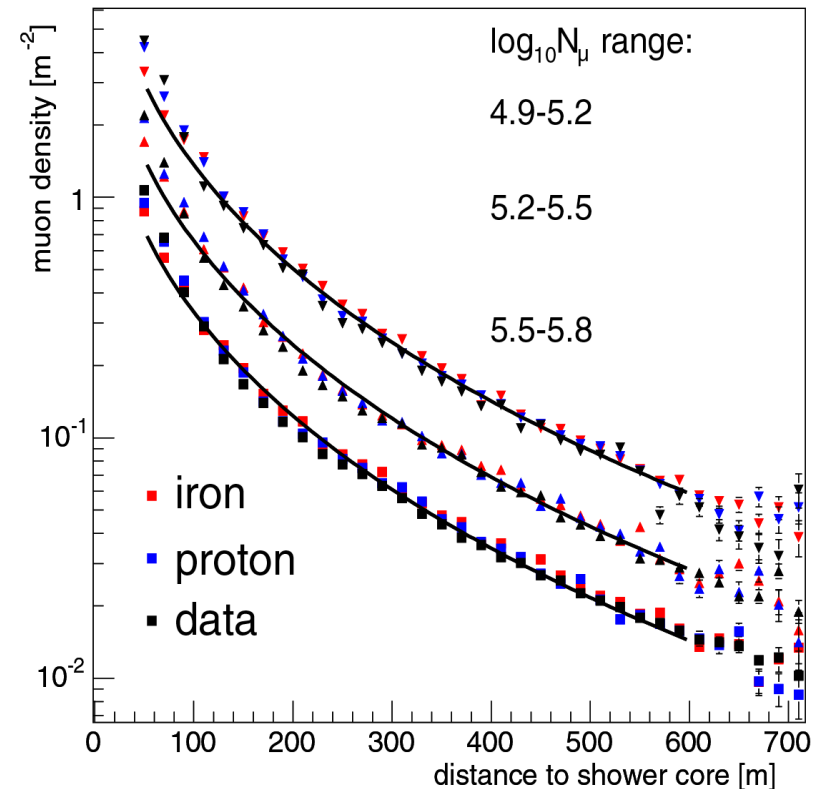
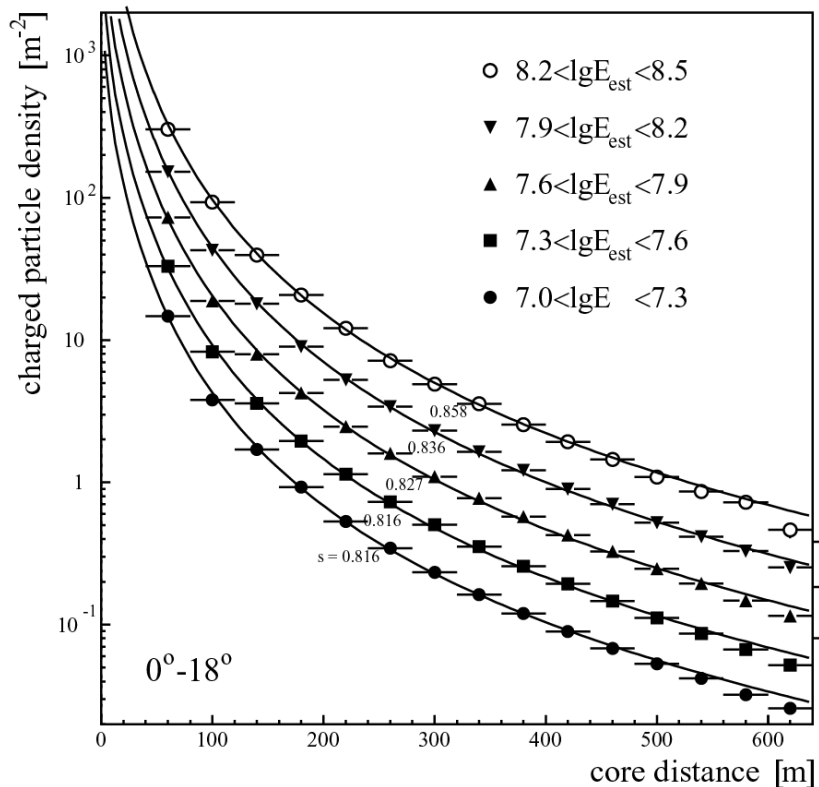J. v. Buren et al., Proc. 29th ICRC, Pune 6 (2005) 301
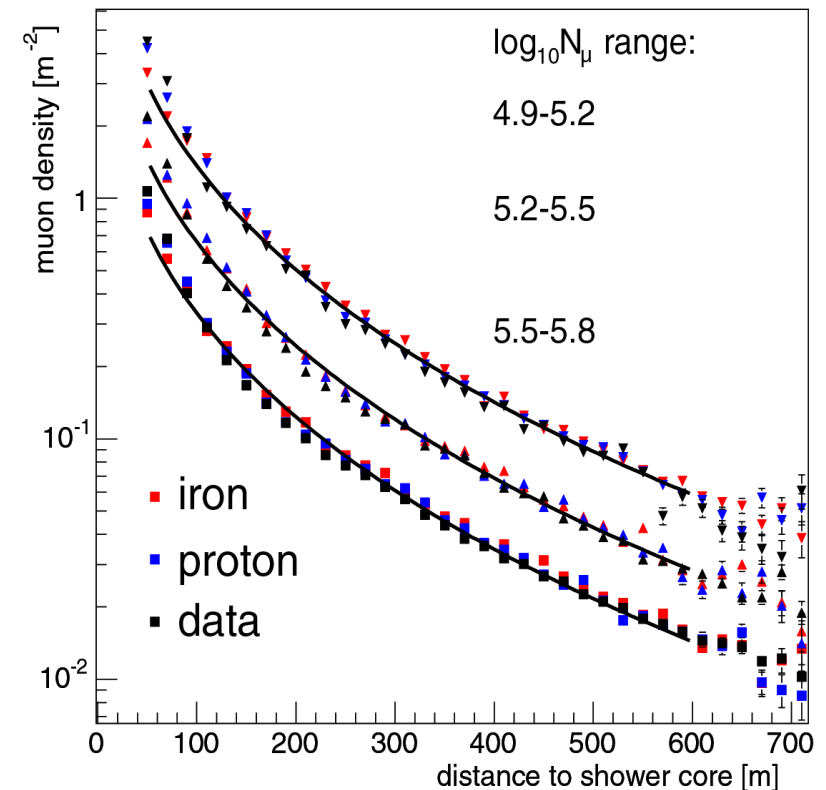
# KASCADE-Grande – Lateral distributions
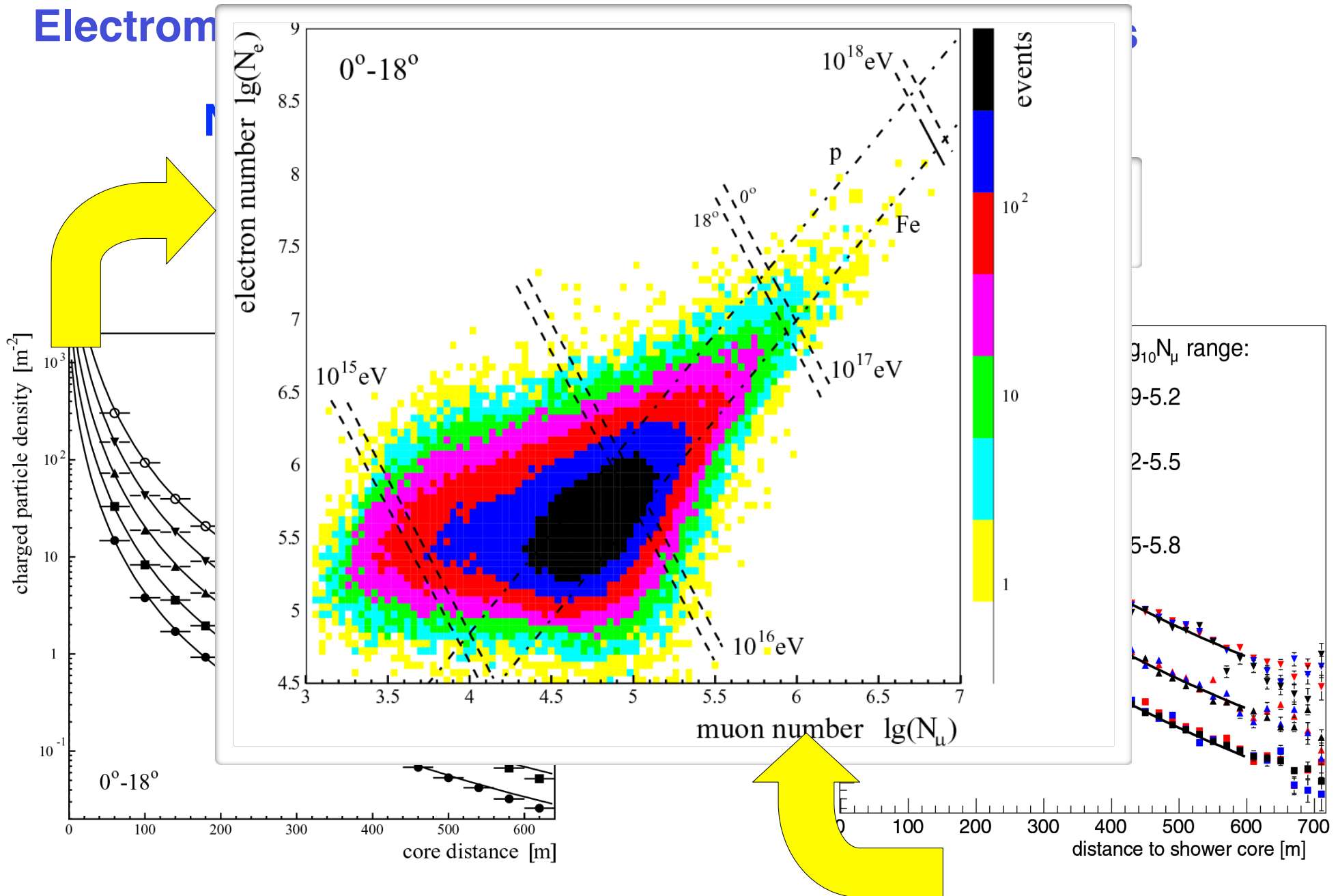
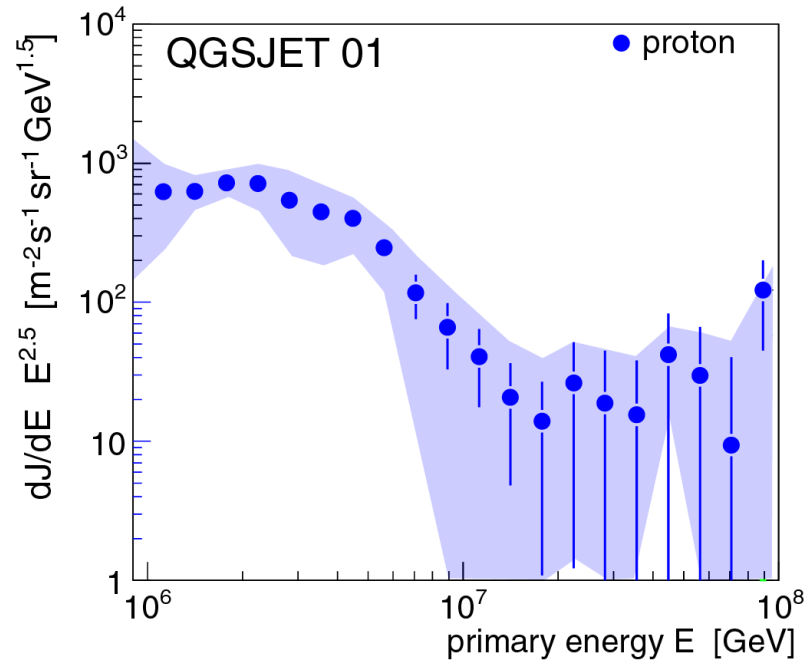**Electromagnetic component**

**Muons**

**NKG function**

$$\rho(r, s, N_e) = \frac{N_e}{r_M^2} \frac{\Gamma(4.5 - s)}{2\pi\Gamma(s)\Gamma(4.5 - 2s)} \left(\frac{r}{r_M}\right)^{s-2} \left(1 + \frac{r}{r_M}\right)^{s-4.5}$$

R. Glasstetter et al., Proc. 29th ICRC, Pune 6 (2005) 293

J. v. Buren et al., Proc. 29th ICRC, Pune 6 (2005) 301

**Electrom**



R. Glasstetter et al., Proc. 29th ICRC, Pune 6 (2005) 293

J. v. Buren et al., Proc. 29th ICRC, Pune 6 (2005) 301

# KASCADE: Energy spectra for elemental groups



T. Antoni et al., Astropart. Phys. 24 (2005) 1

# KASCADE: Energy spectra for elemental groups



T. Antoni et al., Astropart. Phys. 24 (2005) 1

# KASCADE: Energy spectra for elemental groups



T. Antoni et al., Astropart. Phys. 24 (2005) 1

# KASCADE: Energy spectra for elemental groups



T. Antoni et al., Astropart. Phys. 24 (2005) 1

# KASCADE: Energy spectra for elemental groups



T. Antoni et al., Astropart. Phys. 24 (2005) 1

# KASCADE: Energy spectra for elemental groups



T. Antoni et al., Astropart. Phys. 24 (2005) 1

# KASCADE: Energy spectra for elemental groups



➡️ **Knee caused by cut-off for light elements**

**Astrophysical interpretation limited by description of interactions in the atmosphere**

T. Antoni et al., Astropart. Phys. 24 (2005) 1

# KASCADE: Energy spectra for elemental groups



→ **Knee caused by cut-off for light elements**

**Astrophysical interpretation limited by description of interactions in the atmosphere**

T. Antoni et al., Astropart. Phys. 24 (2005) 1

# KASCADE: Energy spectra for elemental groups
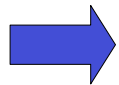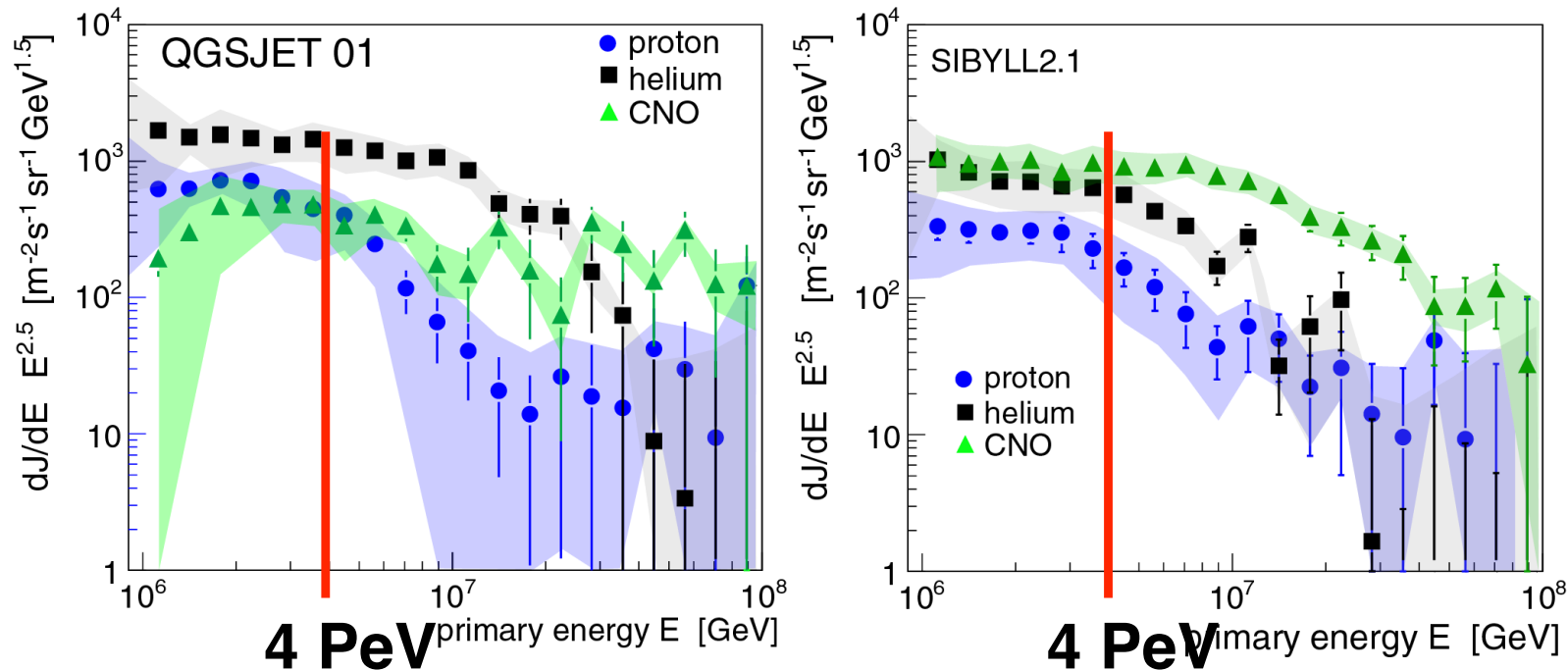


➡ **Knee caused by cut-off for light elements**

**Astrophysical interpretation limited by description of interactions in the atmosphere**

T. Antoni et al., Astropart. Phys. 24 (2005) 1

# Test of hadronic interaction models

## QGSJET 01

**$N_e$-$N_\mu$ analysis**
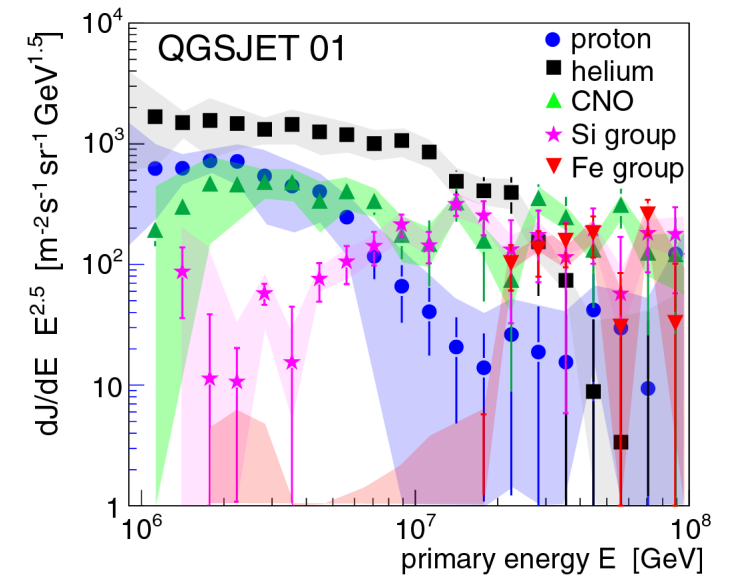


**$\chi^2$ distribution**
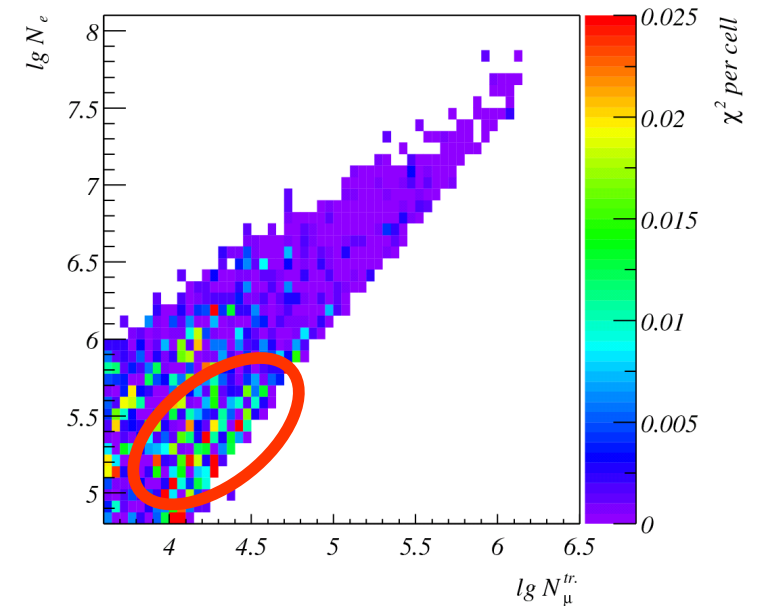
# Test of hadronic interaction models

## QGSJET 01

**Number of hadrons vs. number of muons**
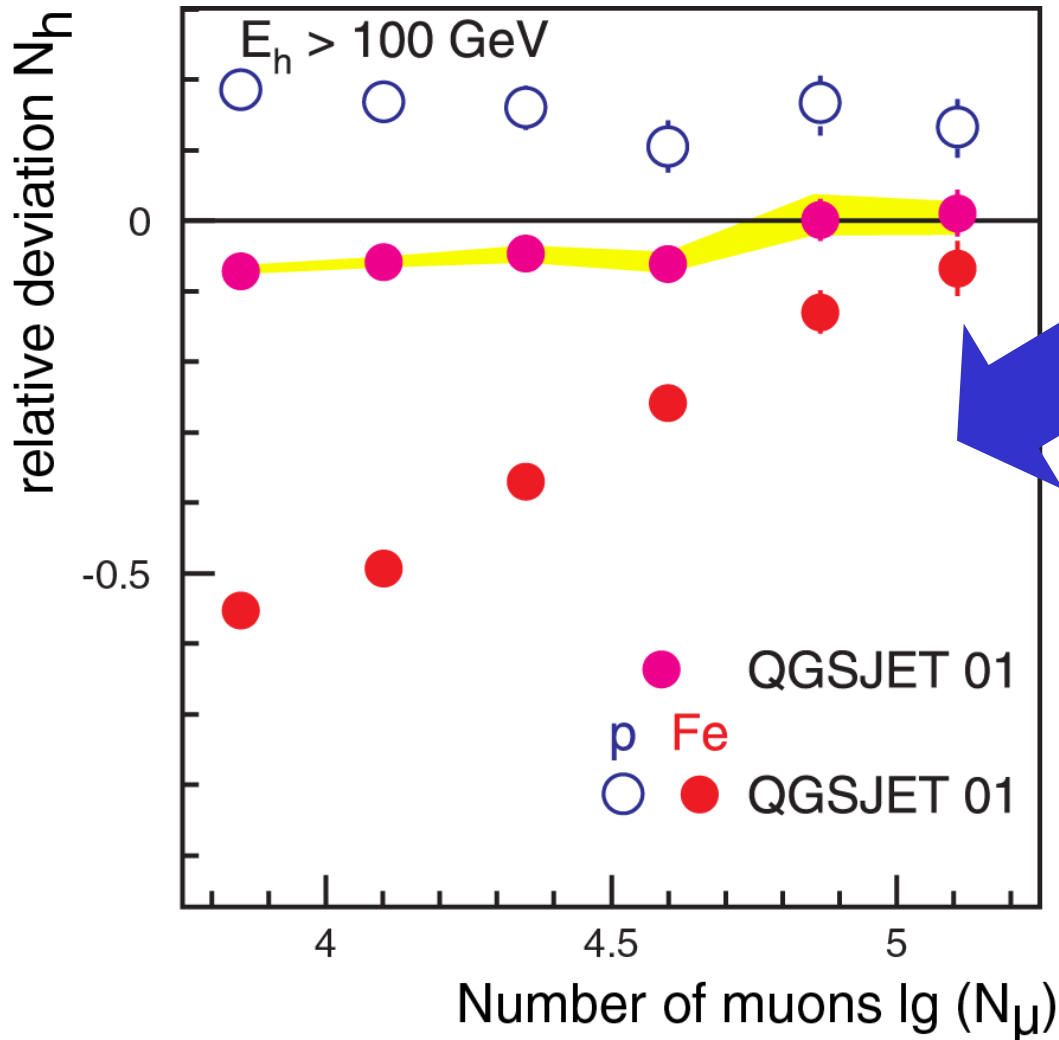


**inconsistencies on 10% level**
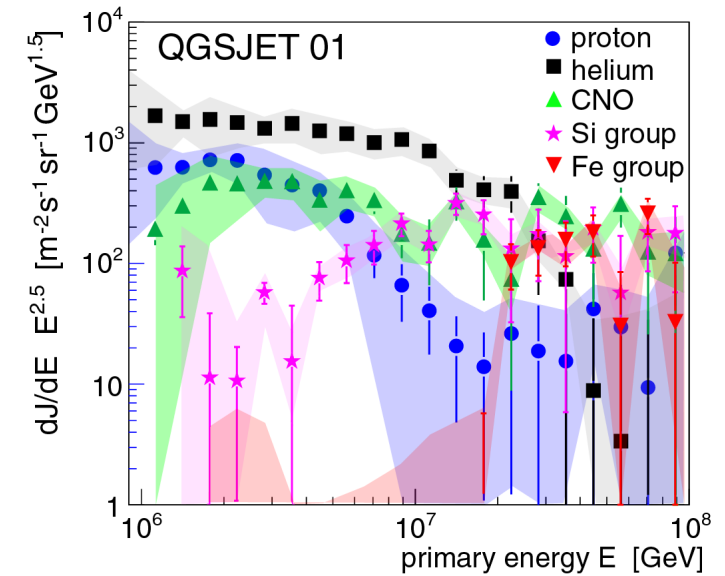
## $N_e$-$N_\mu$ analysis



## $\chi^2$ distribution
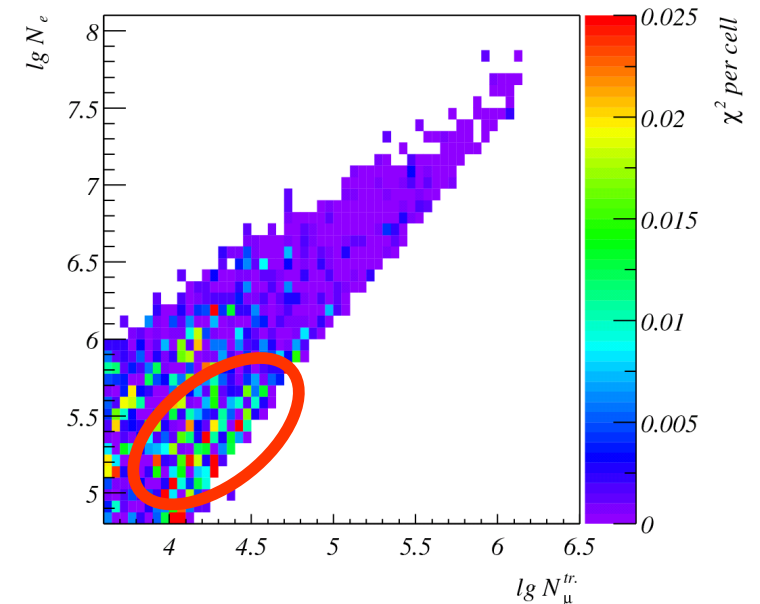
# Test of hadronic interaction models

## QGSJET 01

**Number of hadrons vs. number of muons**
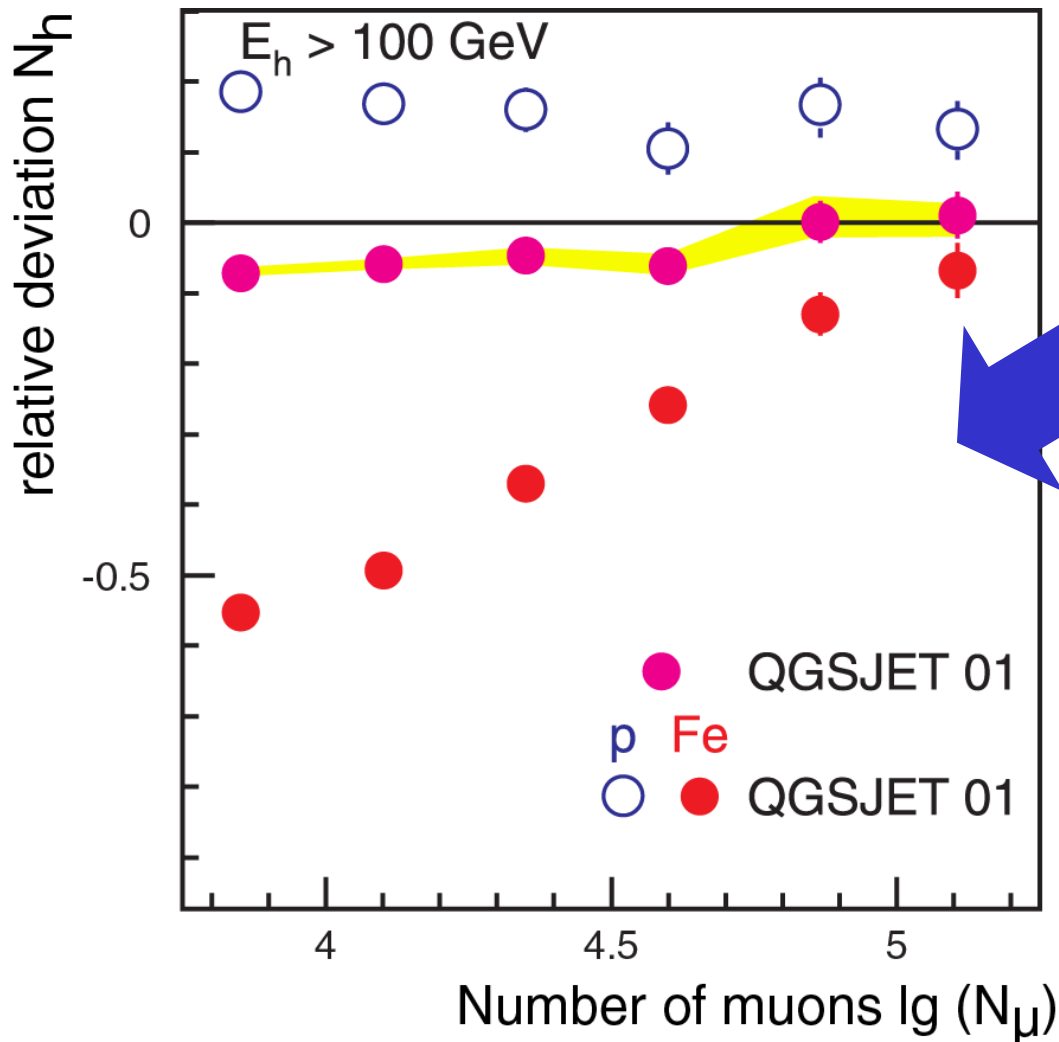


inconsistencies on 10% level

**$N_e$-$N_\mu$ analysis**



*in literature:*
**ideas that knee is caused by new interactions in atmosphere —> energy is carried away by „invisible channels"**
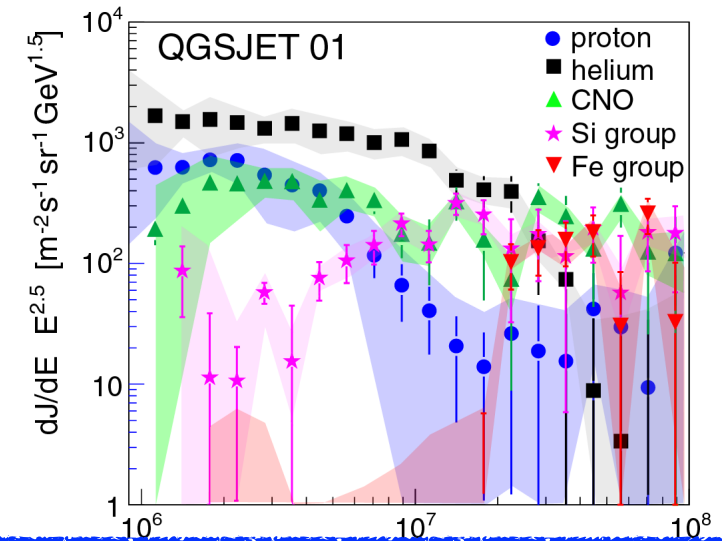


extensive air showers
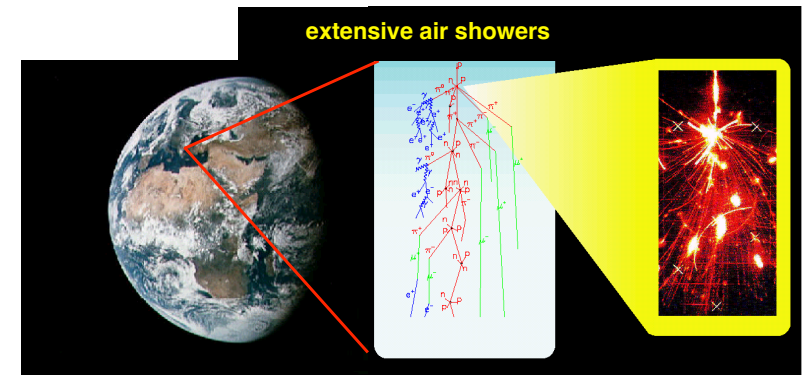
# Test of hadronic interaction models

## QGSJET 01

**Number of hadrons vs. number of muons**

$N_e$-$N_\mu$ analysis
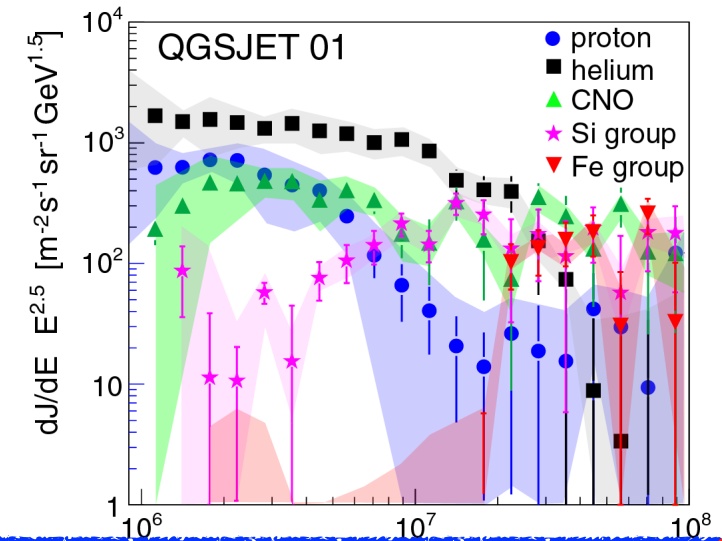


**inconsistencies on 10% level**

*in literature:*
**ideas that knee is caused by new
interactions in atmosphere
—> energy is carried away by
„invisible channels"**

J. Milke et al, Proc. 29th Int. Cosmic Ray Conference Pune 6 (2005) 125
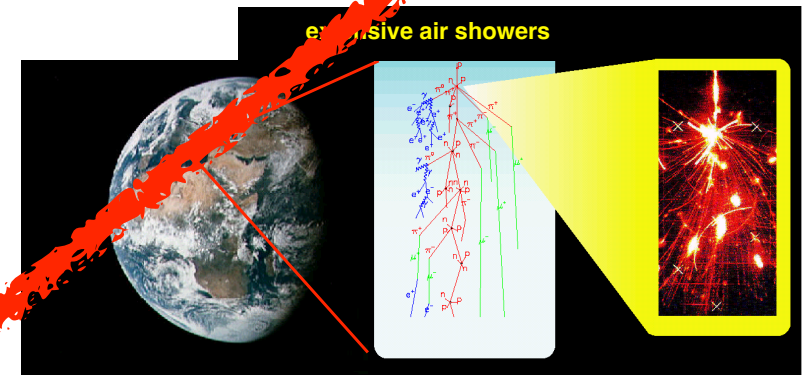
# Electron, muon and hadron size spectra of EAS in the "knee" region

R. Glasstetter[a] and J.R. Hörandel[a] for the KASCADE Collaboration*
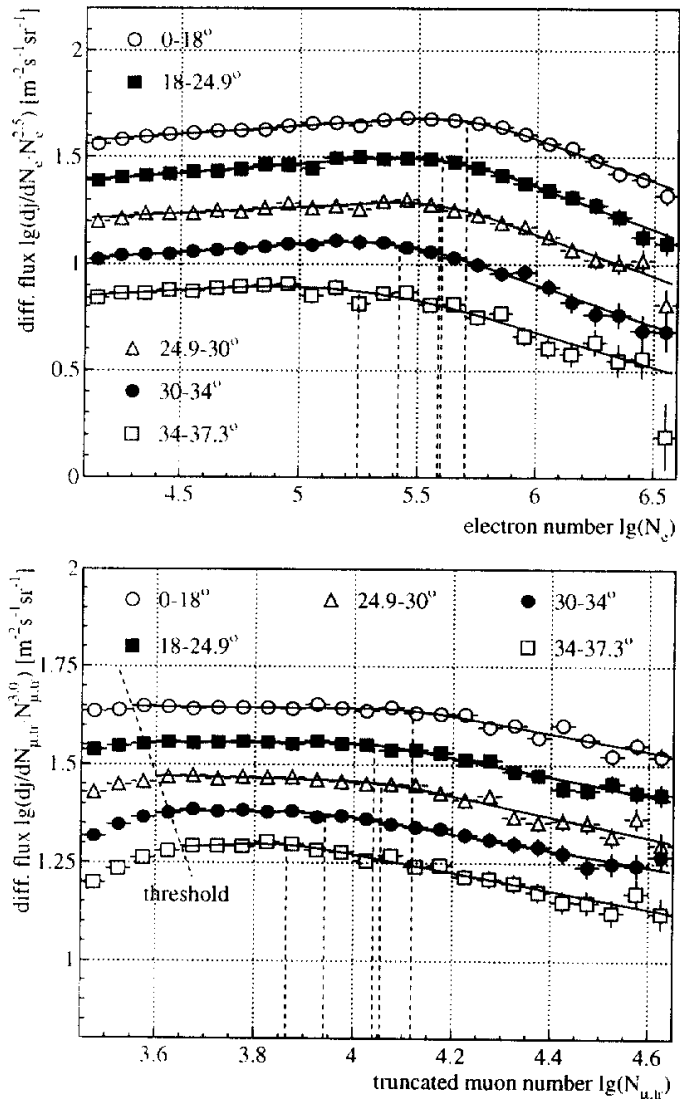
Figure 1. Electromagnetic (top) and muonic (bottom) shower size spectra for different zenith angle bins.
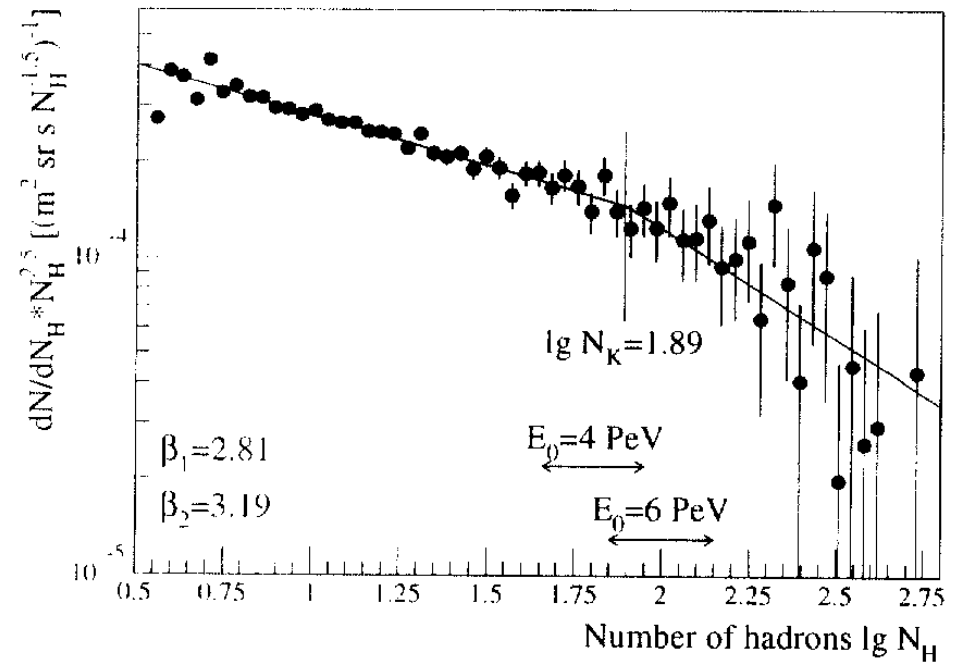


Figure 3. Hadronic shower size spectrum.
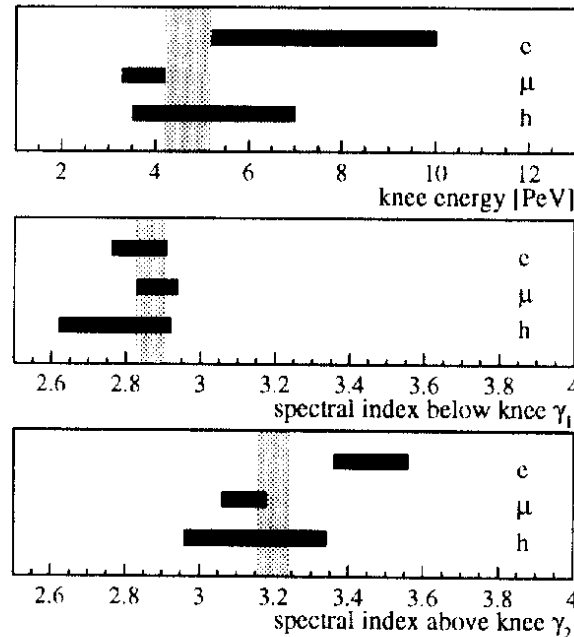


Figure 4. Knee position and spectral indices.

*knee observed in all components, electromagnetic, muonic, and hadronic!*

# KASCADE-Grande
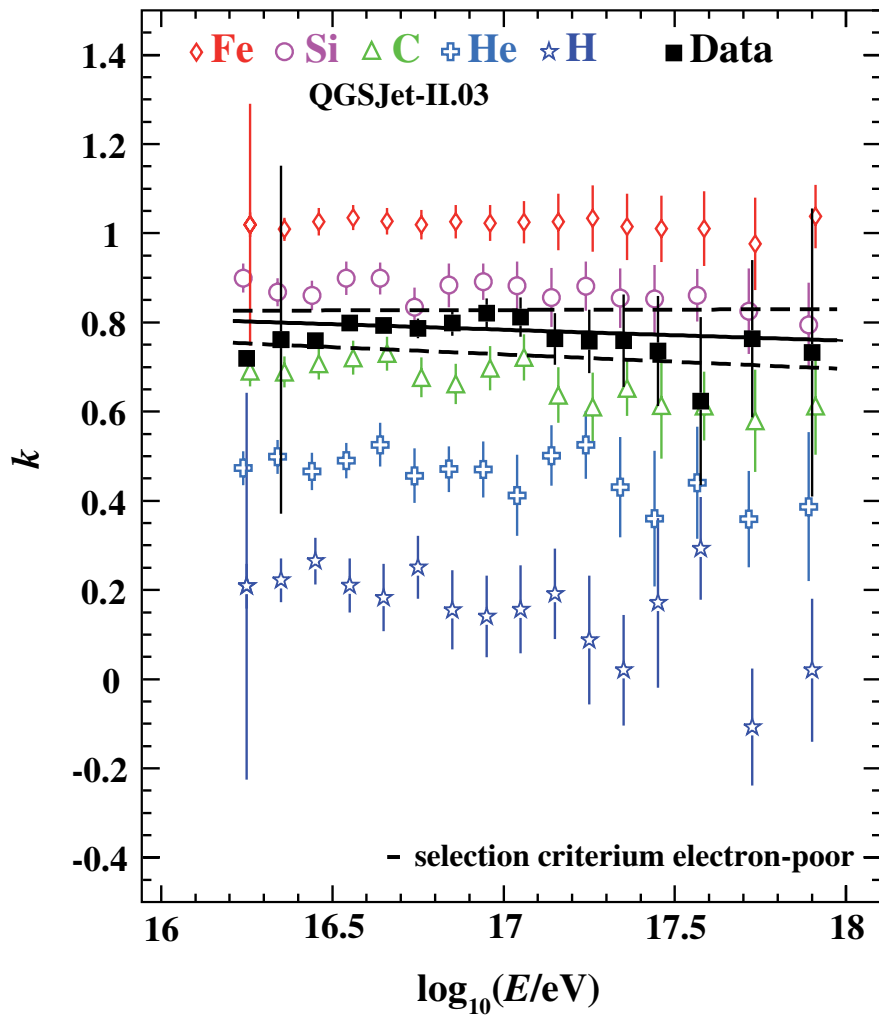


$$k = \frac{\log_{10}(N_{ch}/N_\mu) - \log_{10}(N_{ch}/N_\mu)_H}{\log_{10}(N_{ch}/N_\mu)_{Fe} - \log_{10}(N_{ch}/N_\mu)_H},$$

**W.D. Apel et al., PRL 107 (2011) 171104**

# KASCADE-Grande



$$k = \frac{\log_{10}(N_{ch}/N_\mu) - \log_{10}(N_{ch}/N_\mu)_H}{\log_{10}(N_{ch}/N_\mu)_{Fe} - \log_{10}(N_{ch}/N_\mu)_H},$$

**W.D. Apel et al., PRL 107 (2011) 171104**
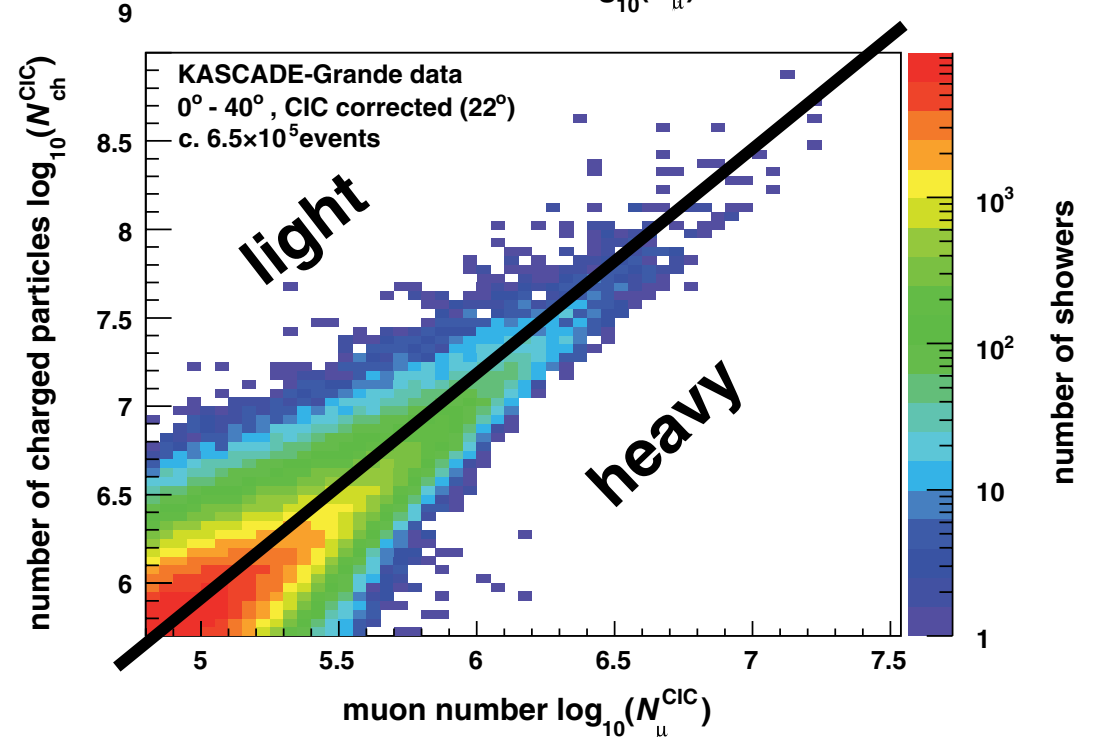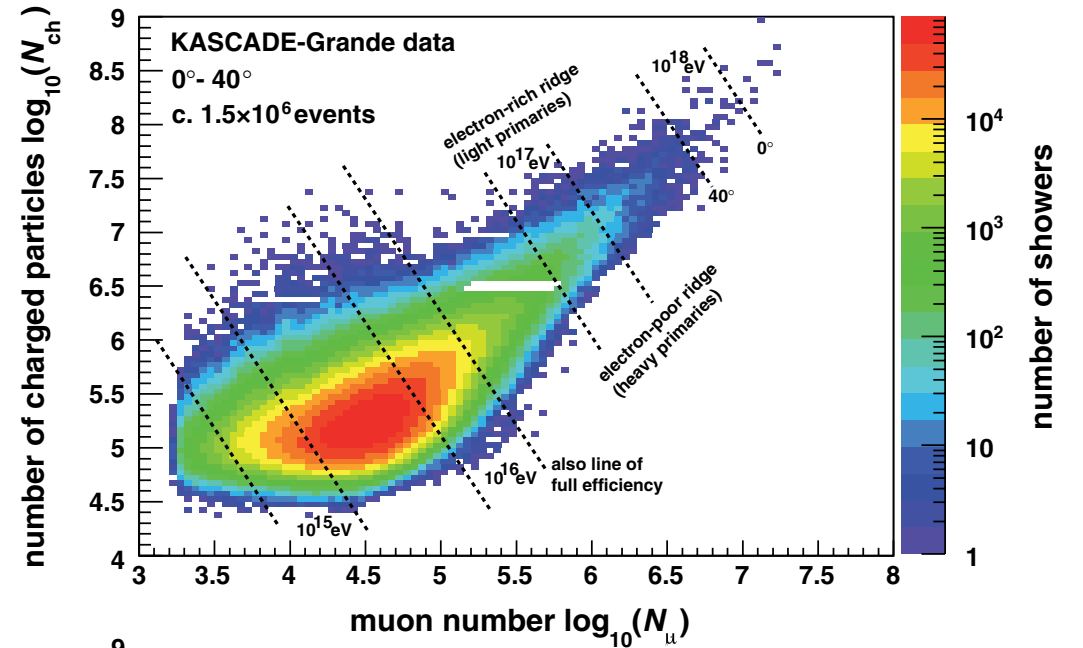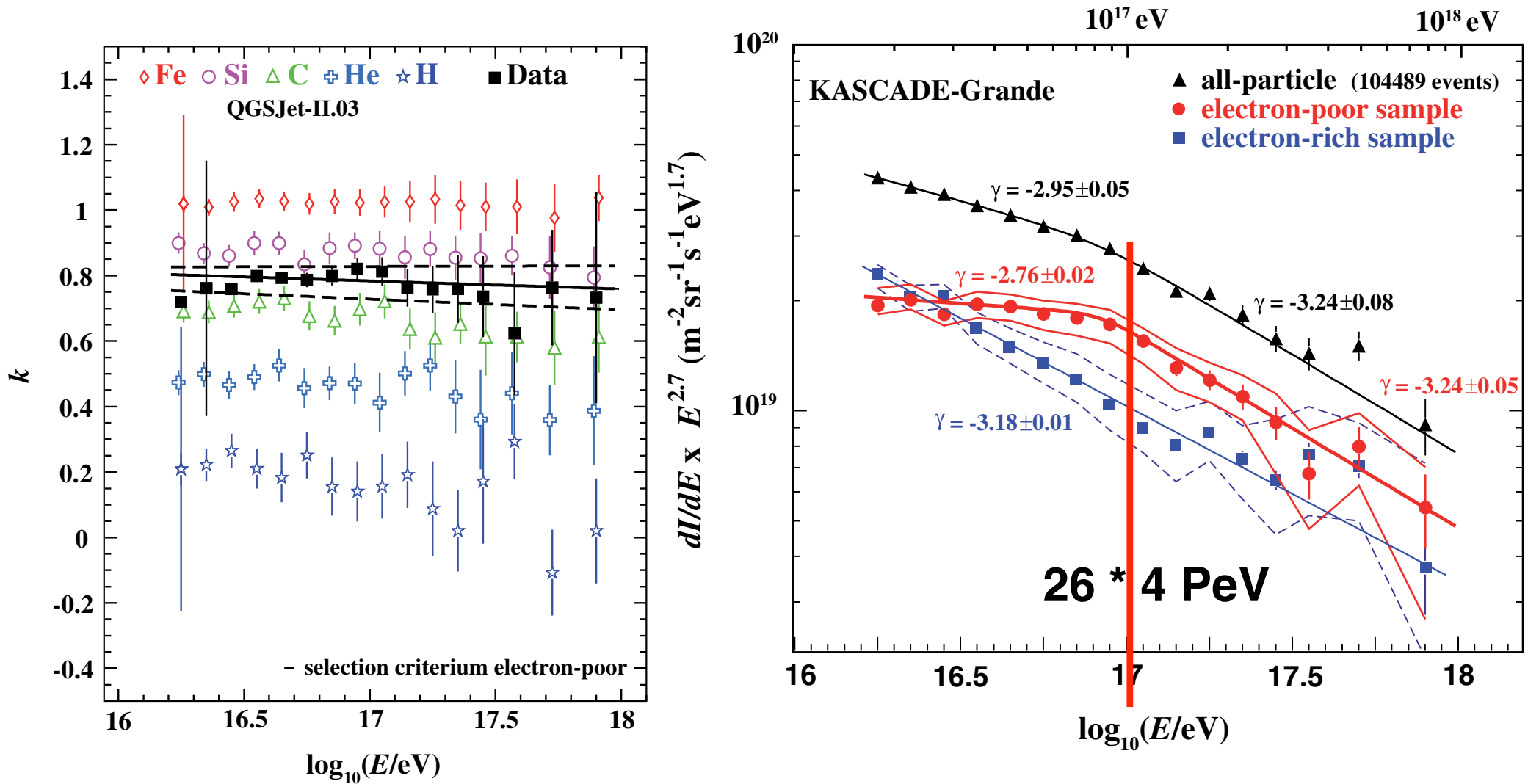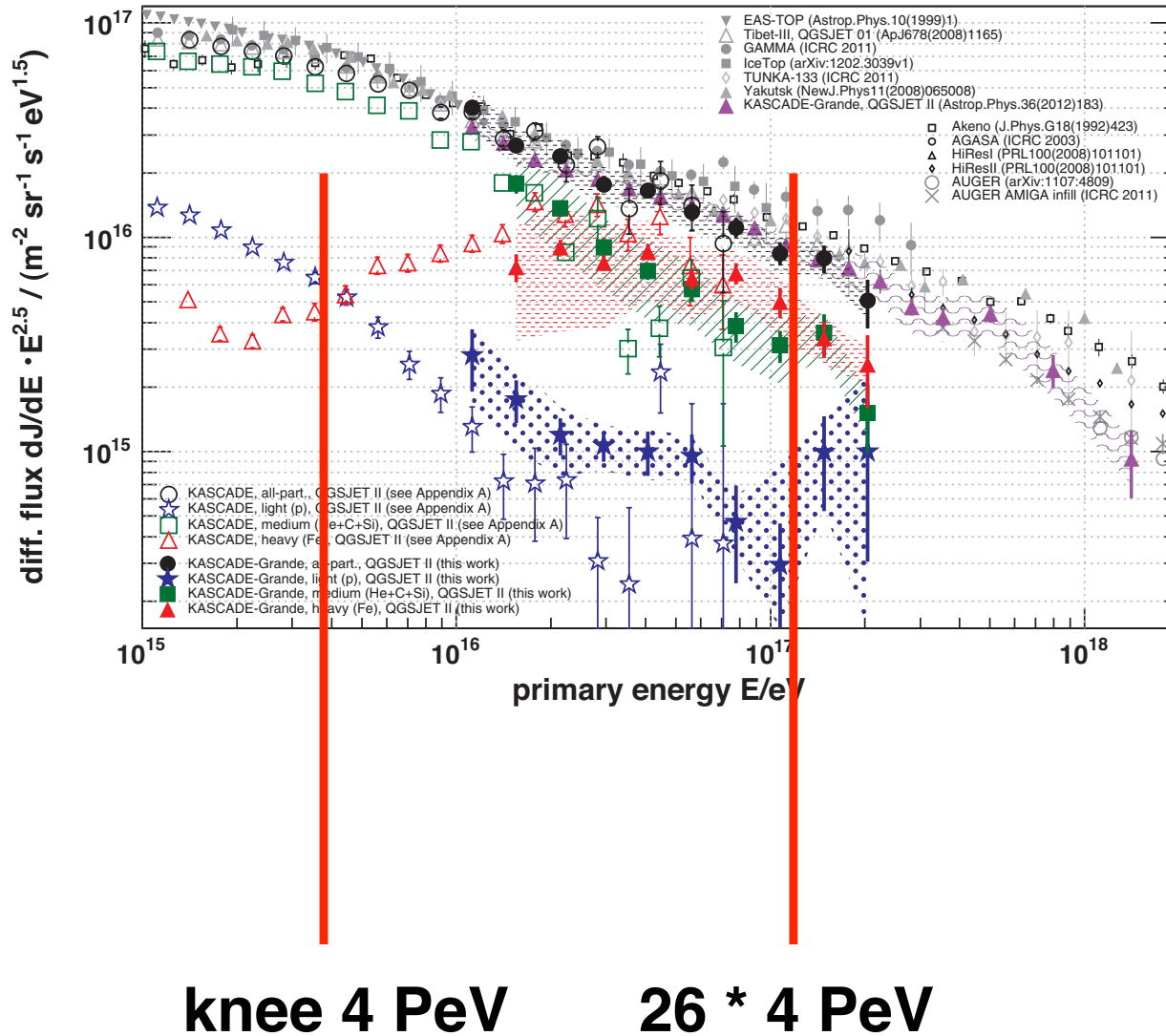
# KASCADE-Grande



**knee 4 PeV**          **26 * 4 PeV**
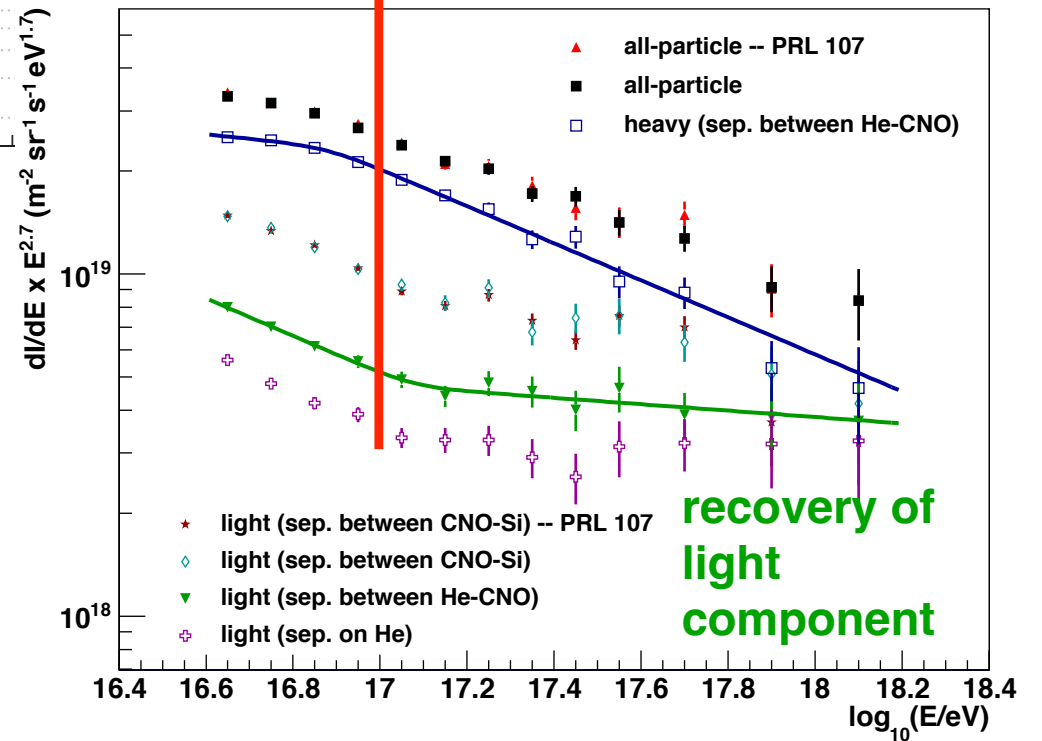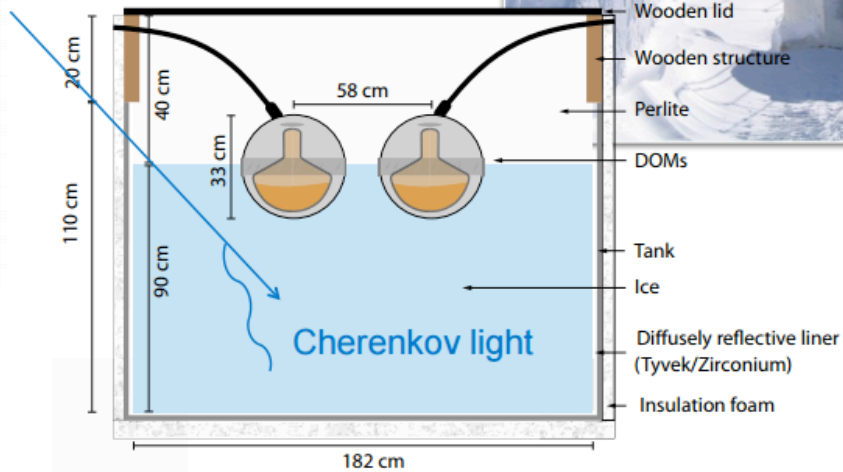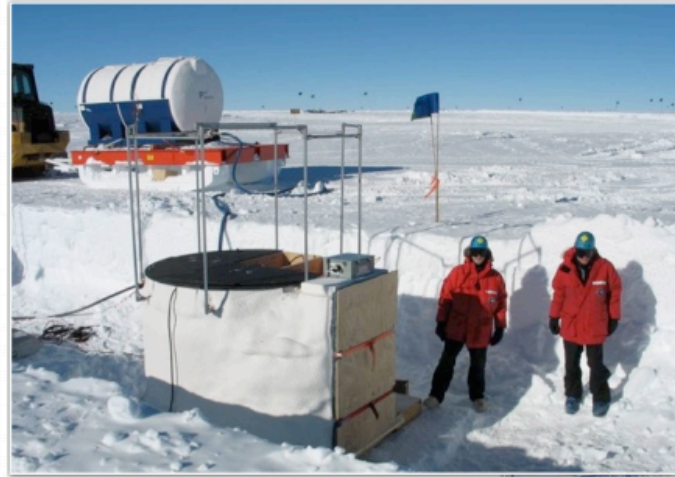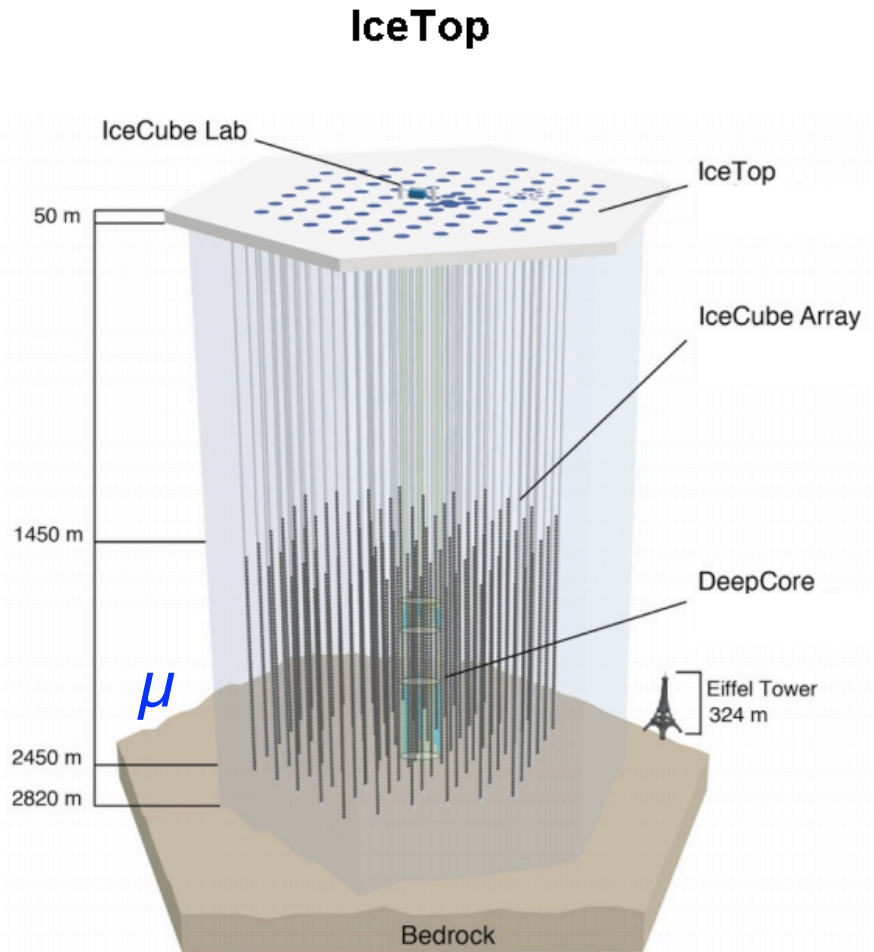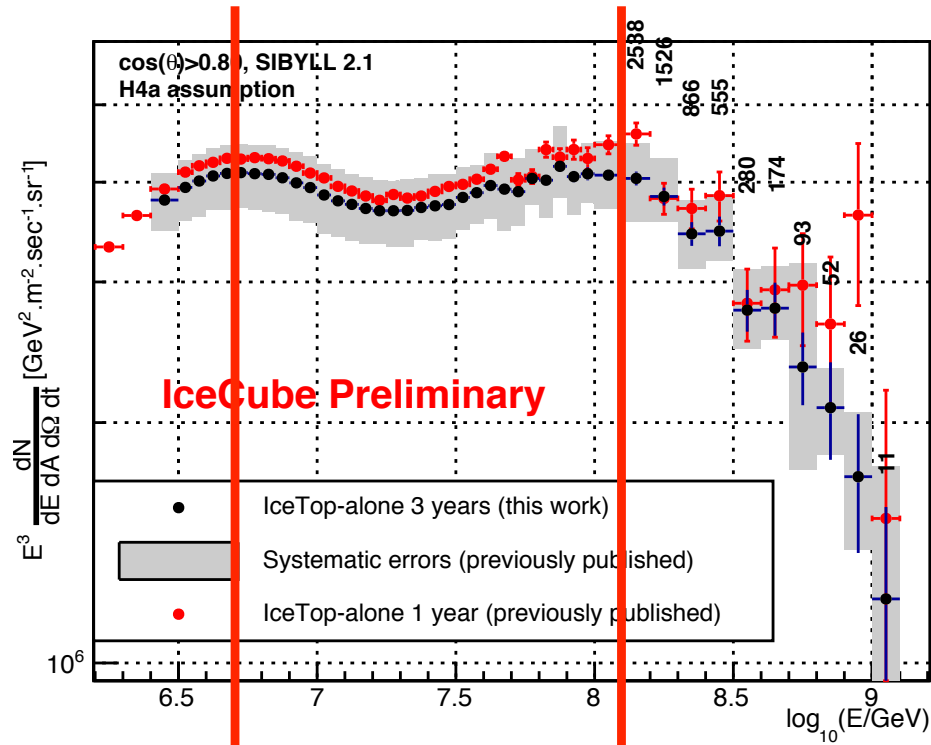
W.D. Apel et al., Astropart. Phys 47 (2013) 54

# KASCADE-Grande



**26 * 4 PeV**

**knee 4 PeV**          **26 * 4 PeV**

**recovery of light component**

# Ice Cube - Ice Top

e/m (+μ)

μ

# Ice Cube - Ice Top



K. Rawlins J Phys Conf. Ser. 718 (2016) 052033

# Ice Cube - Ice Top



**5 PeV**      **26*5 PeV**

**Ice Top only**

**combined**

K. Rawlins J Phys Conf. Ser. 718 (2016) 052033

# Ice Cube - Ice Top





**5 PeV**      **26*5 PeV**

## Ice Top only                     combined

K. Rawlins J Phys Conf. Ser. 718 (2016) 052033

# Ice Cube - Ice Top



K. Rawlins J Phys Conf. Ser. 718 (2016) 052033
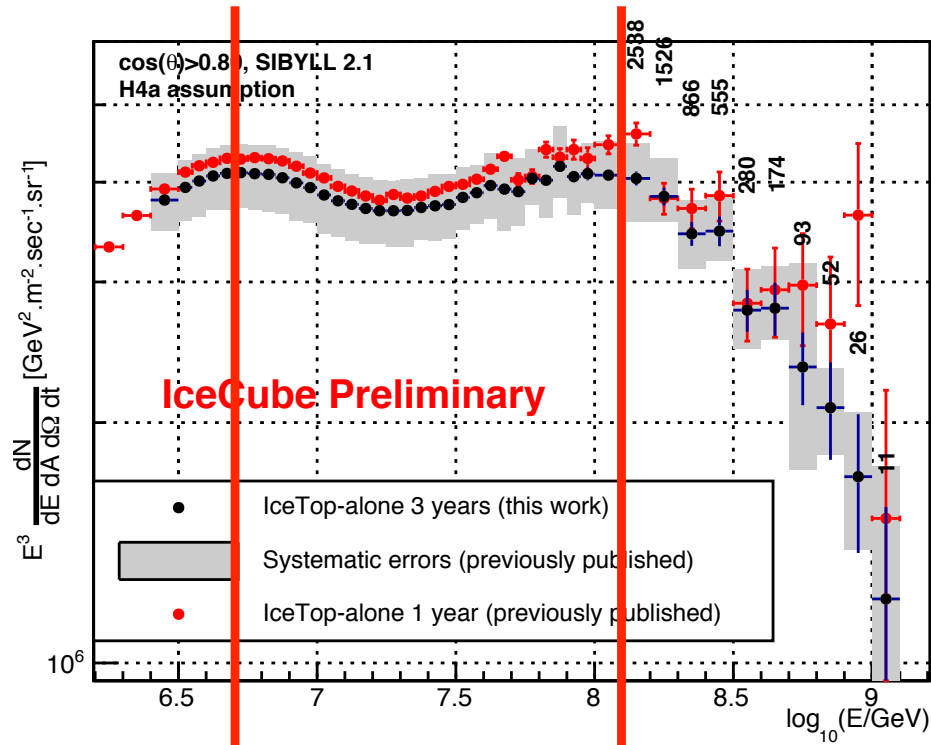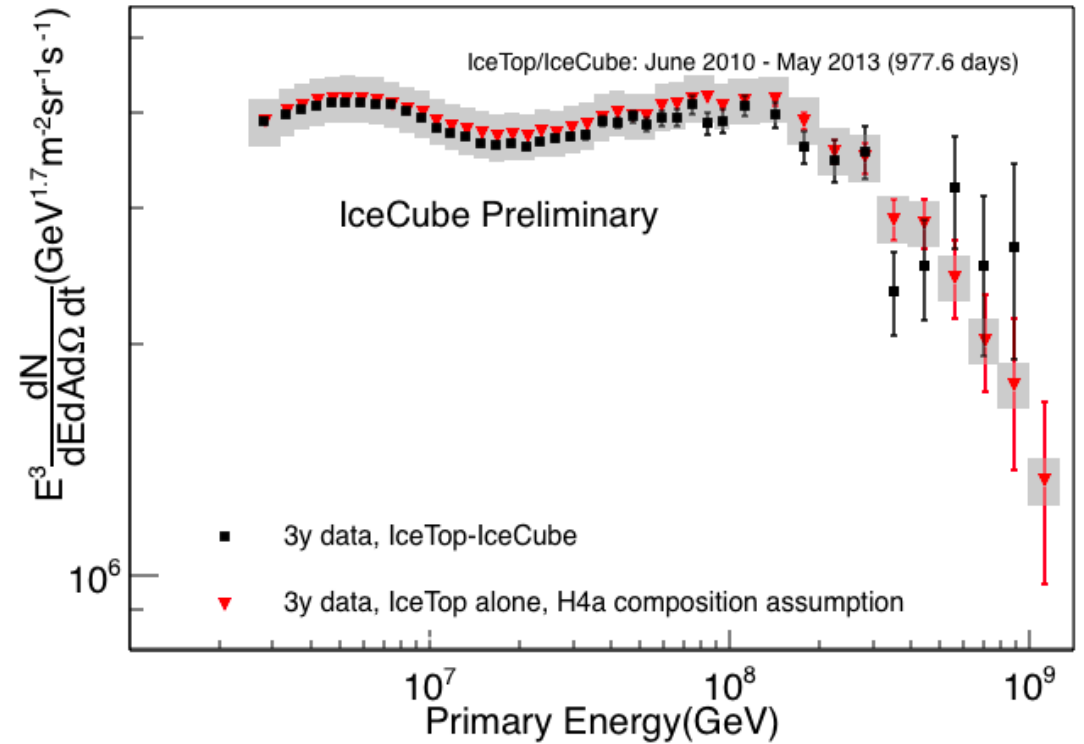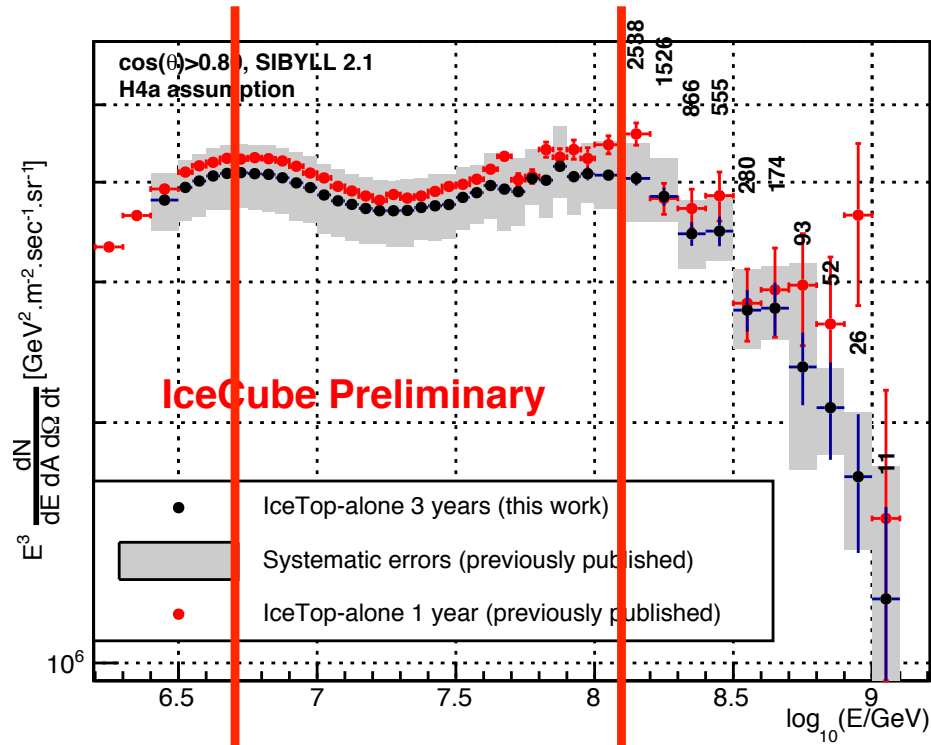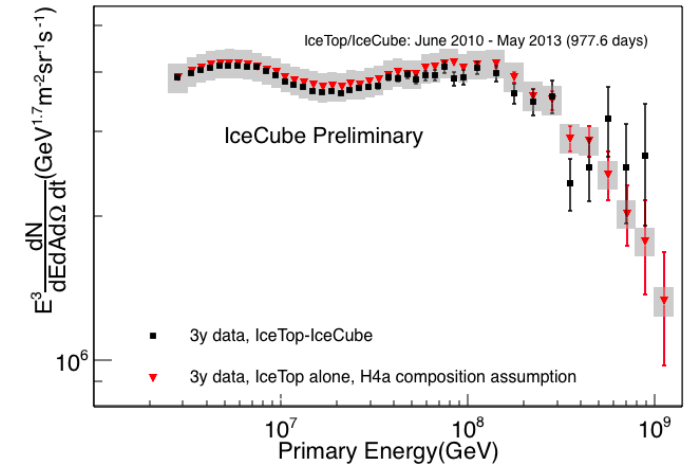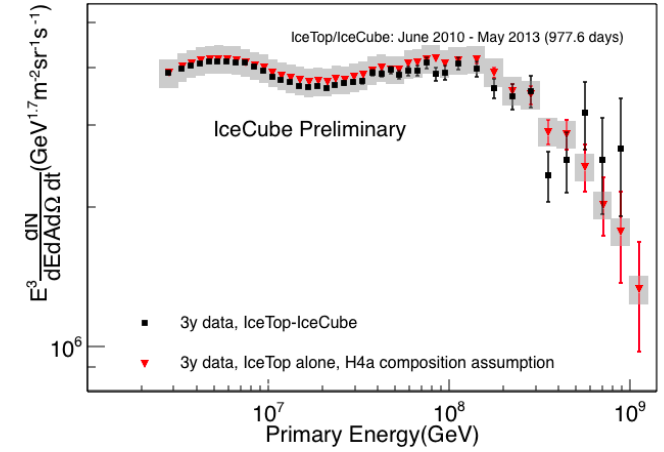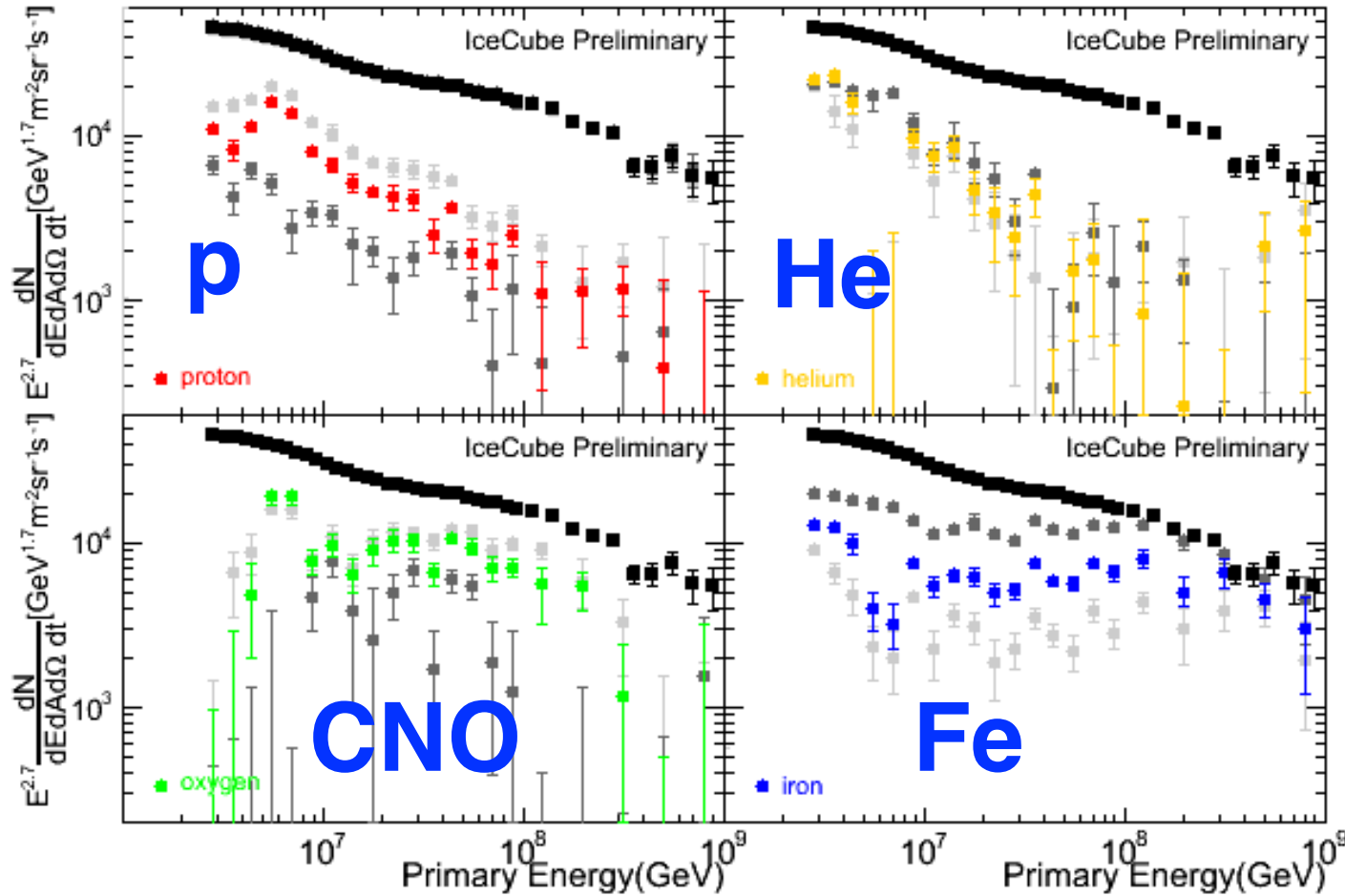
# Cosmic-ray energy spectrum
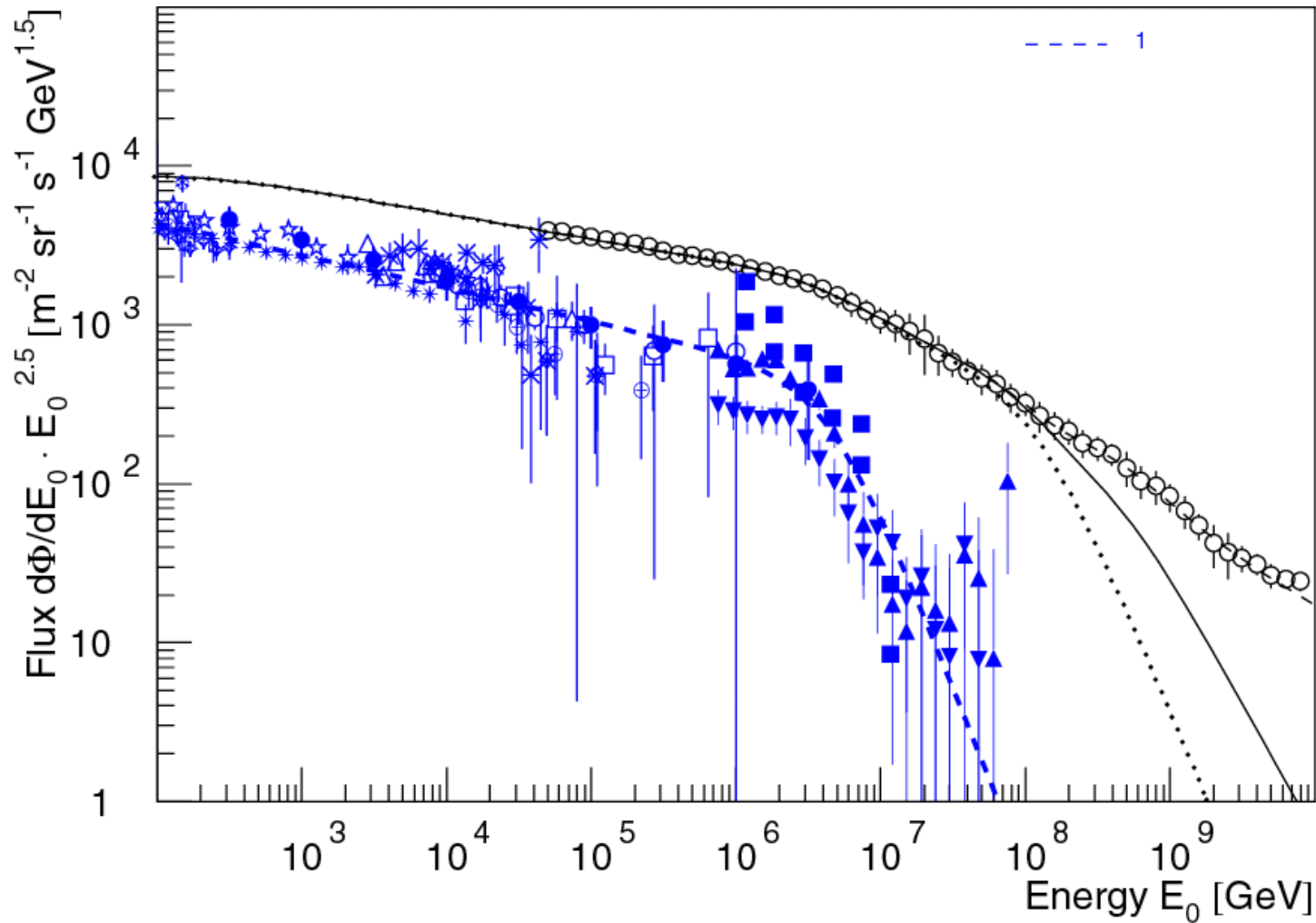
# Cosmic-ray energy spectrum
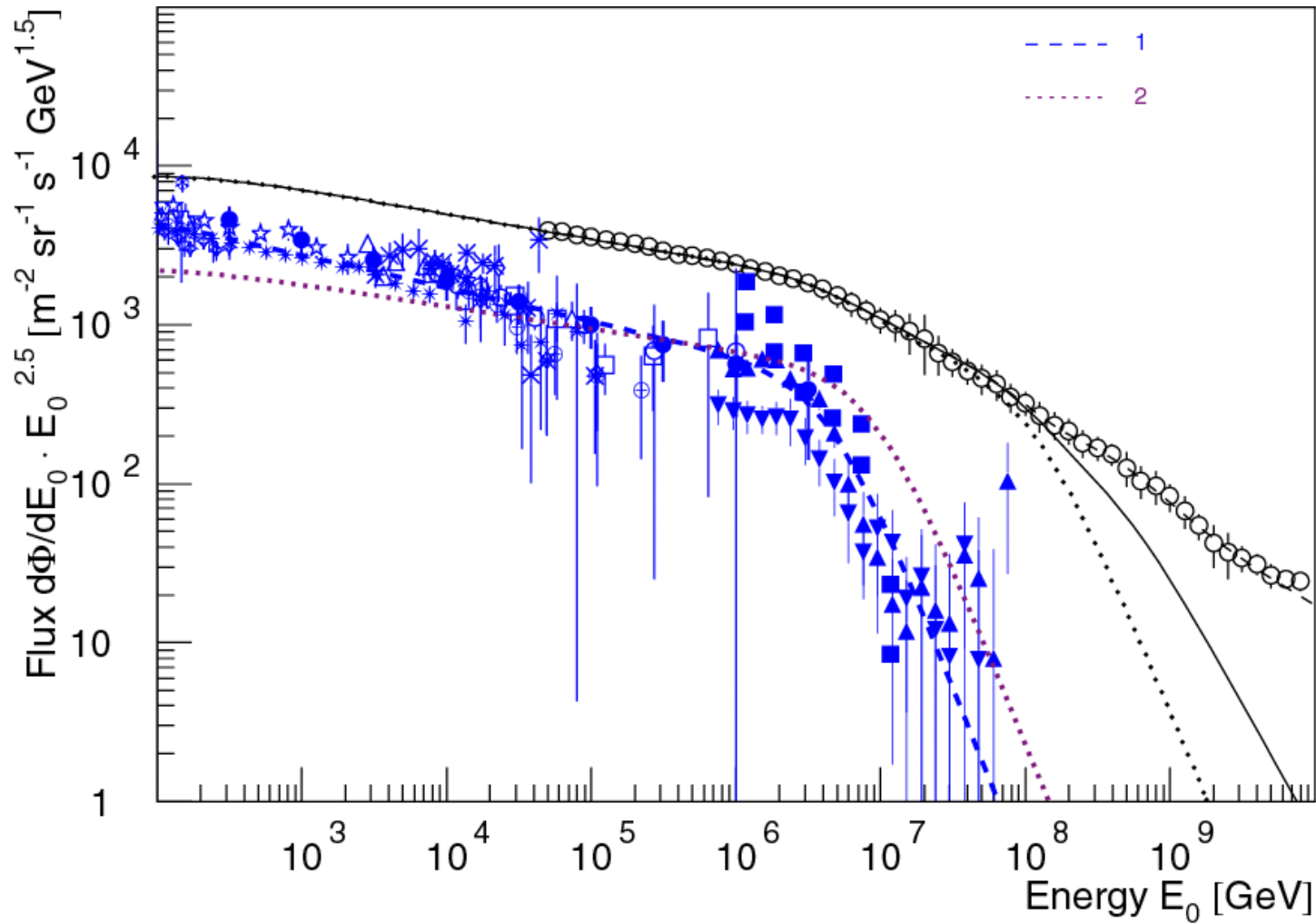
# Cosmic-ray energy spectrum
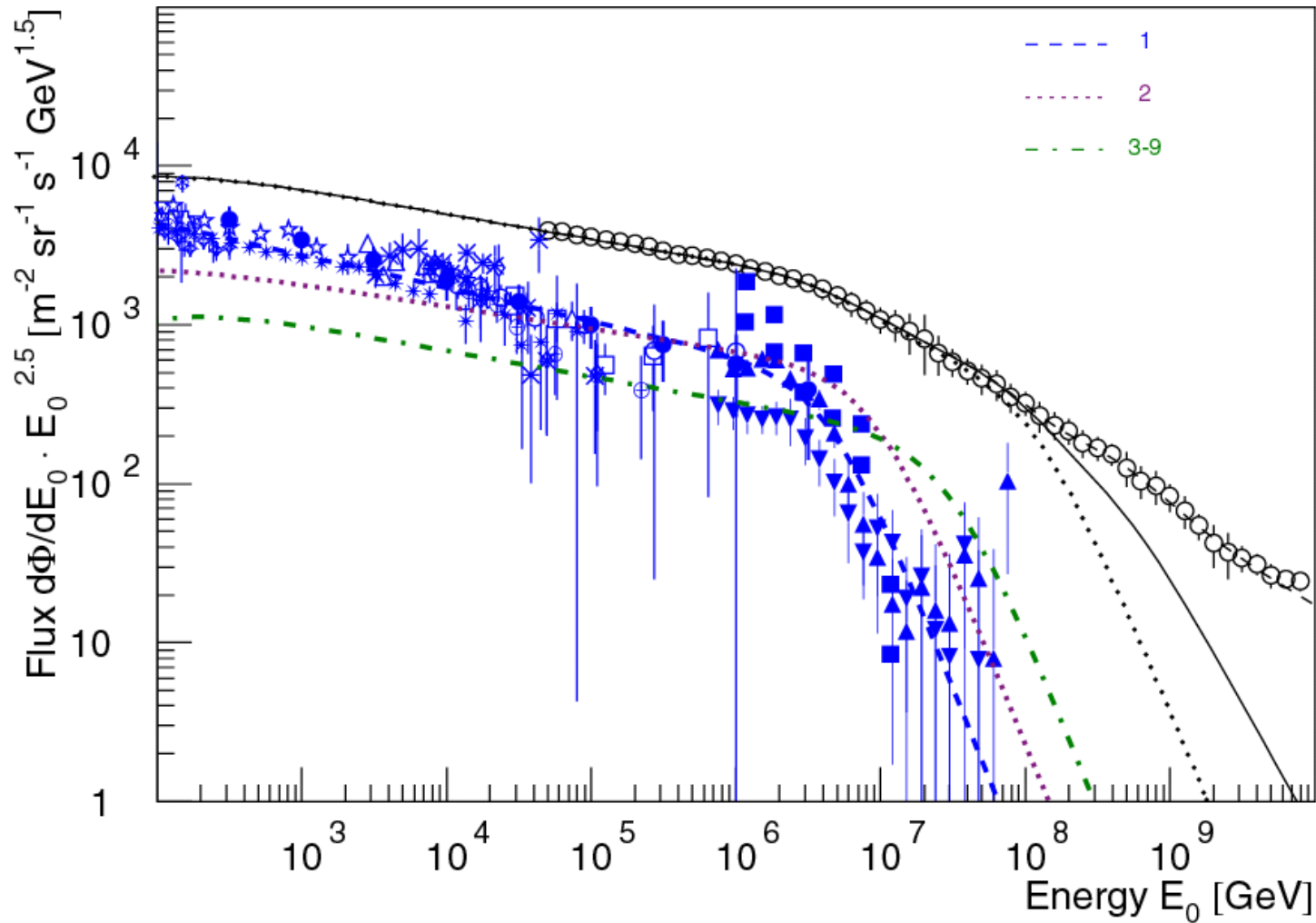
# Cosmic-ray energy spectrum
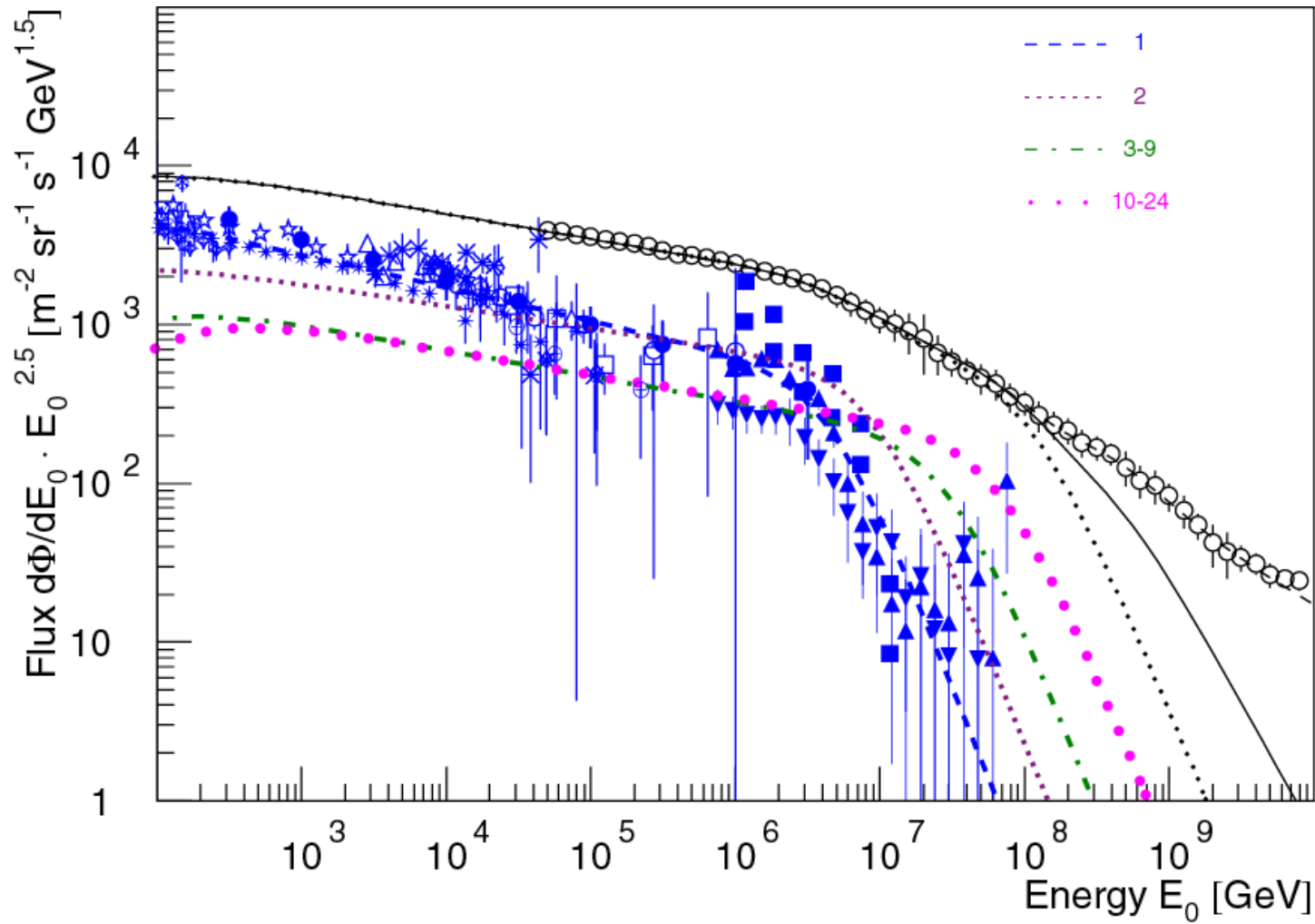
# Cosmic-ray energy spectrum
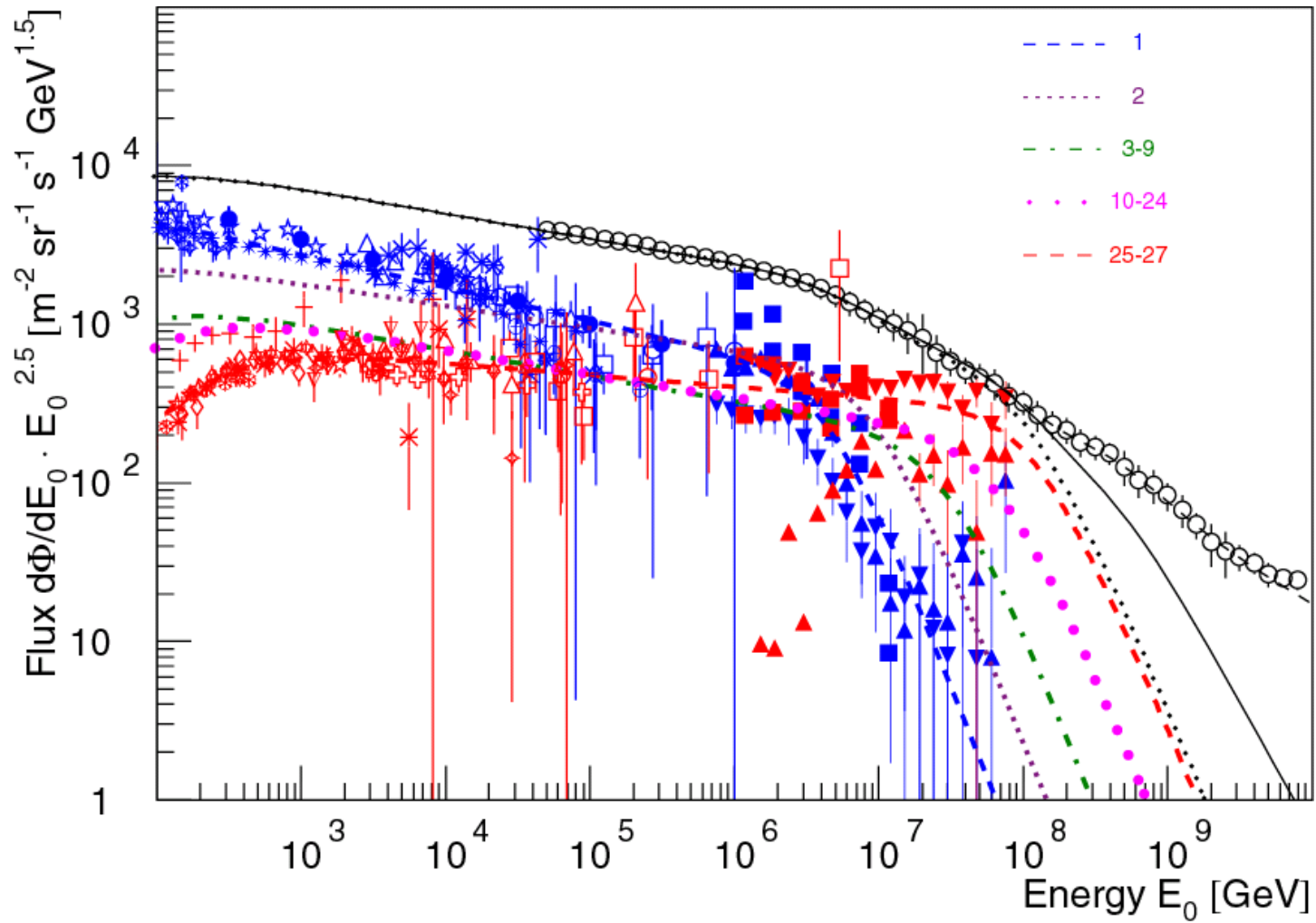
# Cosmic-ray energy spectrum
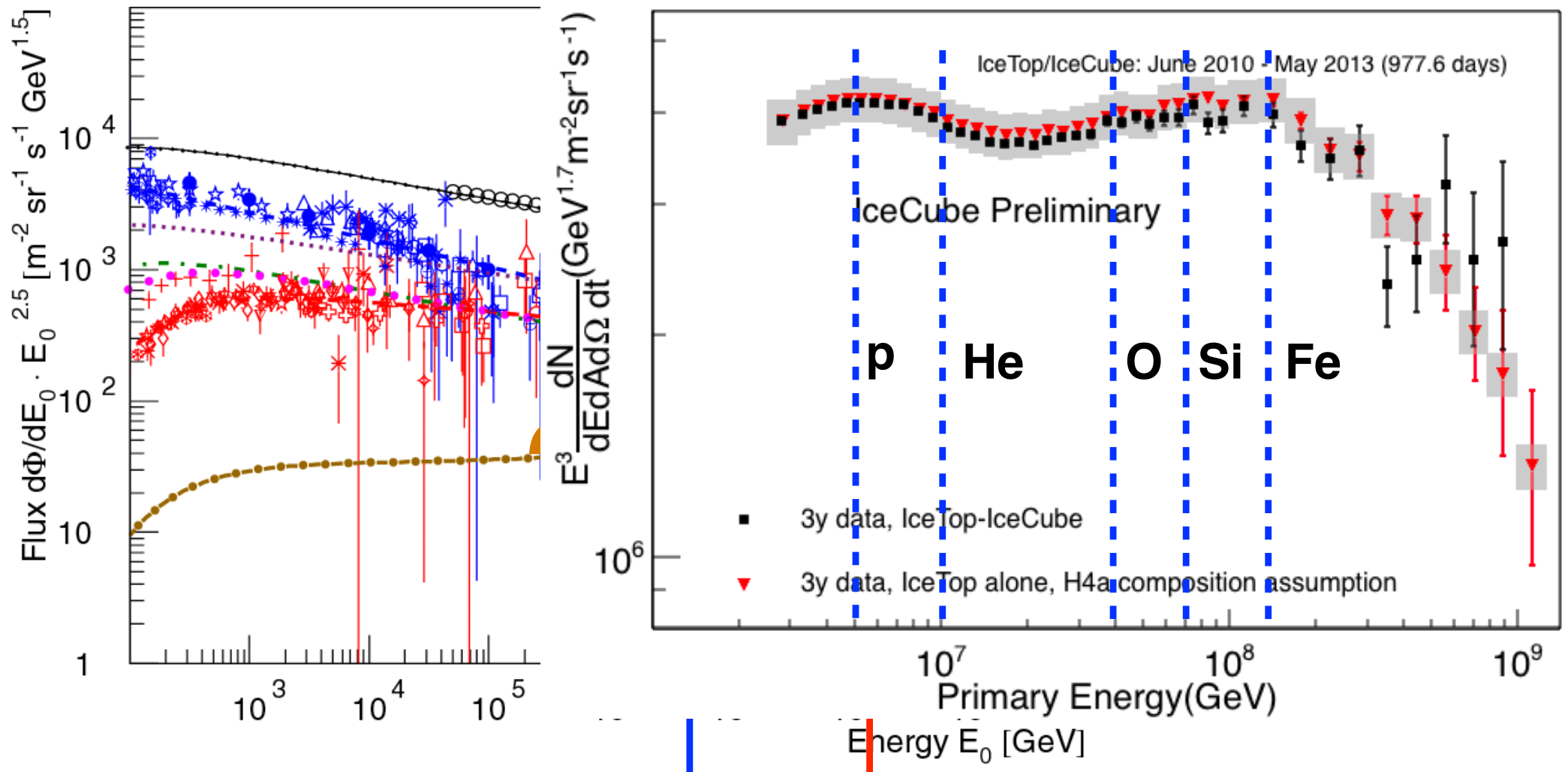
# TALE (TA low-energy extension)
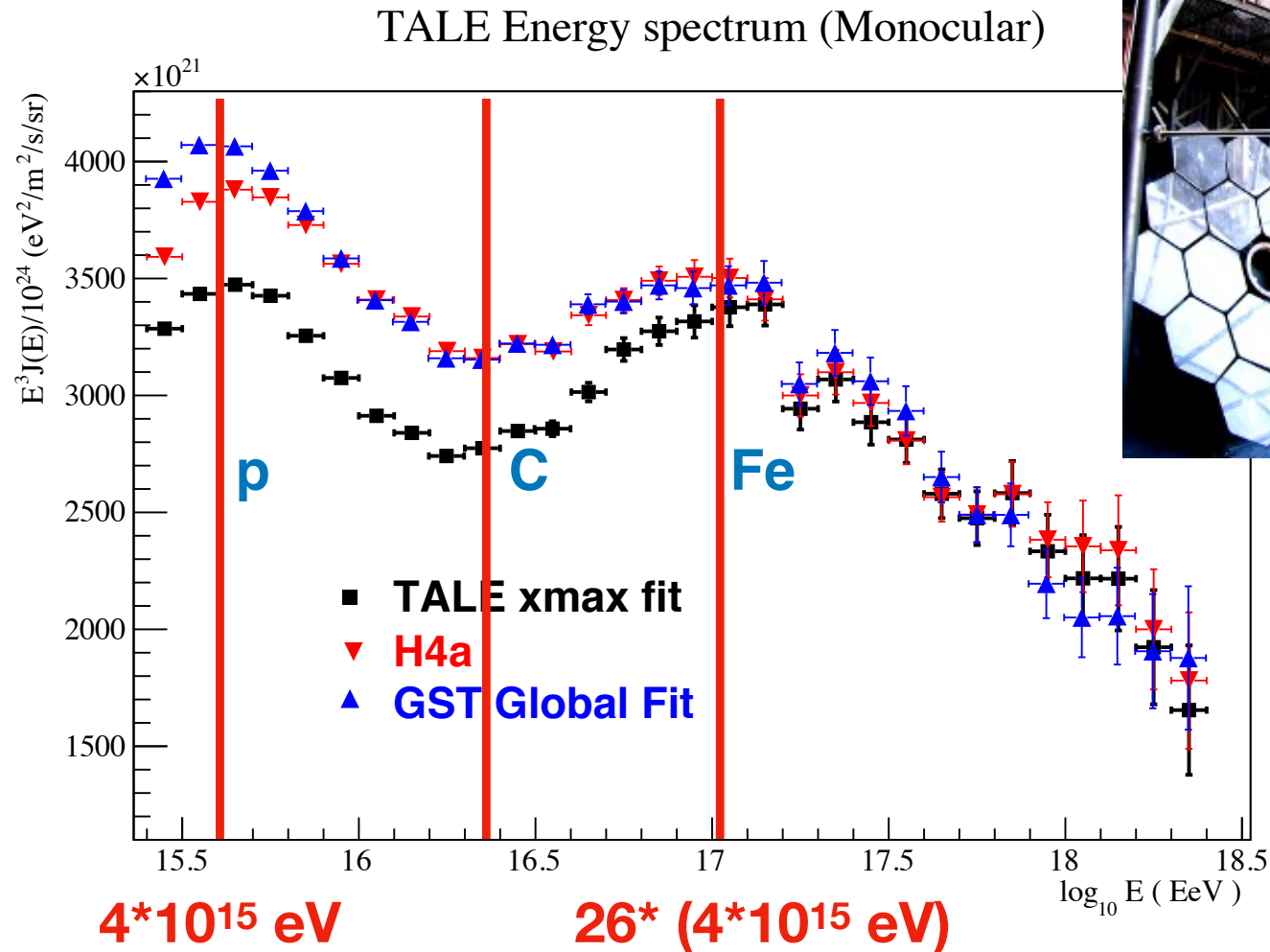


**Figure 3:** TALE Cosmic rays energy spectrum measured with TALE. The result is based on a QGSJet II-3 hadronic model assumption. A mixed primary composition given by the H4a, and "global fit" models, as well as a TALE derived mix was used in the calculations.

Proton / protons

Legend (upper panel):
- ⊗ AMS
- ✳ ATIC-2
- ☆ BESS
- ◇ CAPRICE 98
- ✳ CREAM2011
- ◆ PAMELA2011
- ⊕ RICH-II
- ✂ GRAPES-3 QGS
- ✂ GRAPES-3 SIB
- ▲ KASCADE QGSJET
- ▼ KASCADE SIBYLL
- ● KASCADE SH
- ■ EAS-TOP
- ☰ EAS-TOP SH

Flux $d\Phi/dE_0 \cdot E_0^{2.5}$ $[m^{-2}\ sr^{-1}\ s^{-1}\ GeV^{1.5}]$

Energy $E_0$ [GeV]



Helium / He

Legend (lower panel):
- ⊗ AMS
- ✳ ATIC-2
- ☆ BESS
- ◇ CAPRICE 98
- ✳ CREAM2011
- ◆ PAMELA2011
- ⊕ RICH-II
- ✂ GRAPES-3 QGS
- ✂ GRAPES-3 SIB
- ▲ KASCADE QGSJET
- ▼ KASCADE SIBYLL

Flux $d\Phi/dE_0 \cdot E_0^{2.5}$ $[m^{-2}\ sr^{-1}\ s^{-1}\ GeV^{1.5}]$

Energy $E_0$ [GeV]

**JRH, AIP Conf. Proc. 1516 (2013) 185**

Proton

protons

Flux $d\Phi/dE_0 \cdot E_0^{2.5}$ [m$^{-2}$ sr$^{-1}$ s$^{-1}$ GeV$^{1.5}$]

- ⊗ AMS
- ✳ ATIC-2
- ☆ BESS
- ◇ CAPRICE 98
- ✻ CREAM2011
- ✦ PAMELA2011
- ⊕ RICH-II

- ✻ GRAPES-3 QGS
- ✻ GRAPES-3 SIB
- ▲ KASCADE QGSJET
- ▼ KASCADE SIBYLL
- ● KASCADE SH
- ■ EAS-TOP
- ≡ EAS-TOP SH

Energy E$_0$ [GeV]



Helium

He

Flux $d\Phi/dE_0 \cdot E_0^{2.5}$ [m$^{-2}$ sr$^{-1}$ s$^{-1}$ GeV$^{1.5}$]

- ⊗ AMS
- ✳ ATIC-2
- ☆ BESS
- ◇ CAPRICE 98
- ✻ CREAM2011
- ✦ PAMELA2011
- ⊕ RICH-II

- ✻ GRAPES-3 QGS
- ✻ GRAPES-3 SIB
- ▲ KASCADE QGSJET
- ▼ KASCADE SIBYLL

Energy E$_0$ [GeV]

**JRH, AIP Conf. Proc. 1516 (2013) 185**

**protons**

**He**

**26**

**protons**

**He**

SIBYLL2.1       **KASCADE**

- proton
- helium
- CNO

primary energy E [GeV]

**JRH, AIP Conf. Proc. 1516 (2013) 185**

Jörg R. Hörandel, APP 2023/24   **26**

**protons**

**He**

# Transport equation for cosmic rays in the Galaxy

$$\frac{\partial N_i}{\partial t} = \nabla(D_i \nabla N_i) - \frac{\partial}{\partial E}(b_i N_i) - n\nu\sigma_i N_i - \frac{N_i}{\gamma\tau_i} + Q_i + \sum_{j>i} n\nu\sigma_{ij} N_j + \sum_{j>i} \frac{N_j}{\gamma_j \tau_{ij}}$$
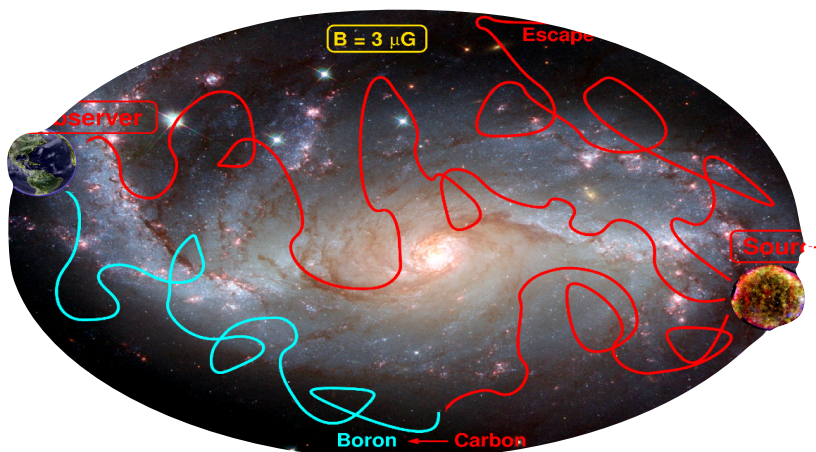
# Transport equation for cosmic rays in the Galaxy

diffusion

$$\frac{\partial N_i}{\partial t} = \nabla(D_i \nabla N_i) - \frac{\partial}{\partial E}(b_i N_i) - n\nu\sigma_i N_i - \frac{N_i}{\gamma\tau_i} + Q_i + \sum_{j>i} n\nu\sigma_{ij} N_j + \sum_{j>i} \frac{N_j}{\gamma_j \tau_{ij}}$$
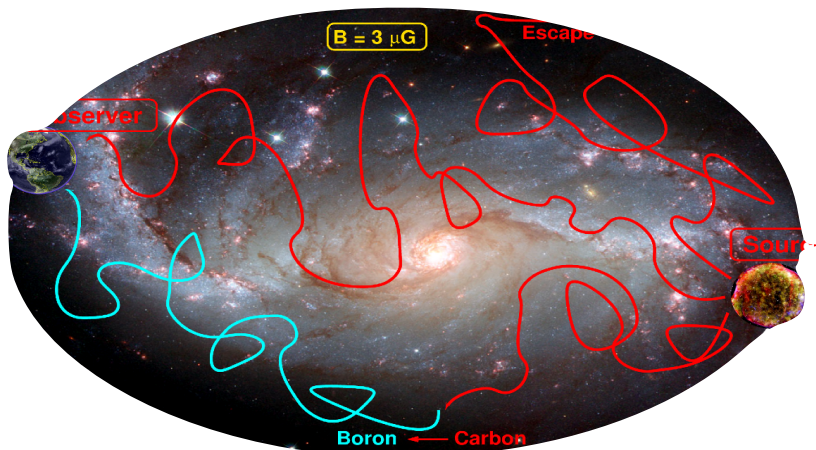
# Transport equation for cosmic rays in the Galaxy

**diffusion**

**energy loss (Bethe Bloch)**

$$\frac{\partial N_i}{\partial t} = \nabla(D_i \nabla N_i) - \frac{\partial}{\partial E}(b_i N_i) - n\nu\sigma_i N_i - \frac{N_i}{\gamma\tau_i} + Q_i + \sum_{j>i} n\nu\sigma_{ij} N_j + \sum_{j>i}\frac{N_j}{\gamma_j \tau_{ij}}$$
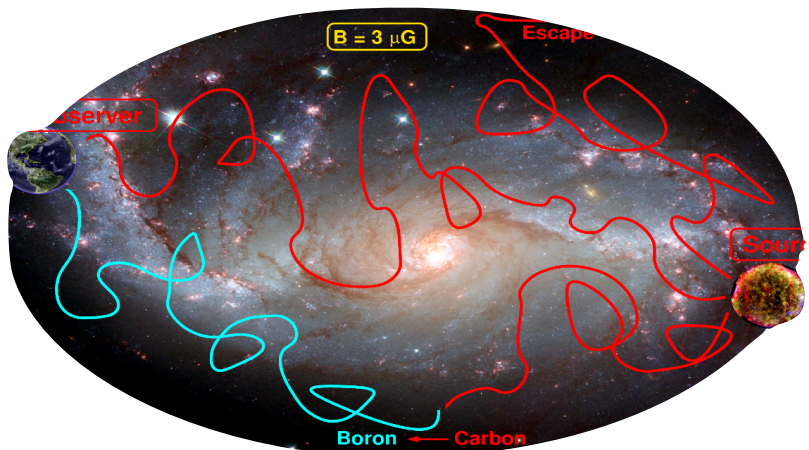
# Transport equation for cosmic rays in the Galaxy

**diffusion**

**energy loss (Bethe Bloch)**

**loss through interactions
with ISM (spallation)**

$$\frac{\partial N_i}{\partial t} = \nabla(D_i \nabla N_i) - \frac{\partial}{\partial E}(b_i N_i) - n\nu\sigma_i N_i - \frac{N_i}{\gamma\tau_i} + Q_i + \sum_{j>i} n\nu\sigma_{ij} N_j + \sum_{j>i} \frac{N_j}{\gamma_j \tau_{ij}}$$

# Transport equation for cosmic rays in the Galaxy

**diffusion**

**energy loss (Bethe Bloch)**

**loss through interactions with ISM (spallation)**

**loss through radioactive decay**

$$\frac{\partial N_i}{\partial t} = \nabla(D_i \nabla N_i) - \frac{\partial}{\partial E}(b_i N_i) - n\nu\sigma_i N_i - \frac{N_i}{\gamma\tau_i} + Q_i + \sum_{j>i} n\nu\sigma_{ij} N_j + \sum_{j>i} \frac{N_j}{\gamma_j \tau_{ij}}$$

# Transport equation for cosmic rays in the Galaxy

**diffusion**

**energy loss (Bethe Bloch)**

**loss through interactions
with ISM (spallation)**

**loss through radioactive decay**

$$\frac{\partial N_i}{\partial t} = \nabla(D_i \nabla N_i) - \frac{\partial}{\partial E}(b_i N_i) - n\nu\sigma_i N_i - \frac{N_i}{\gamma\tau_i} + Q_i + \sum_{j>i} n\nu\sigma_{ij} N_j + \sum_{j>i} \frac{N_j}{\gamma_j\tau_{ij}}$$

**source term**



B = 3 μG
Escape
Observer
Source
Boron — Carbon

# Transport equation for cosmic rays in the Galaxy

diffusion

energy loss (Bethe Bloch)

loss through interactions
with ISM (spallation)

loss through radioactive decay

$$\frac{\partial N_i}{\partial t} = \nabla(D_i \nabla N_i) - \frac{\partial}{\partial E}(b_i N_i) - n\nu\sigma_i N_i - \frac{N_i}{\gamma\tau_i} + Q_i + \sum_{j>i} n\nu\sigma_{ij} N_j + \sum_{j>i} \frac{N_j}{\gamma_j \tau_{ij}}$$

source term

production through spallation
of heavy nuclei

B = 3 μG

Escape

Observer

Source

Boron — Carbon

# Transport equation for cosmic rays in the Galaxy

**diffusion**

**energy loss (Bethe Bloch)**

**loss through interactions with ISM (spallation)**

**loss through radioactive decay**

$$\frac{\partial N_i}{\partial t} = \nabla(D_i \nabla N_i) - \frac{\partial}{\partial E}(b_i N_i) - n\nu\sigma_i N_i - \frac{N_i}{\gamma\tau_i} + Q_i + \sum_{j>i} n\nu\sigma_{ij} N_j + \sum_{j>i} \frac{N_j}{\gamma_j \tau_{ij}}$$

**source term**

**production through spallation of heavy nuclei**

**production through decay of heavy nuclei**

B = 3 μG

Escape

Observer

Source

Boron ← Carbon

# Transport equation f...
# Ga...

**diffusion**

**energy loss (Bethe Bloch**

**loss through i...**
**with ...**



$$\frac{\partial N_i}{\partial t} = \nabla(D_i \nabla N_i) - \frac{\partial}{\partial E}(b_i N_i) - n\nu\sigma_i N_i - \frac{N_i}{\gamma\tau_i} + Q_i + \sum_{j>i} n\nu\sigma_{ij} N_j + \sum_{j>i} \frac{N_j}{\gamma_j \tau_{ij}}$$

**source term**

**production through spallation
of heavy nuclei**

**production through decay
of heavy nuclei**

# Transport equation for cosmic rays in the Galaxy

**diffusion**

**energy loss (Bethe Bloch)**

**loss through interactions with ISM (spallation)**

**loss through radioactive decay**

$$\frac{\partial N_i}{\partial t} = \nabla(D_i \nabla N_i) - \frac{\partial}{\partial E}(b_i N_i) - n\nu\sigma_i N_i - \frac{N_i}{\gamma\tau_i} + Q_i + \sum_{j>i} n\nu\sigma_{ij} N_j + \sum_{j>i} \frac{N_j}{\gamma_j \tau_{ij}}$$
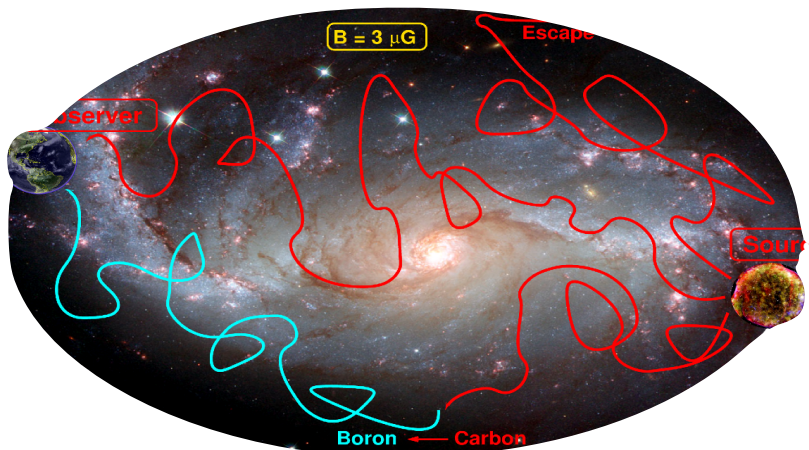
**source term**

**production through spallation of heavy nuclei**

**production through decay of heavy nuclei**

B = 3 μG
Escape
Observer
Source
Boron — Carbon
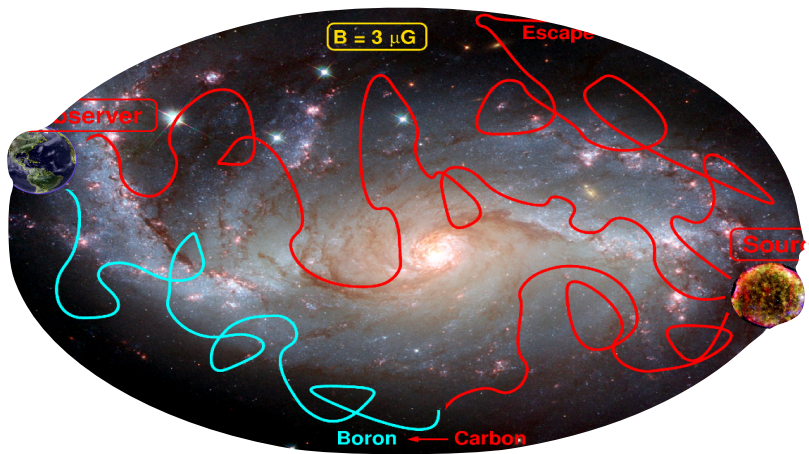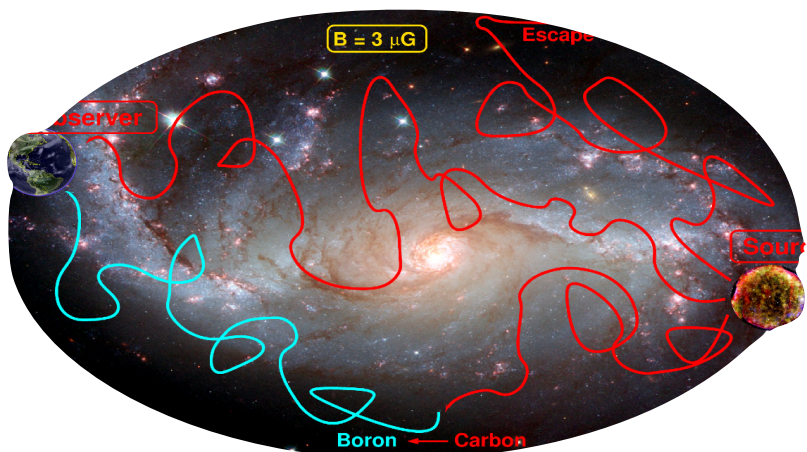
# 1st order Fermi acceleration at strong shock

a) **rest system of unshocked ISM** ISM

$p_2, T_2, \rho_2$      $p_1, T_1, \rho_1$

$U_{Schock}$

$v_2 = 3/4 \, U_s$      $v_1 = 0$

$v_s = U_s$

b) **rest system of unshocked ISM**

$3/4 \, U_s$

c) **rest system of shock front**

$v_2 = 1/4 \, v_1$      $v_1 = |U|$

$v_s = 0$

d) **rest system of shocked ISM**

$3/4 \, U_s$
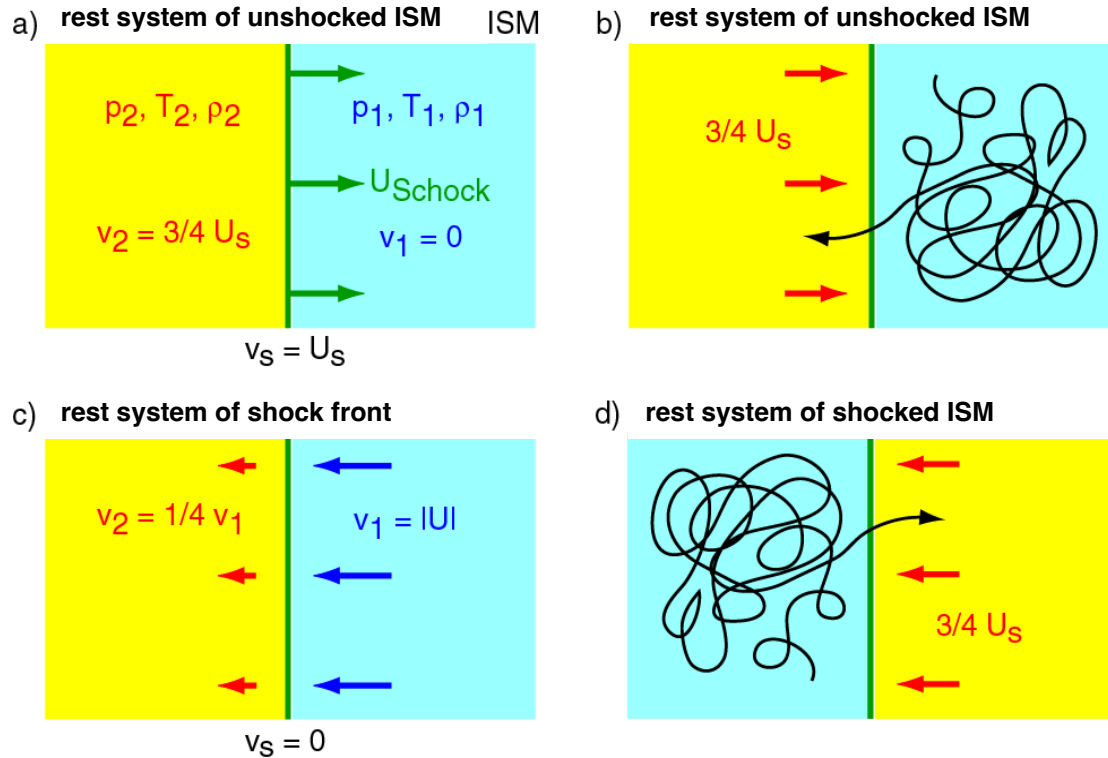
**Bell, Blanford, Ostriker (1978)**
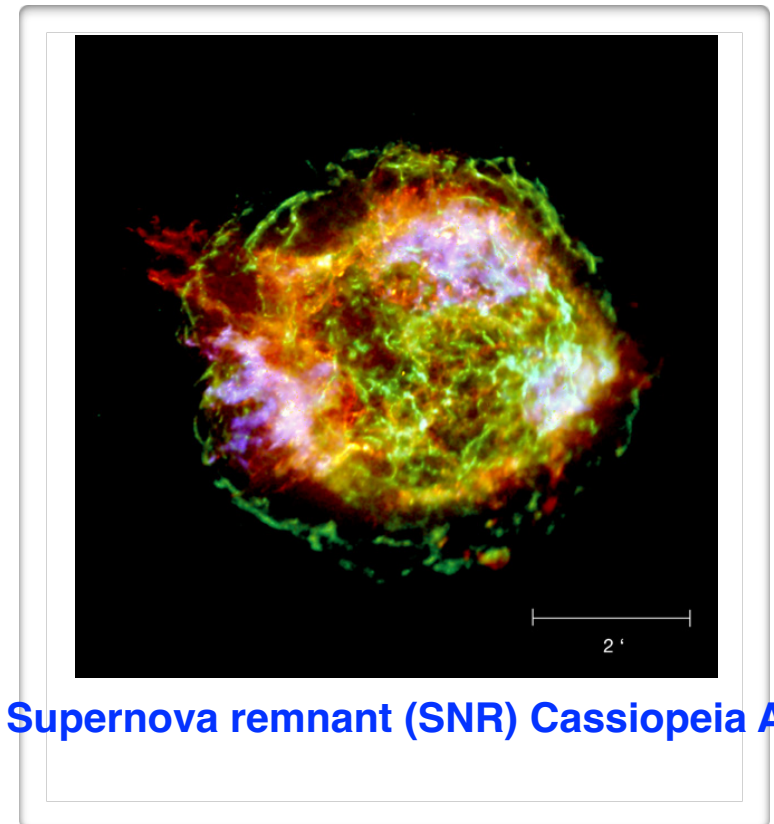
**energy gain** 
$$\frac{\Delta E}{E} \propto \frac{U_s}{c}$$

➡ $$N(E) \, dE \propto E^{-2} \, dE$$

**power law with spectral index
-2.0 ... -2.1**

**Supernova remnant (SNR) Cassiopeia A**

# H.E.S.S. supernova remnant RXJ 1713



$$\frac{dN}{dE_\gamma} \propto E_\gamma^{-\Gamma}$$
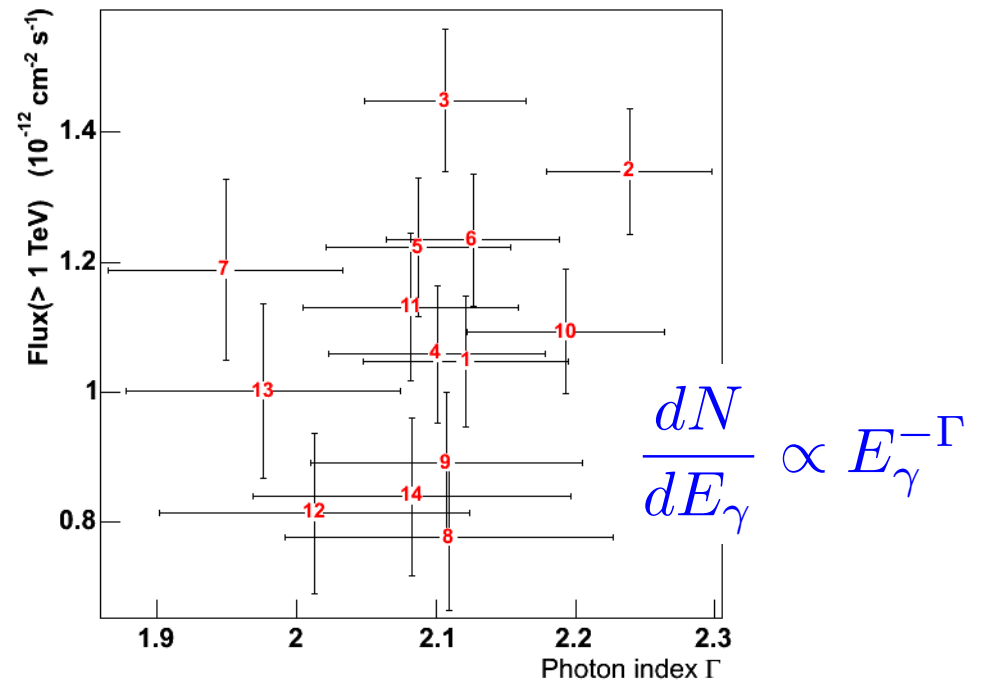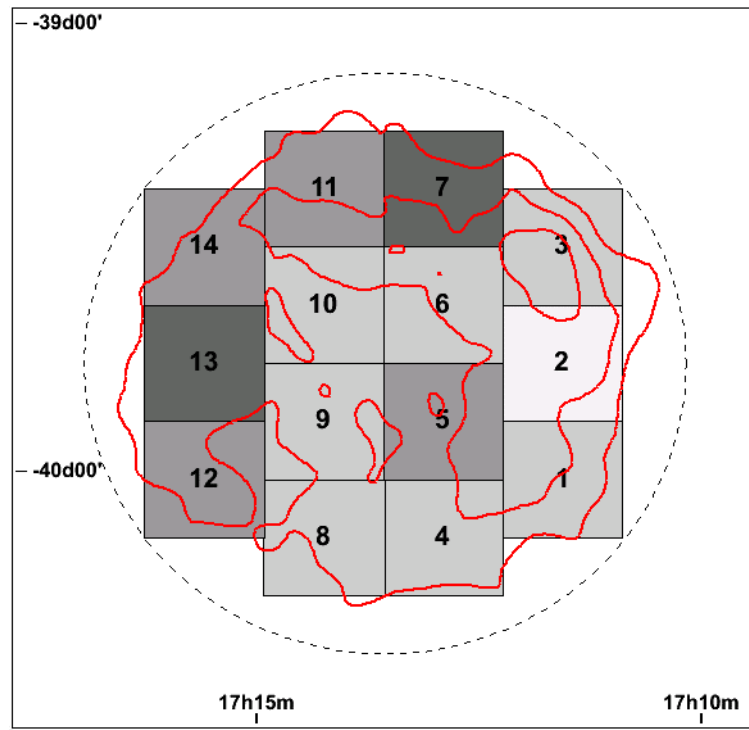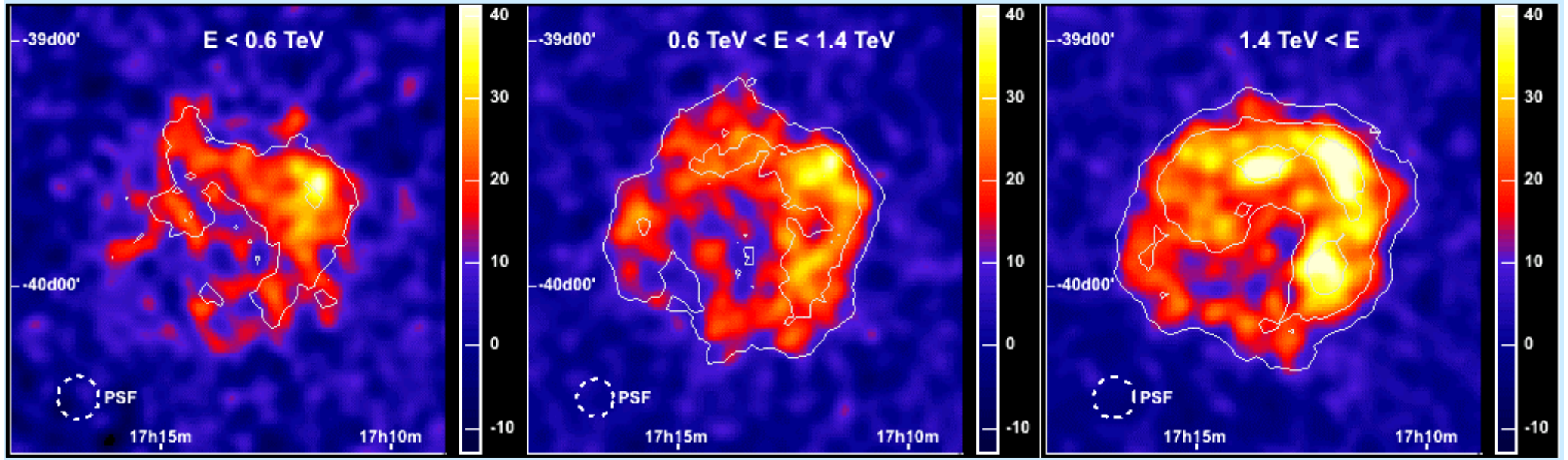
# Acceleration of cosmic rays at SNR



**Figure 3**
Spectral energy distribution of accelerated protons (power-law index $\alpha_{\mathrm{injected}} = 2.0$ and cutoff at 100 TeV) and $\gamma$-rays resulting from inelastic collisions with interstellar material. The dominant emission into photons occurs via the decay $\pi^0 \to \gamma\gamma$ (*solid orange curves*). The $\gamma$-ray spectrum follows the parent protons' spectrum rather closely in the midenergy range and in the high-energy cutoff region. For all proton indices, the low-energy turnover is a characteristic feature of the pion-decay emission. Also shown is the spectrum of electrons resulting from the inelastic proton–proton interactions via the decay chain $\pi^{\pm} \to \mu + \nu_{\mu} \to e^{\pm} \nu_e$ (*dashed gray curve*). For the synchrotron emission from these so-called secondary electrons, a source with age $t_{\mathrm{age}} = 1,000$ years and $B = 30\ \mu$G have been assumed. The shaded gray region shows the sensitive range of current $\gamma$-ray detectors (*Fermi*-LAT, imaging atmospheric Cherenkov detectors).

The emissivity can be turned into a flux at Earth by an astrophysical accelerator that puts a fraction $\epsilon_{\mathrm{CR}}$ of its energy output $E_{\mathrm{pr}}$ into the acceleration of protons:

$$F_\gamma(>100\,\mathrm{MeV}) = 4.4 \times 10^{-7} \epsilon_{\mathrm{CR}} \frac{E_{\mathrm{pr}}}{10^{51}\,\mathrm{erg}} \frac{d}{\mathrm{kpc}}^{-2} \frac{n}{1\,\mathrm{cm}^{-3}}\,\mathrm{cm}^{-2}\,\mathrm{s}^{-1}. \qquad 3.$$

In other words, if the distance $d$ and the density of the interaction region $n$ are known, the amount of energy in protons $E_{\mathrm{pr}}$ at the interaction site can be directly inferred from the $\gamma$-ray flux $F_\gamma$.

# Acceleration of cosmic rays at SNR



$p^+$ spectrum original $\Gamma = \alpha_{\text{injected}} = 2$; $E_c = 100$ TeV

$\pi^0$ decay; $\alpha = 2$

$E_\gamma = 67.5$ MeV

$E_\gamma = 500$ MeV

$\alpha = 1.75$

$\alpha = 2.25$

$\alpha = 2.5$

Synchrotron from secondary $\bar{e}$

Secondary $e$ $\pi^\pm \to \mu \nu_\mu \to e^\pm \nu_e$

**Figure 3**

Spectral energy distribution of accelerated protons (power-law index $\alpha_{\text{injected}} = 2.0$ and cutoff at 100 TeV) and $\gamma$-rays resulting from inelastic collisions with interstellar material. The dominant emission into photons occurs via the decay $\pi^0 \to \gamma\gamma$ (*solid orange curves*). The $\gamma$-ray spectrum follows the parent protons' spectrum rather closely in the midenergy range and in the high-energy cutoff region. For all proton indices, the low-energy turnover is a characteristic feature of the pion-decay emission. Also shown is the spectrum of electrons resulting from the inelastic proton–proton interactions via the decay chain $\pi^\pm \to \mu + \nu_\mu \to e^\pm \nu_e$ (*dashed gray curve*). For the synchrotron emission from these so-called secondary electrons, a source with age $t_{\text{age}} = 1{,}000$ years and $B = 30$ μG have been assumed. The shaded gray region shows the sensitive range of current $\gamma$-ray detectors (*Fermi*-LAT, imaging atmospheric Cherenkov detectors).

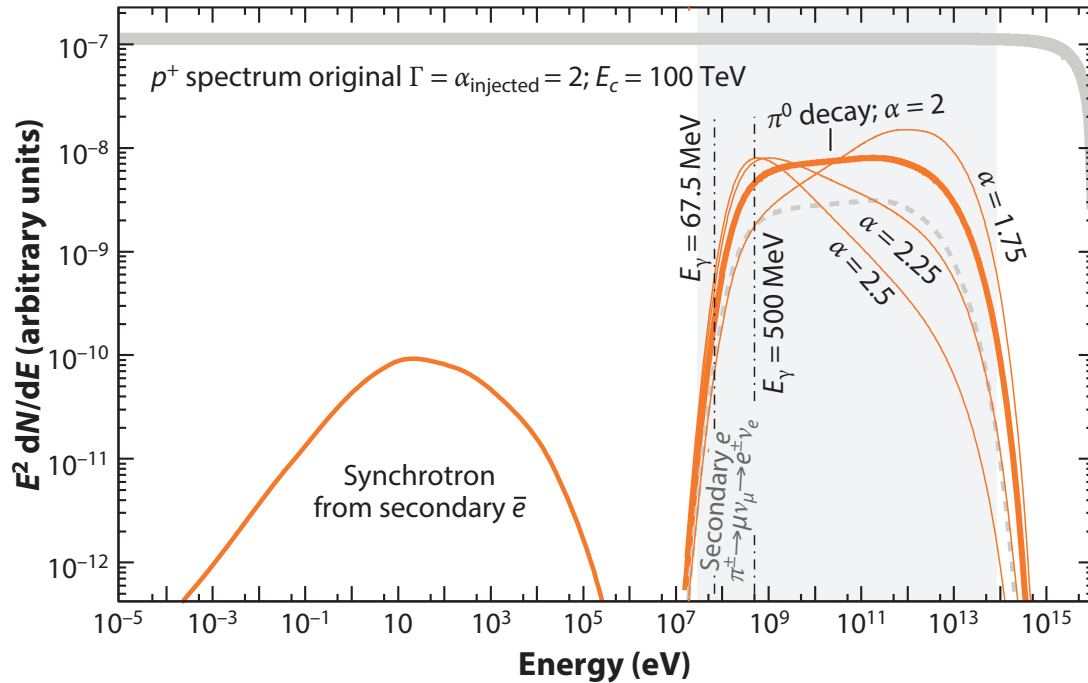The emissivity can be turned into a flux at Earth by an astrophysical accelerator that puts a fraction $\epsilon_{\text{CR}}$ of its energy output $E_{\text{pr}}$ into the acceleration of protons:

$$F_\gamma(>100\,\text{MeV}) = 4.4 \times 10^{-7} \epsilon_{\text{CR}} \frac{E_{\text{pr}}}{10^{51}\,\text{erg}} \frac{d}{\text{kpc}}^{-2} \frac{n}{1\,\text{cm}^{-3}}\,\text{cm}^{-2}\,\text{s}^{-1}. \qquad 3.$$

In other words, if the distance $d$ and the density of the interaction region $n$ are known, the amount of energy in protons $E_{\text{pr}}$ at the interaction site can be directly inferred from the $\gamma$-ray flux $F_\gamma$.



**Figure 6**

Typical $\gamma$-ray energy spectra for several of the most prominent supernova remnants (SNRs). Young SNRs (<1,000 years) are shown in green. These typically show smaller $\gamma$-ray fluxes but rather hard spectra in the GeV and TeV bands. The older (but still referred to as young) shell-type SNRs RX J1713.7-3946 and RX J0852.0-4622 (Vela Junior) of ages ~2,000 years are shown in shades of red. These show very hard spectra in the GeV band ($\Gamma = 1.5$) and a peak in the TeV band with an exponential cutoff beyond 10 TeV. The middle-aged SNRs (~20,000 years) interacting with molecular clouds (W44, W51C, and IC443) are shown in blue. Also shown are hadronic fits to the data (*solid lines*).
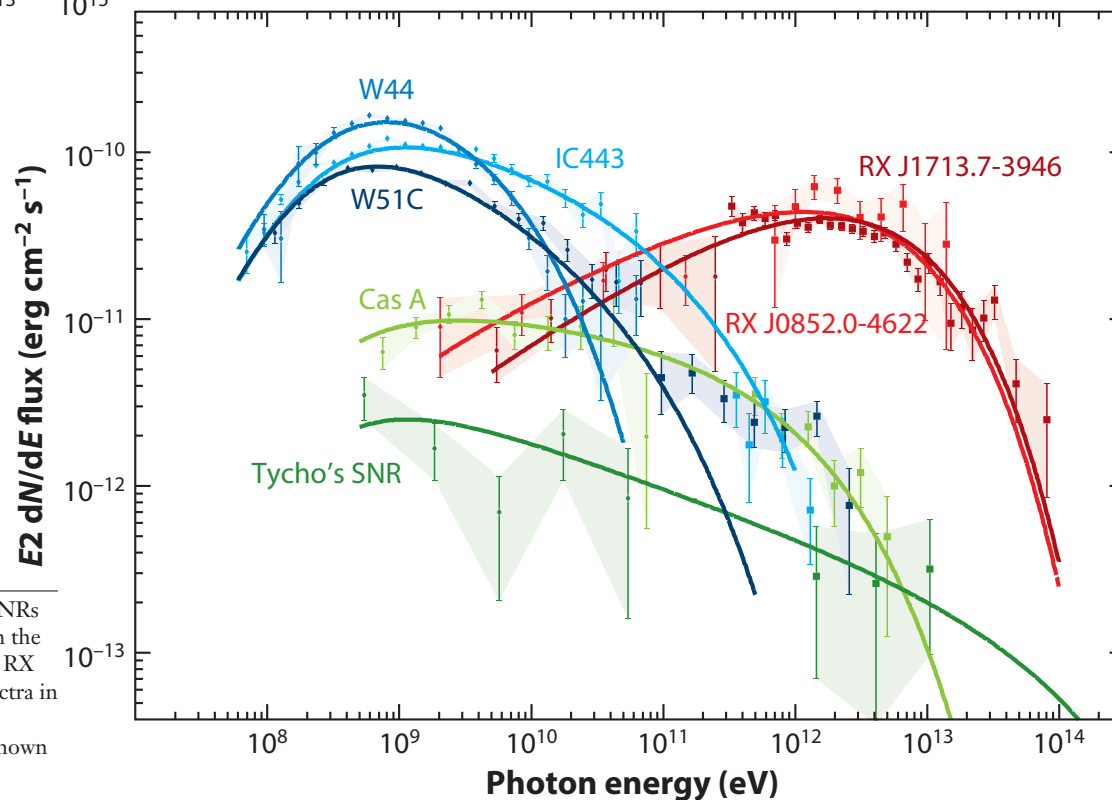
## general considerations about accelerators

**trajectory of particle in B field**

**centripedal force = Lorentz force**

$$m\frac{v^2}{r} = q \cdot v \cdot B \qquad\qquad m \cdot v = p \quad \textbf{momentum}$$

$$\frac{p}{r} = Z \cdot e \cdot B$$

$$r_L = \frac{p}{z \cdot e \cdot B} \qquad \textbf{Larmor radius}$$

*L* **dimension of accelerator**

*L > 2 r$_L$*

**closer look (Hillas 1984):**

$$L > \frac{2r_L}{\beta}$$

**velocity of scattering centers**

$$\beta = \frac{v}{c}$$

$$L > \frac{2 \cdot p}{z \cdot e \cdot B \cdot \beta}$$



$$B \cdot L > \frac{2 \cdot p}{z \cdot e \cdot \beta} \qquad \textbf{Hillas criterion}$$

**in astrophyscial units**

$$r_L = 1.08 \text{ pc } \frac{E_{15}}{Z \cdot B_{\mu G}}$$

$$B_{\mu G} \cdot L_{pc} > \frac{2 \cdot E_{15}}{Z \cdot \beta} \qquad \textbf{necessary condition}$$
$$\textbf{not sufficient}$$

$$E_{15} < Z \cdot B_{\mu G} \cdot L_{pc} \cdot \frac{\beta}{2}$$

**Fig. 1.** Energy spectra for different cosmic-ray elements. *Solid line*: Model prediction for the SNR-CRs. *Data*: CREAM (Ahn et al. 2009; Yoon et al. 2011), ATIC-2 (Panov et al. 2007), AMS-02 (Aguilar et al. 2015a,b), PAMELA (Adriani et al. 2011), CRN (Müller et al. 1991; Swordy et al. 1990), HEAO (Engelmann et al. 1990), TRACER (Obermeier et al. 2011), and KASCADE (Antoni et al. 2005). Cosmic-ray source parameters $(q, f)$ used in the calculation are given in Table 1. For the other model parameters $(D_0, a, \eta, s)$, see text for details.
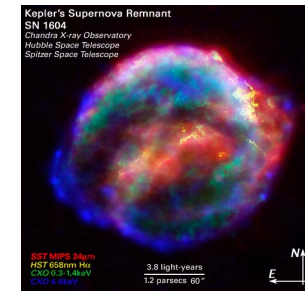
# Contribution of (regular) SNR-CR

$$E_c = Z \cdot 4.5 \ 10^6 \ \text{GeV}$$

$$Q(p) = A Q_0 (Ap)^{-q} \exp\left(-\frac{Ap}{Zp_c}\right),$$

**Table 1.** Source spectral indices, $q$, and energy injected per supernova, $f$, for the different species of cosmic rays used in the calculation of the SNR-CRs spectra shown in Figures 1 and 2.

| Particle type | $q$ | $f \ (\times 10^{49} \ \text{ergs})$ |
|---|---|---|
| Proton | 2.24 | 6.95 |
| Helium | 2.21 | 0.79 |
| Carbon | 2.21 | $2.42 \times 10^{-2}$ |
| Oxygen | 2.25 | $2.52 \times 10^{-2}$ |
| Neon | 2.25 | $3.78 \times 10^{-3}$ |
| Magnesium | 2.29 | $5.17 \times 10^{-3}$ |
| Silicon | 2.25 | $5.01 \times 10^{-3}$ |
| Iron | 2.25 | $4.95 \times 10^{-3}$ |

# Transport equation for cosmic rays in the Galaxy

**diffusion**

**energy loss (Bethe Bloch)**

**loss through interactions with ISM (spallation)**

**loss through radioactive decay**

$$\frac{\partial N_i}{\partial t} = \nabla(D_i \nabla N_i) - \frac{\partial}{\partial E}(b_i N_i) - n\nu\sigma_i N_i - \frac{N_i}{\gamma\tau_i} + Q_i + \sum_{j>i} n\nu\sigma_{ij} N_j + \sum_{j>i} \frac{N_j}{\gamma_j\tau_{ij}}$$

**source term**

**production through spallation of heavy nuclei**

**production through decay of heavy nuclei**
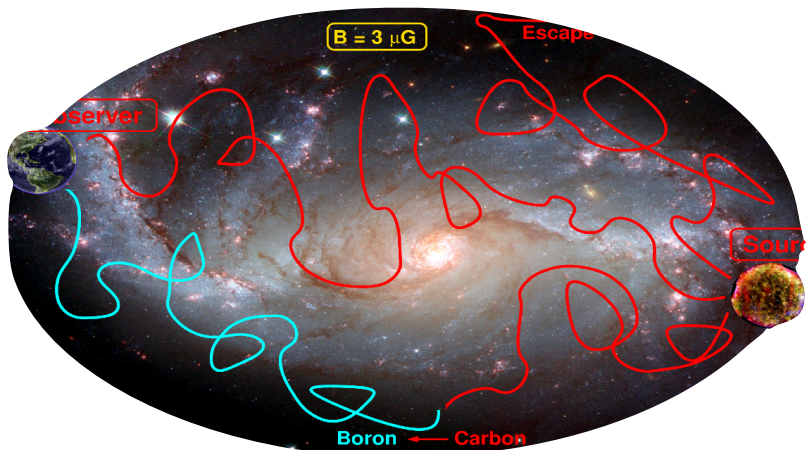
## TRACER balloon experiment
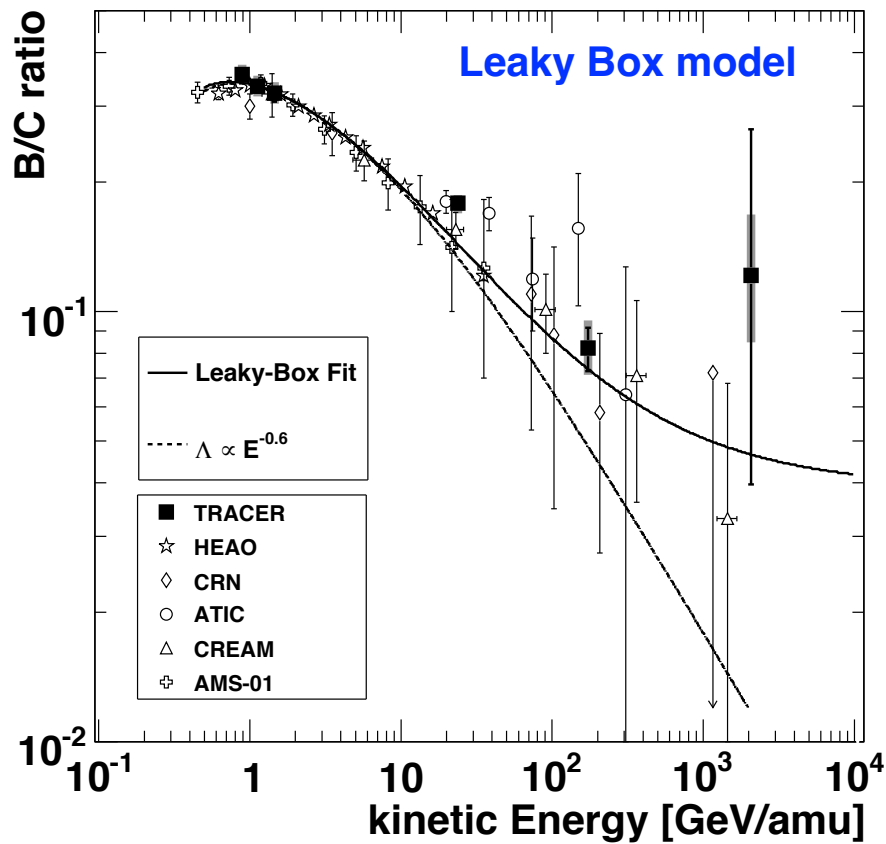


Escape Path Length:

$$\Lambda_{esc}(E) = CE^{-\delta} + \Lambda_0$$

▶ Propagation index:
  $\delta = 0.64 \pm 0.02$.

▶ Residual path length:
  $\Lambda_0 = 0.7 \pm 0.2$ g/cm$^2$.

$$\Lambda(R) = \frac{26.7\beta}{(\beta R)^\delta + (0.714 \cdot \beta \ldots)^{-1.4}} + \Lambda_0 \ \text{g/cm}^2,$$

A. Obermeier et al., ApJ 752 (2012) 69
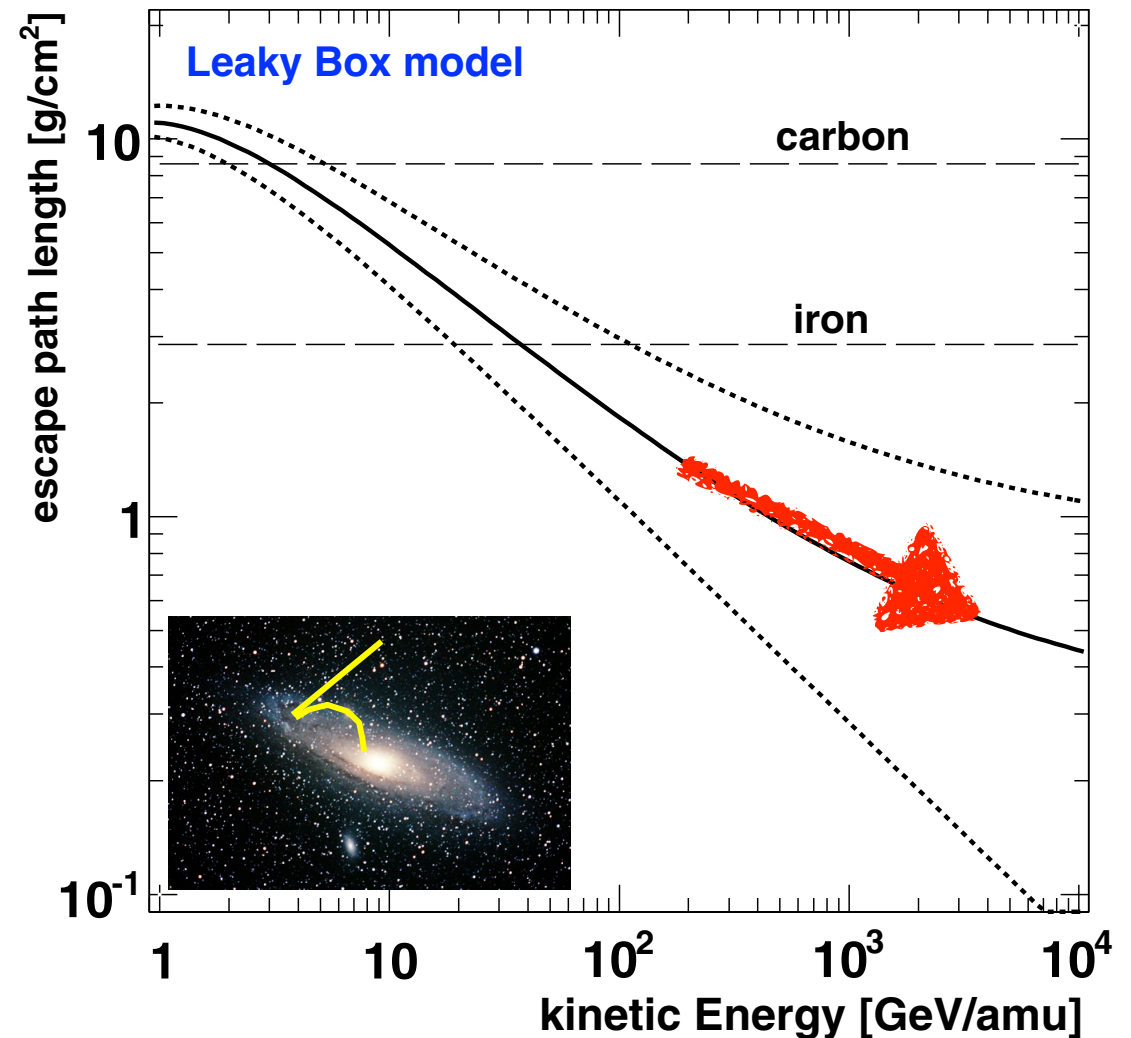
# Pathlength vs. interaction length

| pathlength in Galaxy | $\lambda_{esc} = 5 - 10 \ \text{g/cm}^2$ |
|---|---|

**interaction length**

**nuclear radius**

$$r = r_0 A^{1/3} \qquad r_0 = 1.3 \cdot 10^{-13} \ \text{cm}$$

**cross section**

$$\sigma_{p-A} = \pi (r_p + r_0 A^{1/3})^2$$

**ISM: protons**

$$n = 1/\text{cm}^3 \quad \rho = 1.67 \cdot 10^{-24} \ \text{g/cm}^3$$

**interaction length**

$$\lambda_{p-A} = \frac{\rho}{\sigma_{p-A} \cdot n}$$

$$\lambda_{p-p} = 21 \ \text{g/cm}^2 \qquad > \lambda_{esc}$$

$$\lambda_{p-Fe} = 1.6 \ \text{g/cm}^2 \qquad < \lambda_{esc}$$

# Shape of energy spectrum
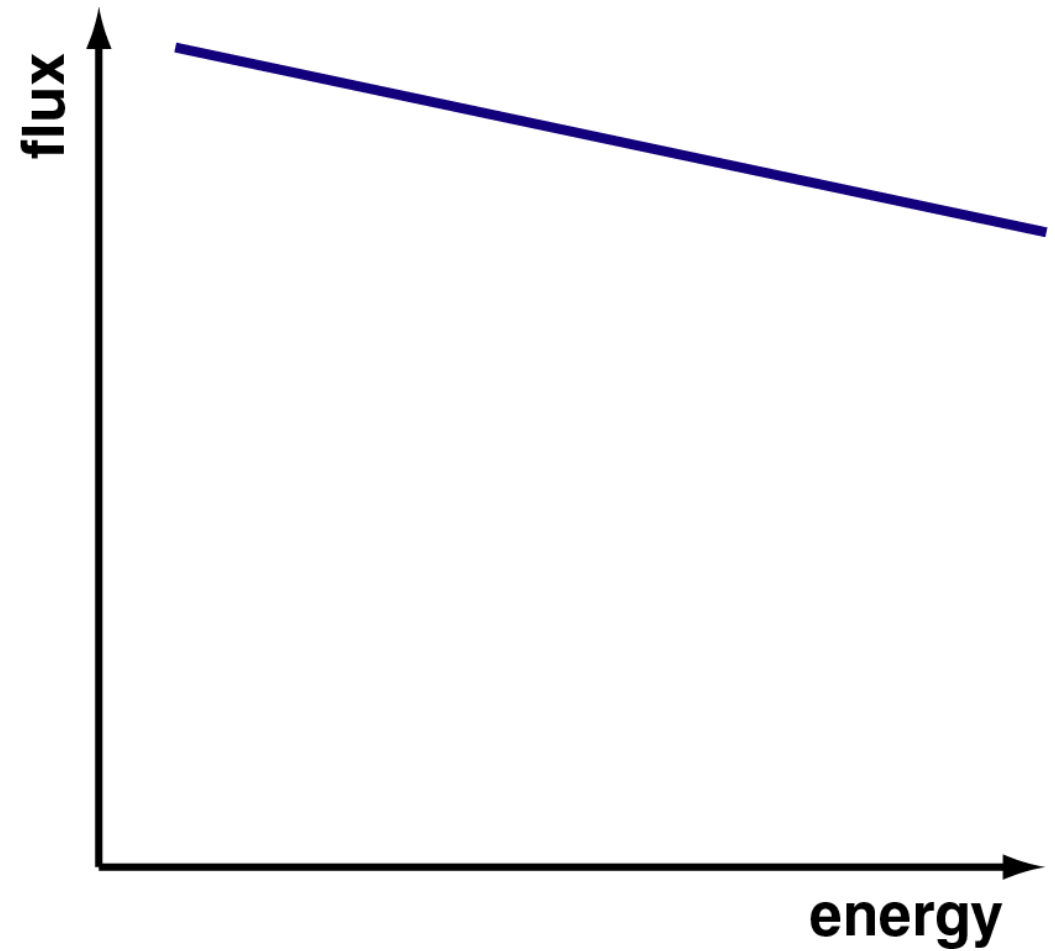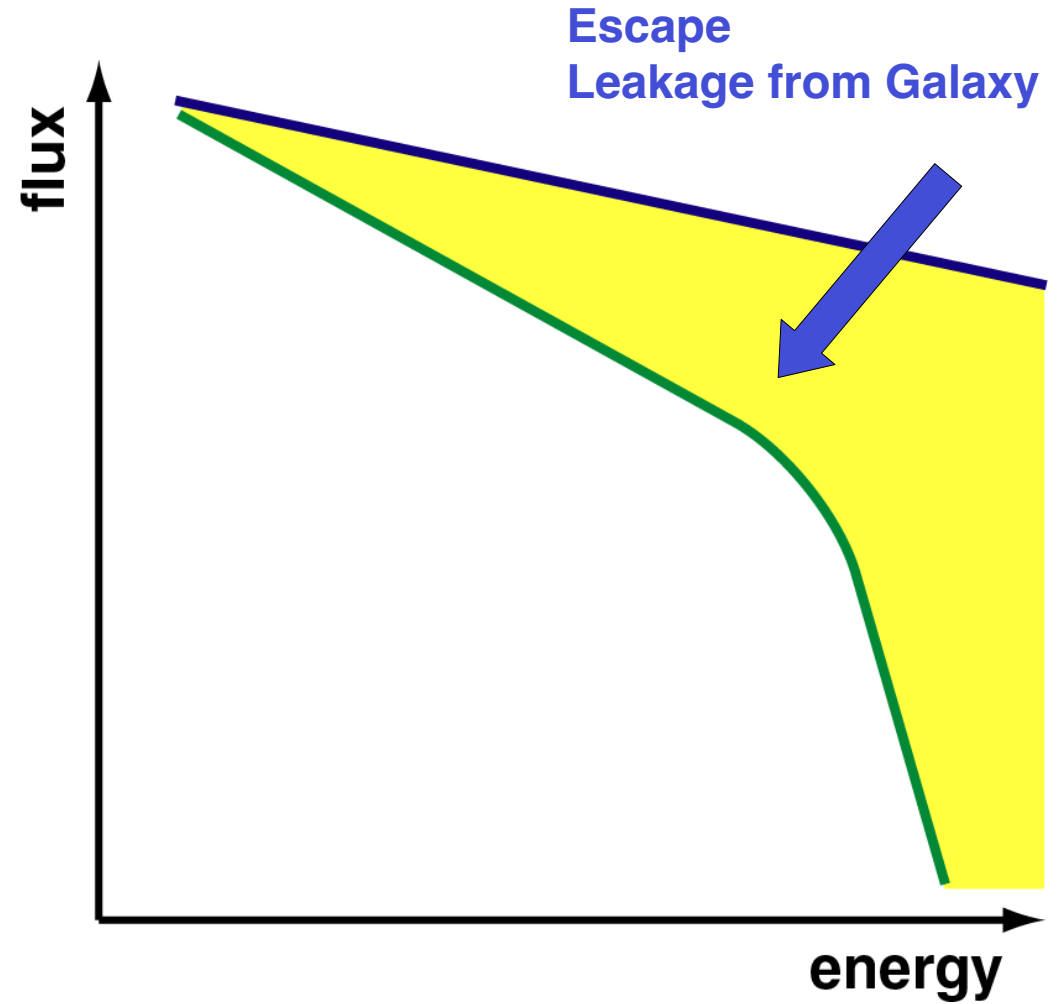
$$\frac{dN}{dE} \propto E_0^{\gamma}$$

**at source** $\gamma \sim$ **-2.1**

# Shape of energy spectrum

$$\frac{dN}{dE} \propto E_0^{\gamma}$$

**at source** $\gamma \sim$ **-2.1**

# Shape of energy spectrum

$$\frac{dN}{dE} \propto E_0^{\gamma}$$

**at source** γ ~ -2.1

**at Earth** γ ~ -2.6 to -2.7

**Escape Leakage from Galaxy**

**fragmentation**
σ ~ **A**$^{2/3}$

**flux**
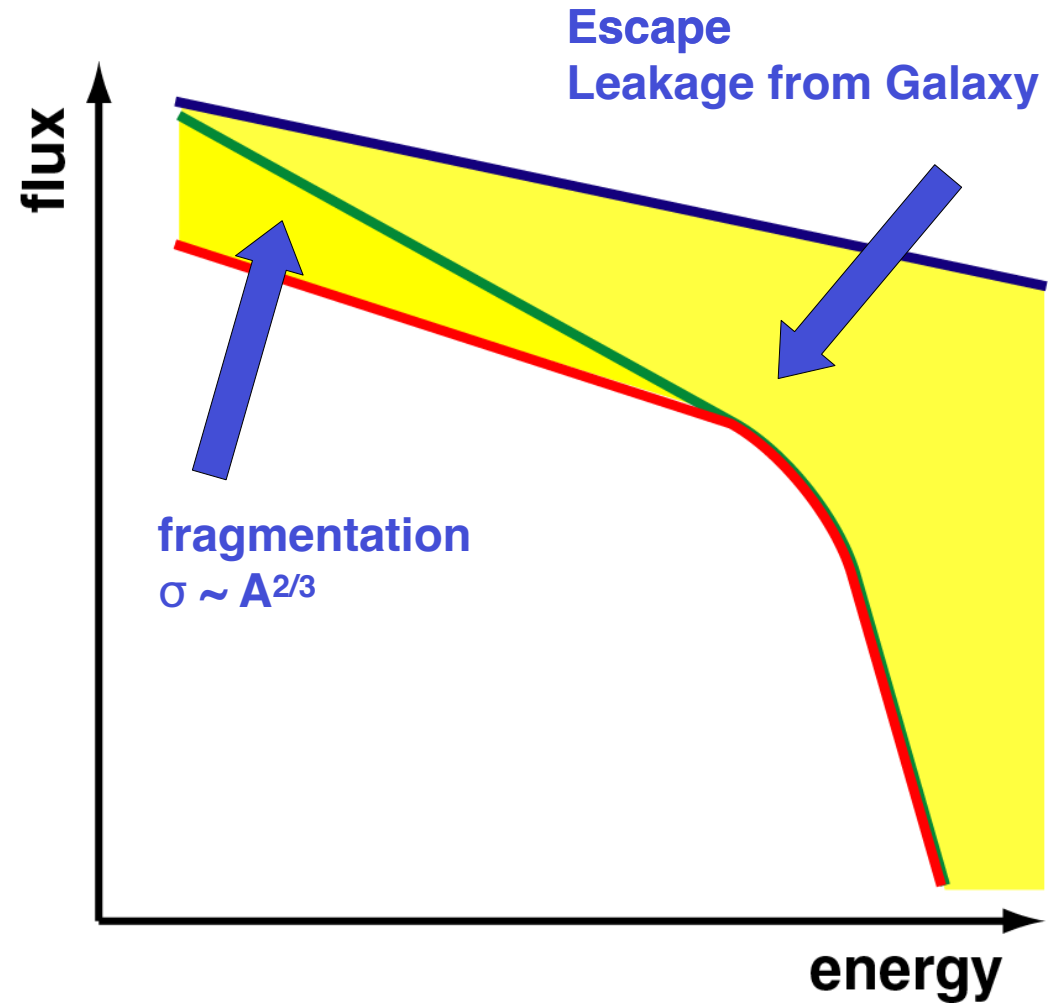
**energy**

# Shape of energy spectrum

$$\frac{dN}{dE} \propto E_0^{\gamma}$$

**at source γ ~ -2.1**

**at Earth γ ~ -2.6 to -2.7**
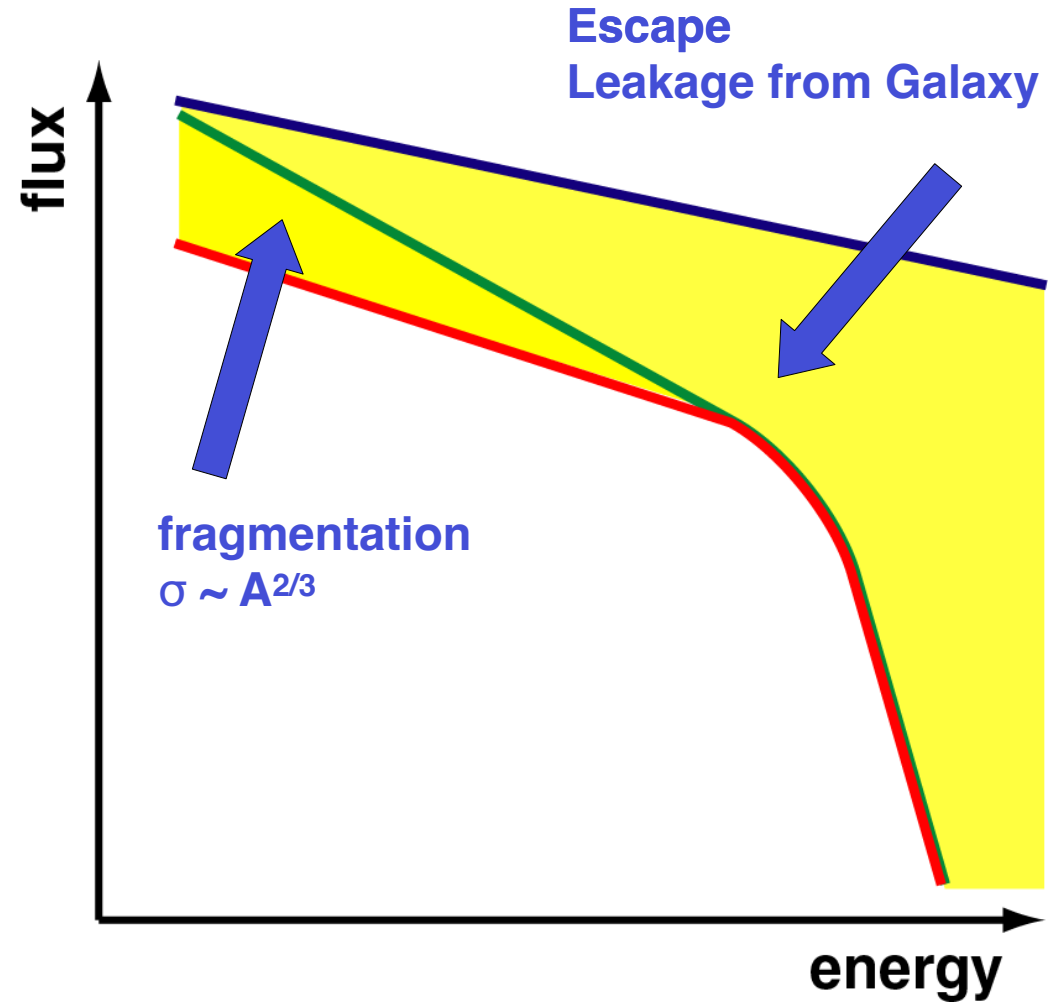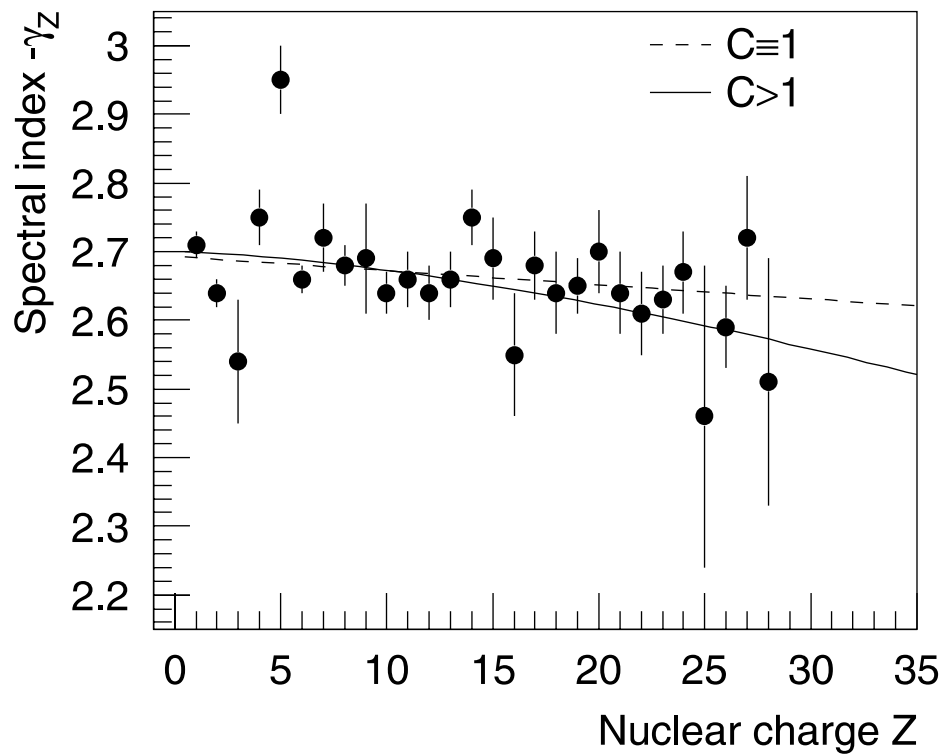


Fig. 5. Spectral index $\gamma_Z$ versus nuclear charge $Z$ (see Table 1). The solid line represents a three parameter fit according to Eq. (6), the dashed graph a linear fit.



**Escape Leakage from Galaxy**

**fragmentation σ ~ A^{2/3}**

# Transport equation for cosmic rays in the Galaxy

**diffusion**

**energy loss (Bethe Bloch)**

**loss through interactions with ISM (spallation)**

**loss through radioactive decay**

$$\frac{\partial N_i}{\partial t} = \nabla(D_i \nabla N_i) - \frac{\partial}{\partial E}(b_i N_i) - n v \sigma_i N_i - \frac{N_i}{\tau_i} + Q_i + \sum_{j>i} n v \sigma_{ij} N_j + \sum_{j>i} \frac{N_j}{\gamma_j \tau_{ij}}$$

**source term**

**production through spallation of heavy nuclei**

**production through decay of heavy nuclei**

B = 3 μG

Escape

Observer

Source

Boron — Carbon

ELSEVIER

# Propagation of super-high-energy cosmic rays in the Galaxy

Jörg R. Hörandel [a,*], Nikolai N. Kalmykov [b], Aleksei V. Timokhin [c]

The steady-state diffusion equation for the cosmic-ray density $N(r)$ is (neglecting nuclear interactions and energy losses)

$$-\nabla_i D_{ij}(r) \nabla_j N(r) = Q(r). \tag{1}$$

$Q(r)$ is the cosmic-ray source term and $D_{ij}(r)$ the diffusion tensor.

ELSEVIER

# Propagation of super-high-energy cosmic rays in the Galaxy

Jörg R. Hörandel [a,*], Nikolai N. Kalmykov [b], Aleksei V. Timokhin [c]

The steady-state diffusion equation for the cosmic-ray density $N(r)$ is (neglecting nuclear interactions and energy losses)

$$-\nabla_i D_{ij}(r)\nabla_j N(r) = Q(r). \tag{1}$$

$Q(r)$ is the cosmic-ray source term and $D_{ij}(r)$ the diffusion tensor.

Under the assumption of azimuthal symmetry and taking into account the predominance of the toroidal component of the magnetic field, Eq. (1) is presented in cylindrical coordinates as

$$\left[-\frac{1}{r}\frac{\partial}{\partial r}rD_\perp\frac{\partial}{\partial r} - \frac{\partial}{\partial z}D_\perp\frac{\partial}{\partial z} - \frac{\partial}{\partial z}D_A\frac{\partial}{\partial r}\right.$$
$$\left.+ \frac{1}{r}\frac{\partial}{\partial r}rD_A\frac{\partial}{\partial z}\right]N(r,z) = Q(r,z), \tag{2}$$

where $N(r,z)$ is the cosmic-ray density averaged over the large-scale fluctuations with a characteristic scale $L \sim 100$ pc [3]. $D_\perp \propto E^m$ is the diffusion coefficient, where $m$ is much less than one ($m \approx 0.2$), and $D_A \propto E$ the Hall diffusion coefficient. The influence of Hall diffusion becomes predominant at high energies ($>10^{15}$ eV). The sharp

# Propagation of super-high-energy cosmic rays in the Galaxy

Jörg R. Hörandel [a,*], Nikolai N. Kalmykov [b], Aleksei V. Timokhin [c]

The steady-state diffusion equation for the cosmic-ray density $N(r)$ is (neglecting nuclear interactions and energy losses)

$$-\nabla_i D_{ij}(r)\nabla_j N(r) = Q(r). \qquad (1)$$

$Q(r)$ is the cosmic-ray source term and $D_{ij}(r)$ the diffusion tensor.

Under the assumption of azimuthal symmetry and taking into account the predominance of the toroidal component of the magnetic field, Eq. (1) is presented in cylindrical coordinates as

$$\left[-\frac{1}{r}\frac{\partial}{\partial r}rD_\perp\frac{\partial}{\partial r} - \frac{\partial}{\partial z}D_\perp\frac{\partial}{\partial z} - \frac{\partial}{\partial z}D_A\frac{\partial}{\partial r}\right.$$
$$\left. + \frac{1}{r}\frac{\partial}{\partial r}rD_A\frac{\partial}{\partial z}\right]N(r,z) = Q(r,z), \qquad (2)$$

where $N(r,z)$ is the cosmic-ray density averaged over the large-scale fluctuations with a characteristic scale $L \sim 100$ pc [3]. $D_\perp \propto E^m$ is the diffusion coefficient, where $m$ is much less than one ($m \approx 0.2$), and $D_A \propto E$ the Hall diffusion coefficient. The influence of Hall diffusion becomes predominant at high energies ($>10^{15}$ eV). The sharp

The magnetic field of the Galaxy consists of a large-scale regular and a chaotic, irregular component $\vec{B} = \vec{B}_{reg} + \vec{B}_{irr}$. A purely azimuthal magnetic field was assumed for the regular field

$$B_z = 0, \quad B_r = 0, \quad B_\phi = 1\,\mu G\exp\left(-\frac{z^2}{z_0^2} - \frac{r^2}{r_0^2}\right),$$

where $z_0 = 5$ kpc and $r_0 = 10$ kpc are constants [3].

Available online at www.sciencedirect.com

ScienceDirect

Astroparticle
Physics

Astroparticle Physics 27 (2007) 119–126

www.elsevier.com/locate/astropart

ELSEVIER

**example of knee due to propagation/leakage from Galaxy**

# Propagation of super-high-energy cosmic rays in the Galaxy

Jörg R. Hörandel [a,*], Nikolai N. Kalmykov [b], Aleksei V. Timokhin [c]

The steady-state diffusion equation for the cosmic-ray density $N(r)$ is (neglecting nuclear interactions and energy losses)

$$-\nabla_i D_{ij}(r) \nabla_j N(r) = Q(r). \tag{1}$$

$Q(r)$ is the cosmic-ray source term and $D_{ij}(r)$ the diffusion tensor.

Under the assumption of azimuthal symmetry and taking into account the predominance of the toroidal component of the magnetic field, Eq. (1) is presented in cylindrical coordinates as

$$\left[ -\frac{1}{r}\frac{\partial}{\partial r} r D_\perp \frac{\partial}{\partial r} - \frac{\partial}{\partial z} D_\perp \frac{\partial}{\partial z} - \frac{\partial}{\partial z} D_A \frac{\partial}{\partial r} \right.$$
$$\left. + \frac{1}{r}\frac{\partial}{\partial r} r D_A \frac{\partial}{\partial z} \right] N(r,z) = Q(r,z), \tag{2}$$

where $N(r,z)$ is the cosmic-ray density averaged over the large-scale fluctuations with a characteristic scale $L \sim 100$ pc [3]. $D_\perp \propto E^m$ is the diffusion coefficient, where $m$ is much less than one ($m \approx 0.2$), and $D_A \propto E$ the Hall diffusion coefficient. The influence of Hall diffusion becomes predominant at high energies ($>10^{15}$ eV). The sharp

The magnetic field of the Galaxy consists of a large-scale regular and a chaotic, irregular component $\vec{B} = \vec{B}_{\text{reg}} + \vec{B}_{\text{irr}}$. A purely azimuthal magnetic field was assumed for the regular field

$$B_z = 0, \quad B_r = 0, \quad B_\phi = 1\,\mu\text{G}\exp\left(-\frac{z^2}{z_0^2} - \frac{r^2}{r_0^2}\right),$$

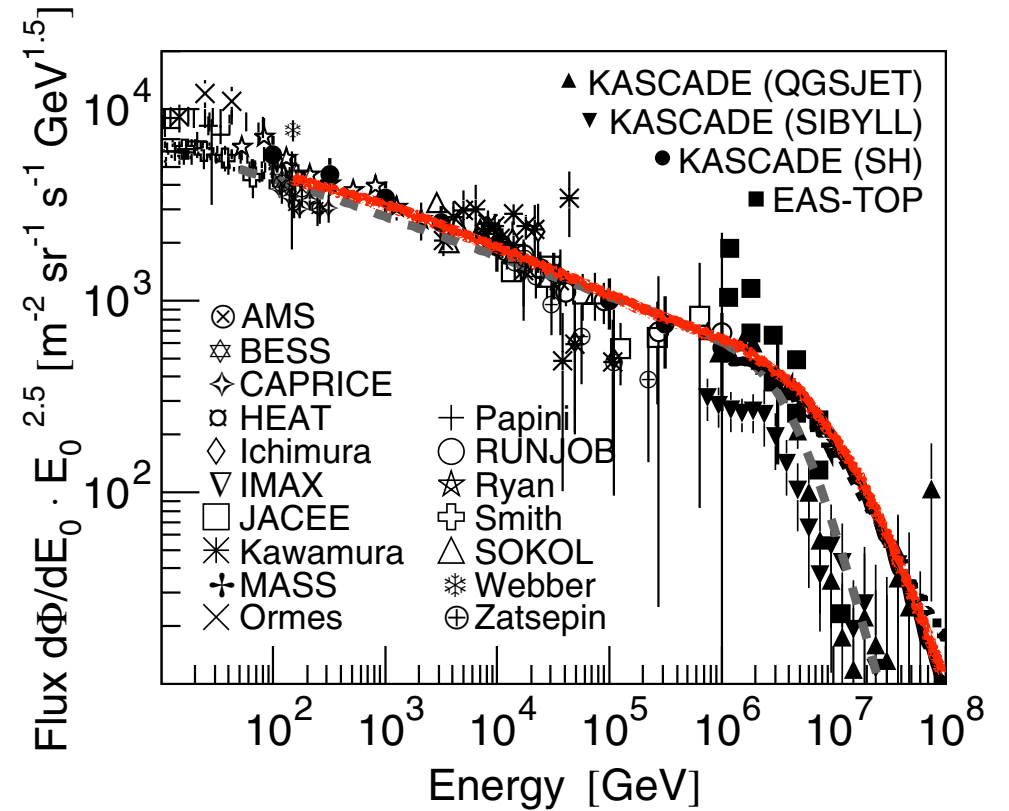where $z_0 = 5$ kpc and $r_0 = 10$ kpc are constants [3].



Fig. 7. Proton flux as obtained from various measurements, for references see [28], compared to the spectra shown in Fig. 6 (black lines) and the *poly-gonato* model [26] (grey, dashed line).
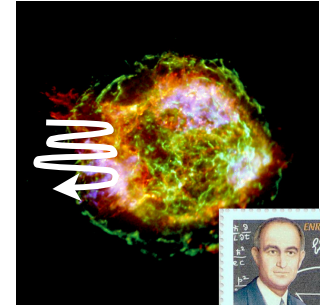
# Origin of the knee?

**Acceleration (SNR)**

| | |
|---|---|
| .. in SNR | Berezhko & Ksenofontov |
| .. in SNR + radio galaxies | Stanev .. |
| .. in oblique shocks | Kobayakawa .. |
| .. in variety of SNR | Sveshnikova |
| Single source model | Erlykin & Wolfendale |
| Reacceleration in galactic wind | Völk & Zirakashvili |

# Origin of the knee?

## Acceleration (SNR)

.. in SNR      Berezhko & Ksenofontov

.. in SNR + radio galaxies      Stanev ..

.. in oblique shocks      Kobayakawa ..

.. in variety of SNR      Sveshnikova

Single source model      Erlykin & Wolfendale

Reacceleration in galactic wind      Völk & Zirakashvili

## Leakage from Galaxy

Minimum pathlength model      Swordy

Anomalous diffusion model      Lagutin ..

Hall diffusion model      Ptuskin .., Kalmykov ..

Diffusion in turbulent magnetic fields      Ogio & Kakimoto

Diffusion and drift      Roulet ..

# Origin of the knee?

JRH, Astropart. Phys. 21 (2004) 241 (updated)

## Acceleration (SNR)

.. in SNR                  Berezhko & Ksenofontov

.. in SNR + radio galaxies    Stanev ..

.. in oblique shocks         Kobayakawa ..

.. in variety of SNR         Sveshnikova

Single source model        Erlykin & Wolfendale

Reacceleration in galactic wind  Völk & Zirakashvili

## Leakage from Galaxy

Minimum pathlength model    Swordy

Anomalous diffusion model    Lagutin ..

Hall diffusion model        Ptuskin .., Kalmykov ..

Diffusion in turbulent magnetic fields  Ogio & Kakimoto

Diffusion and drift          Roulet ..

## $\gamma$-ray bursts

Cannonball model          Plaga

Acceleration in GRB + diffusion  Wick ..

Acceleration in GRB $E_{max} \sim A$  Dar ..

propagation through galaxy

$B = 3~\mu G$

800 ITALIA

Jörg R. Hörandel, APP 2023/24   **44**

# Origin of the knee?

## Acceleration (SNR)

.. in SNR                              Berezhko & Ksenofontov
.. in SNR + radio galaxies             Stanev ..
.. in oblique shocks                   Kobayakawa ..
.. in variety of SNR                   Sveshnikova
Single source model                    Erlykin & Wolfendale
Reacceleration in galactic wind        Völk & Zirakashvili

## Leakage from Galaxy

Minimum pathlength model               Swordy
Anomalous diffusion model              Lagutin ..
Hall diffusion model                   Ptuskin .., Kalmykov ..
Diffusion in turbulent magnetic fields Ogio & Kakimoto
Diffusion and drift                    Roulet ..

propagation through galaxy

B = 3 μG

## γ-ray bursts

Cannonball model                       Plaga
Acceleration in GRB + diffusion        Wick ..
Acceleration in GRB  $E_{max}$ ~A      Dar ..
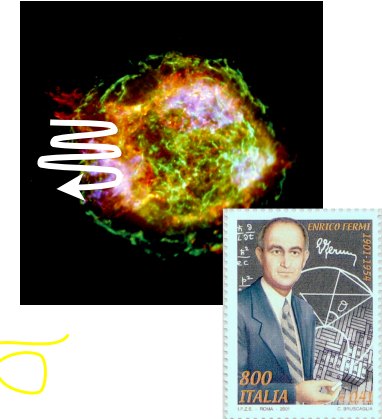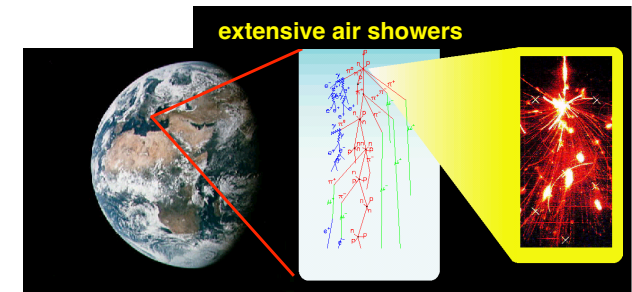
## Interaction with background particles

Diffusion model + photo-disintegration    Tkaczyk
Interaction with neutrinos in galactic halo    Dova ..
Photo-disintegration (optical and UV photons)    Candia ..

# Origin of the knee?

## Acceleration (SNR)

.. in SNR                                   Berezhko & Ksenofontov
.. in SNR + radio galaxies                  Stanev ..
.. in oblique shocks                        Kobayakawa ..
.. in variety of SNR                        Sveshnikova
Single source model                         Erlykin & Wolfendale
Reacceleration in galactic wind             Völk & Zirakashvili

## Leakage from Galaxy

Minimum pathlength model                    Swordy
Anomalous diffusion model                   Lagutin ..
Hall diffusion model                        Ptuskin .., Kalmykov ..
Diffusion in turbulent magnetic fields      Ogio & Kakimoto
Diffusion and drift                          Roulet ..

## $\gamma$-ray bursts

Cannonball model                            Plaga
Acceleration in GRB + diffusion              Wick ..
Acceleration in GRB  $E_{max}$ ~A            Dar ..

## Interaction with background particles

Diffusion model + photo-disintegration   Tkaczyk
Interaction with neutrinos in galactic halo      Dova ..
Photo-disintegration (optical and UV photons)    Candia ..

## Particle physics in atmosphere
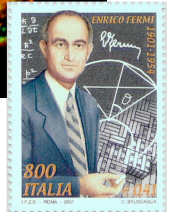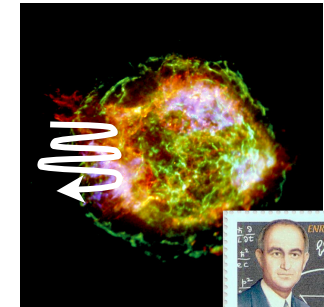
Gravitons, SUSY                             Kazanas & Nicolaidis

# Origin of the knee?

## Acceleration (SNR)

.. in SNR                                         Berezhko & Ksenofontov

.. in SNR + radio galaxies              Stanev ..

.. in oblique shocks                        Kobayakawa ..

.. in variety of SNR                        Sveshnikova

Single source model                       Erlykin & Wolfendale

Reacceleration in galactic wind     Völk & Zirakashvili

## Leakage from Galaxy

Minimum pathlength model           Swordy

Anomalous diffusion model           Lagutin ..

Hall diffusion model                        Ptuskin .., Kalmykov ..

Diffusion in turbulent magnetic fields    Ogio & Kakimoto

Diffusion and drift                           Roulet ..


propagation through galaxy

B = 3 μG

## γ-ray bursts

Cannonball model                          Plaga

Acceleration in GRB + diffusion     Wick ..

Acceleration in GRB, $E_{max} \sim A$    Dar ..

## Interaction with background particles

Diffusion model + photo-disintegration    Tkaczyk

Interaction with neutrinos in galactic halo    Dova ..
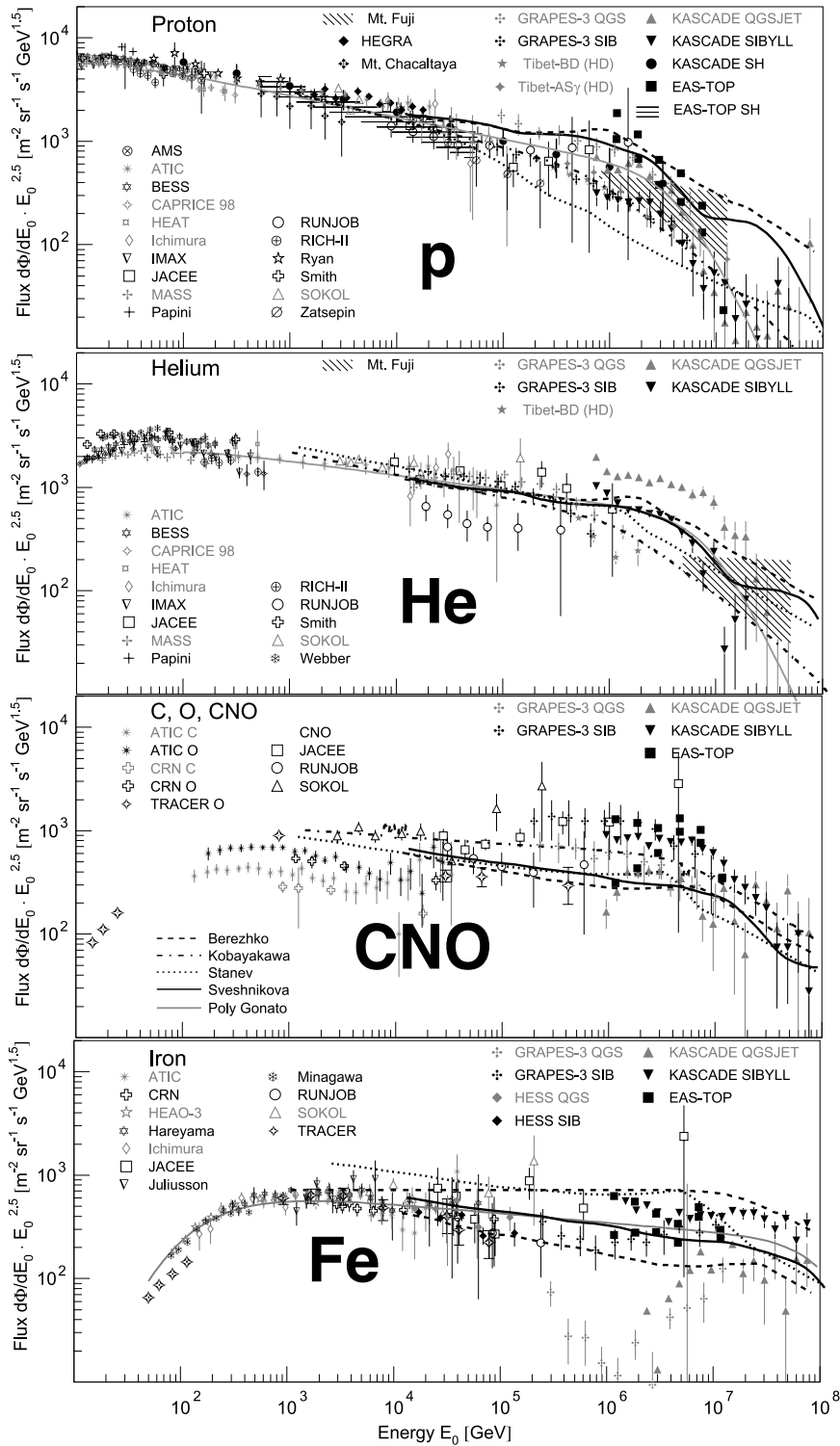
Photo-disintegration (optical and UV photons)    Candia ..

extensive air showers

## Particle physics in atmosphere

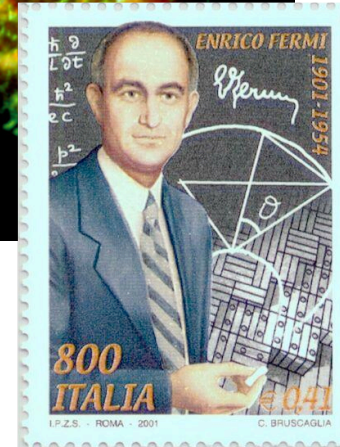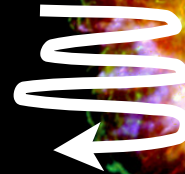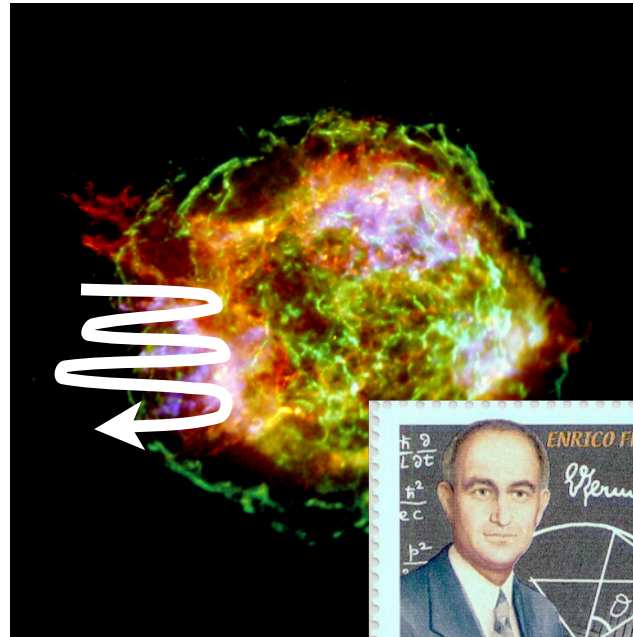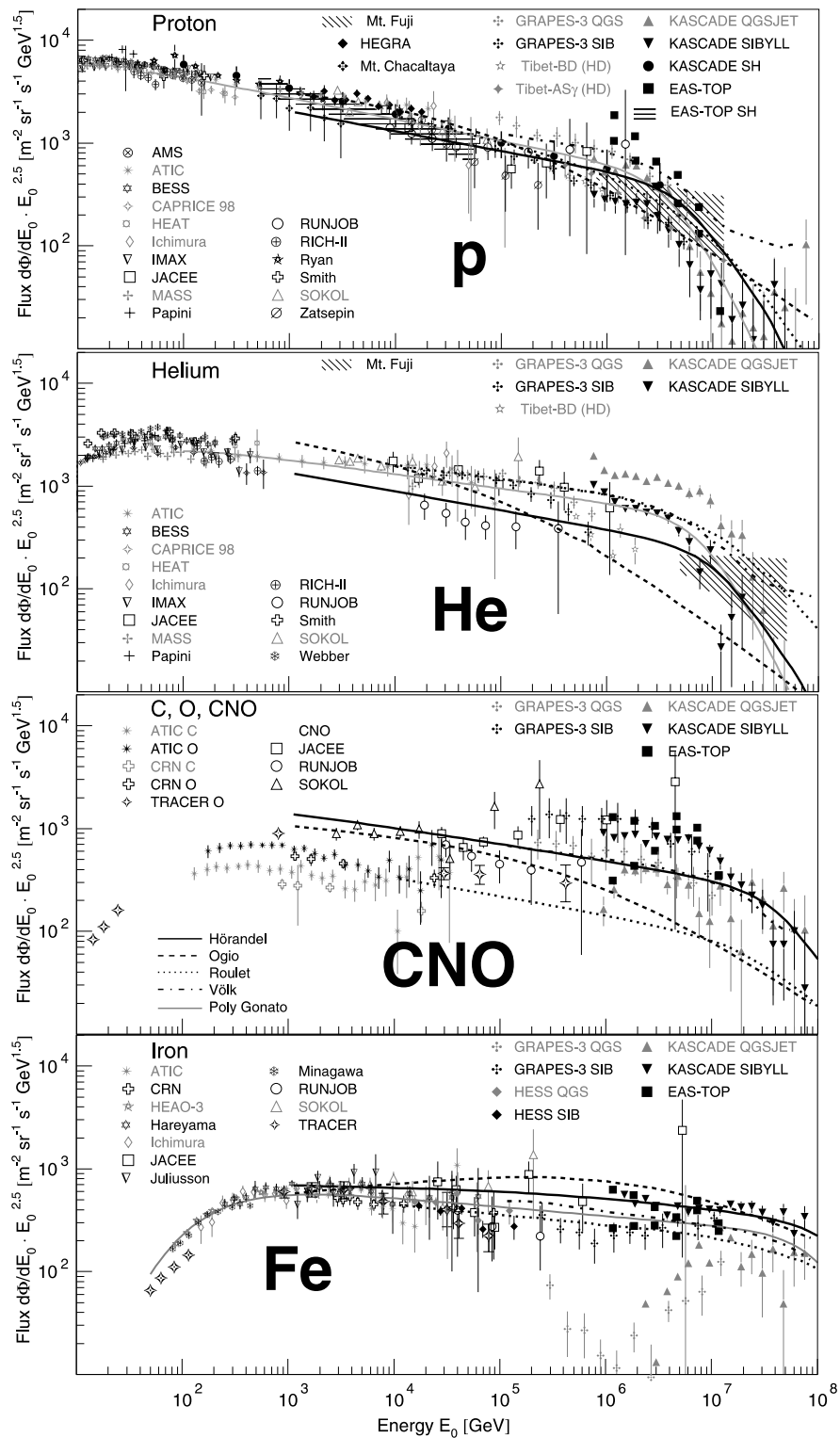Gravitons, SUSY                            Kazanas & Nicolaidis

# maximum energy

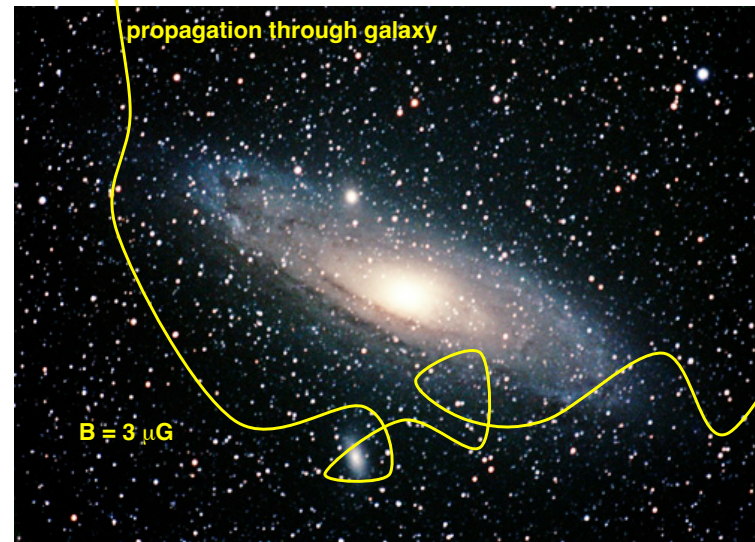$$E_{max} \propto B \cdot Z$$

$$E_{max} \approx Z \cdot 100 \text{ TeV} \dots Z \cdot 5 \text{ PeV}$$

# leakage from Galaxy

$$E_k \propto Z$$

propagation through galaxy

B = 3 μG
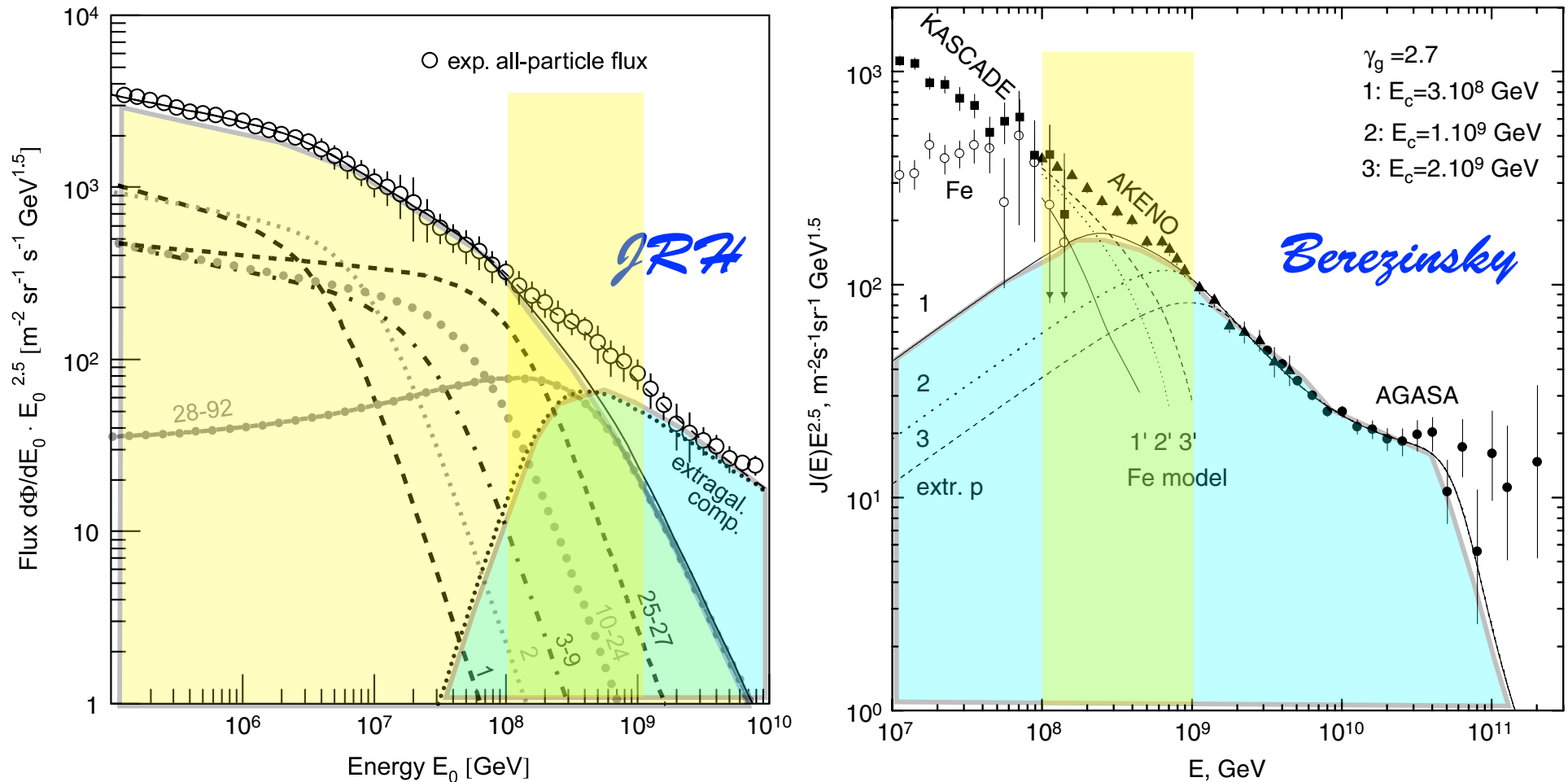
# Transition to extragalactic CR component

**Fig. 26.** *Left panel*: Cosmic-ray energy spectra according to the poly-gonato model [2]. The spectra for groups of elements are labeled by their respective nuclear charge numbers. The sum of all elements yields the galactic all-particle spectrum (—) which is compared to the average measured flux. In addition, a hypothetical extragalactic component is shown to account for the observed all-particle flux (- - -). *Right panel*: Transition from galactic to extragalactic cosmic rays according to Berezinsky et al. [451]. Calculated spectra of extragalactic protons (curves 1, 2, 3) and of galactic iron nuclei (curves 1′, 2′, 3′) are compared with the all-particle spectrum from the Akeno and AGASA experiments. KASCADE data are shown as filled squares for the all-particle flux and as open circles for the flux of iron nuclei.

# Transition to extragalactic CR component
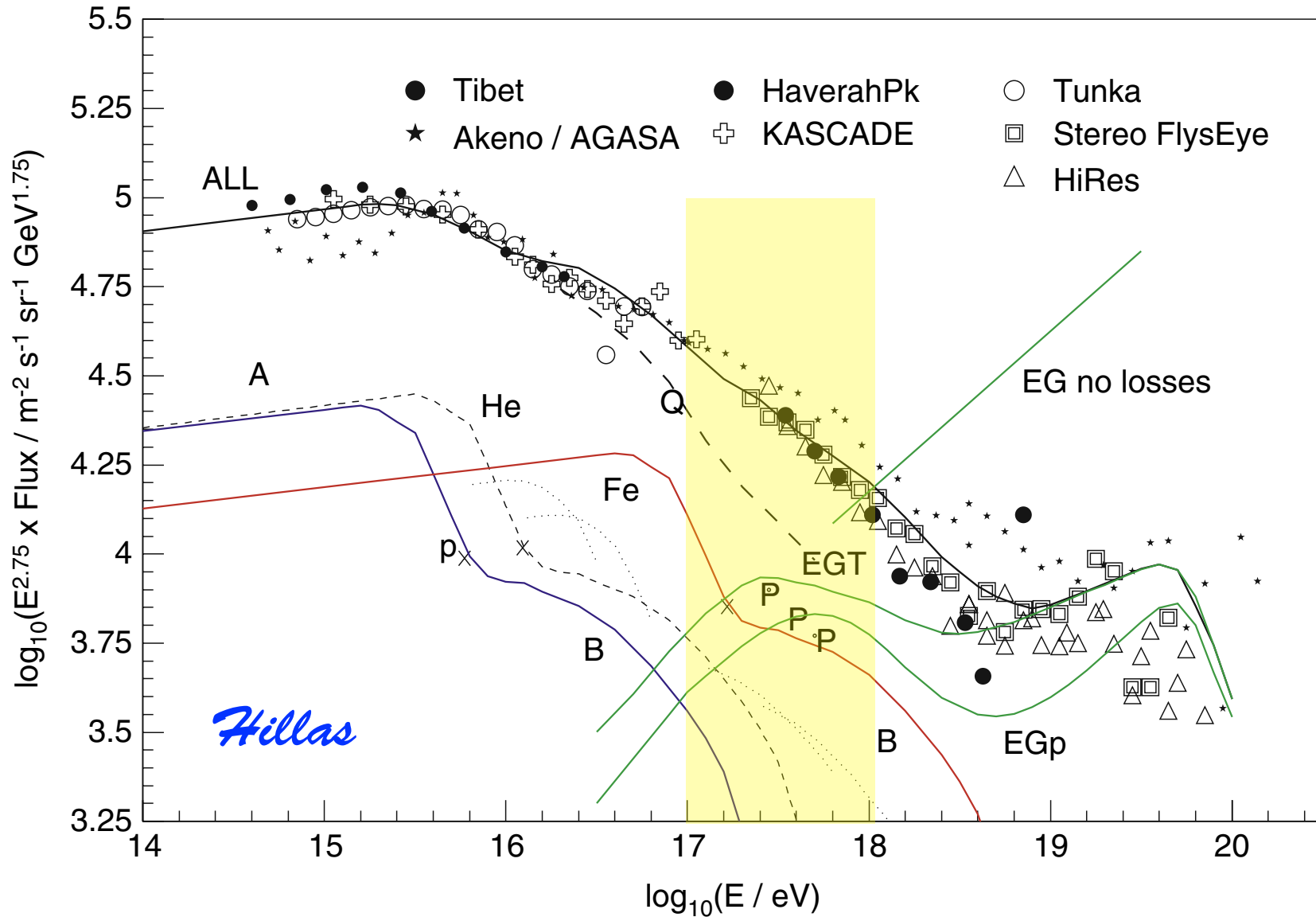


**„classical" supernovae + additional component**

M. Hillas, J. Phys. G 31 (2005) R95

Jörg R. Hörandel, APP 2023/24   48

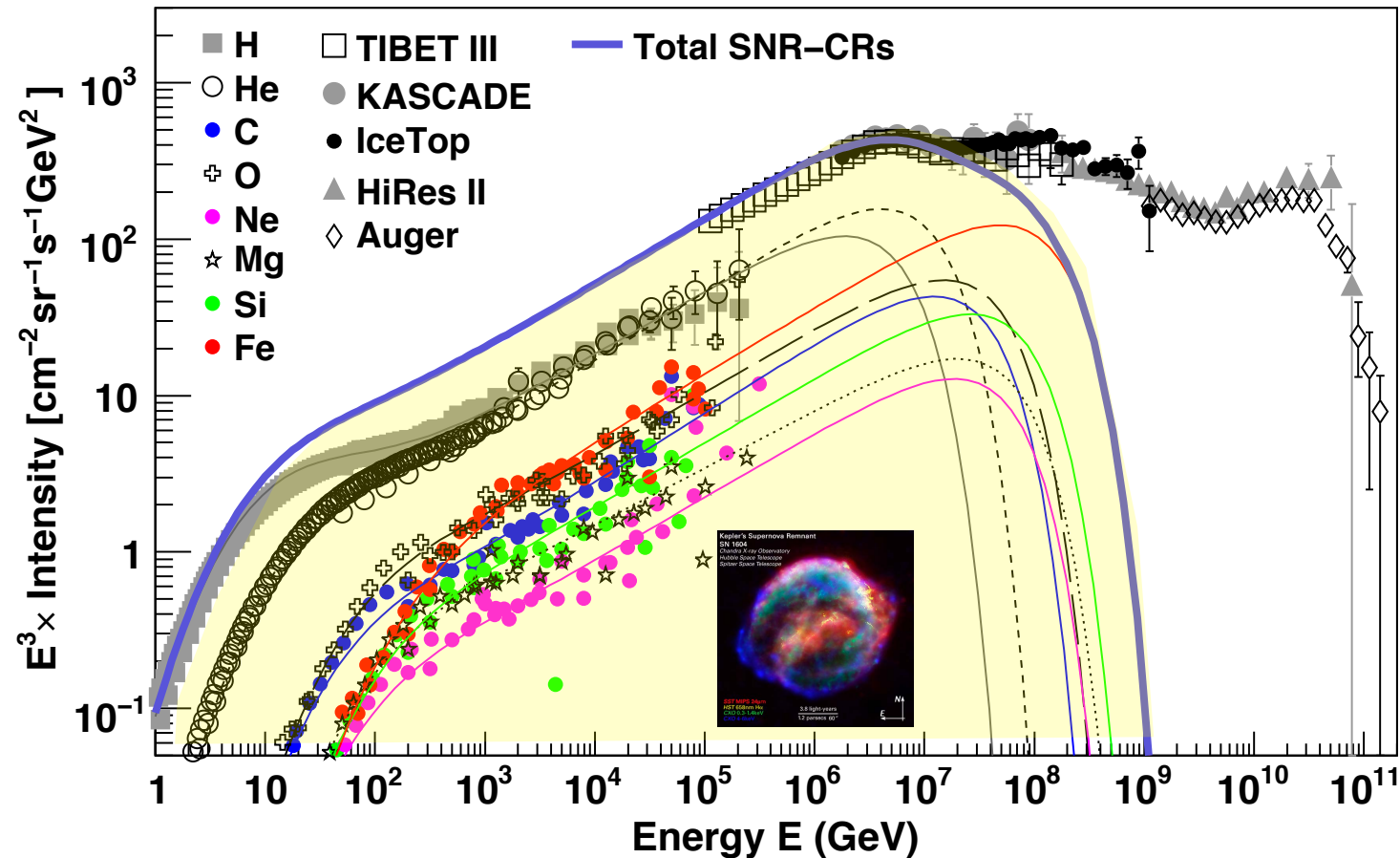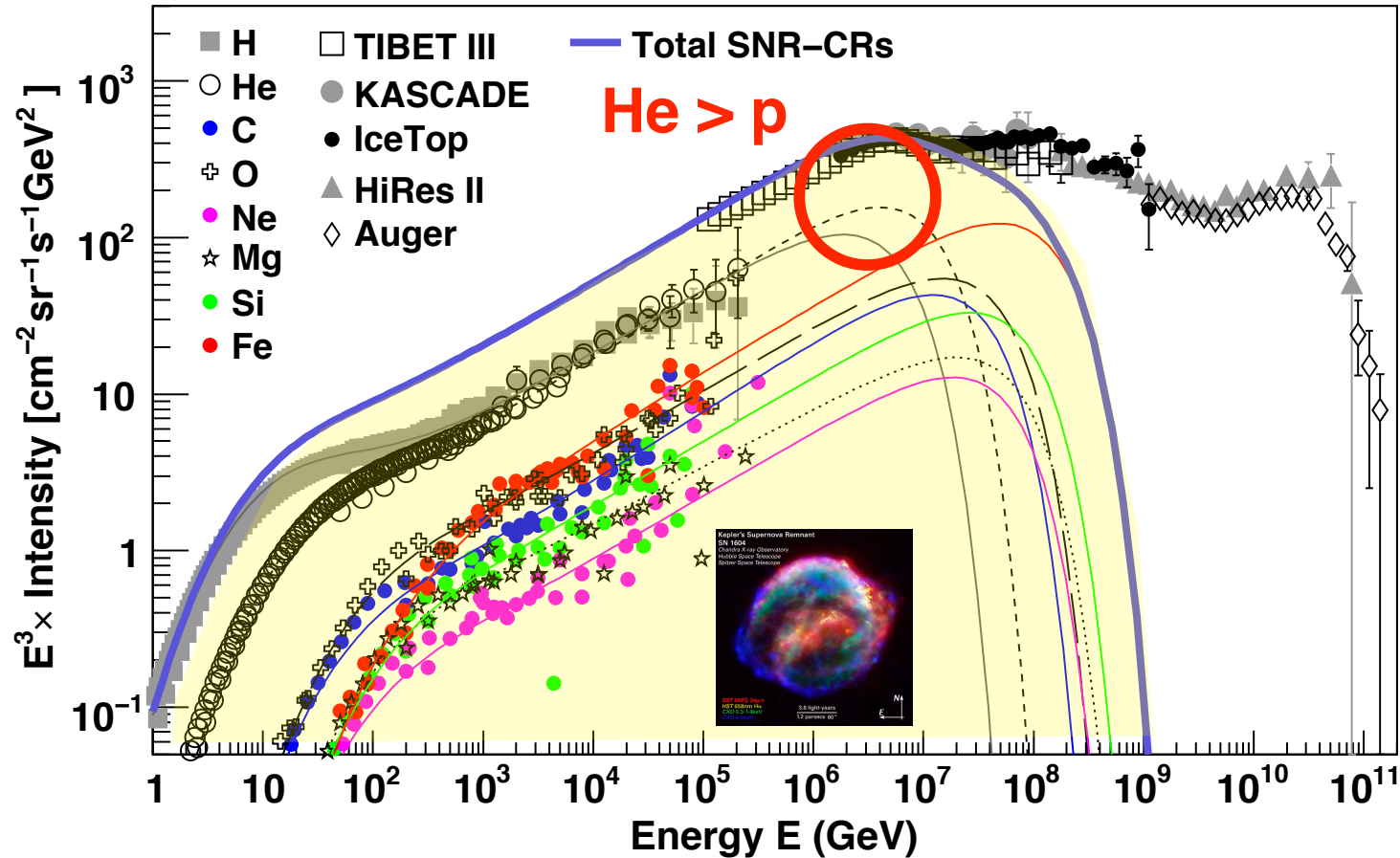# Contribution of (regular) SNR-CR to all-particle spectrum



**Fig. 2.** Contribution of SNR-CRs to the all-particle cosmic-ray spectrum. The thin lines represent spectra for the individual elements, and the thick-solid line represents the total contribution. The calculation assumes an exponential cut-off energy for protons at $E_c = 4.5 \times 10^6$ GeV. Other model parameters, and the low-energy data are the same as in Figure 1. Error bars are shown only for the proton and helium data. High-energy data: KASCADE (Antoni et al. 2005), IceTop (Aartsen et al. 2013), Tibet III (Amenomori et al. 2008), the Pierre Auger Observatory (Schulz et al. 2013), and HiRes II (Abbasi et al. 2009).

**~8% of mechanical power of SN --> CRs**

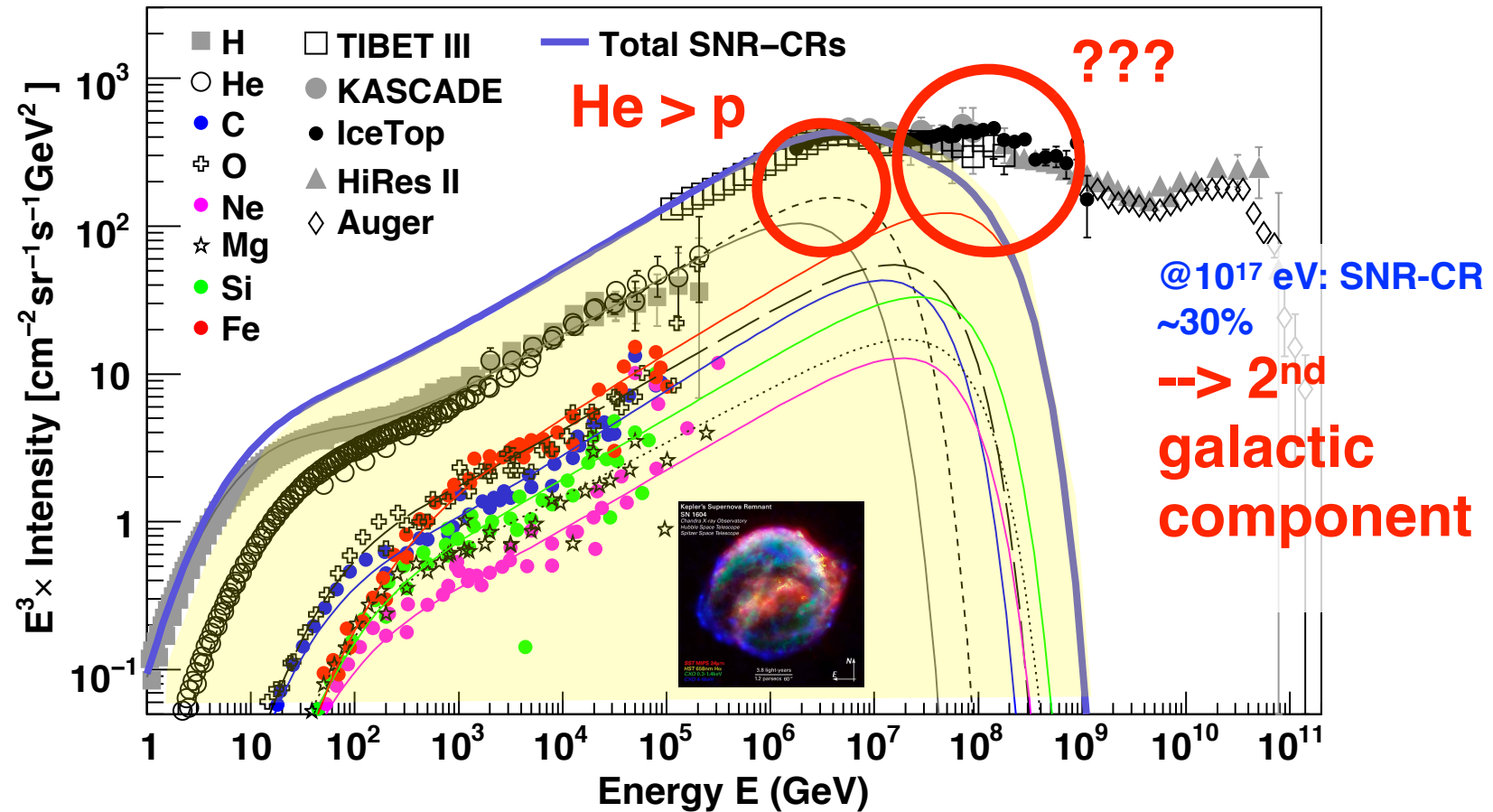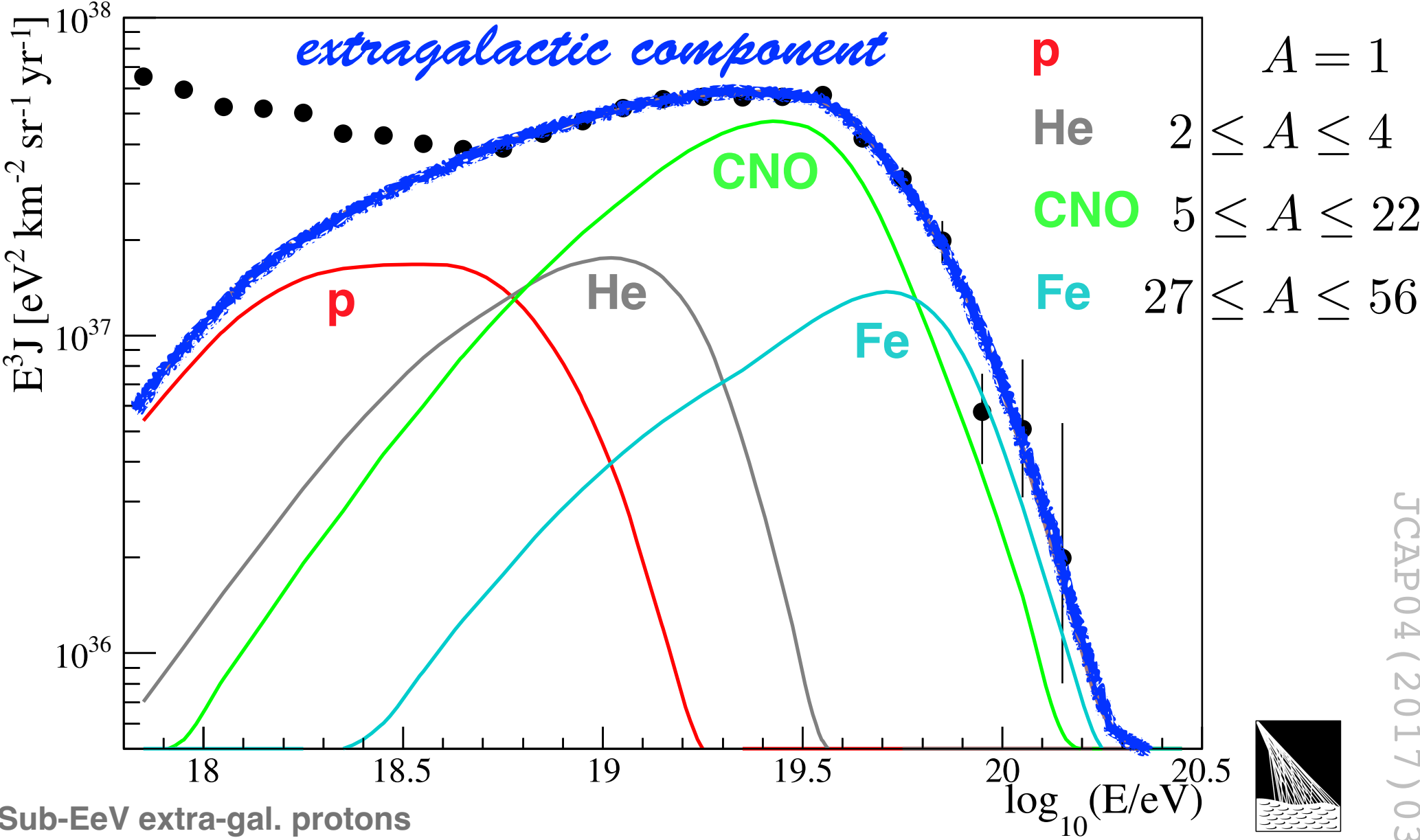# Contribution of (regular) SNR-CR to all-particle spectrum



**Fig. 2.** Contribution of SNR-CRs to the all-particle cosmic-ray spectrum. The thin lines represent spectra for the individual elements, and the thick-solid line represents the total contribution. The calculation assumes an exponential cut-off energy for protons at $E_c = 4.5 \times 10^6$ GeV. Other model parameters, and the low-energy data are the same as in Figure 1. Error bars are shown only for the proton and helium data. High-energy data: KASCADE (Antoni et al. 2005), IceTop (Aartsen et al. 2013), Tibet III (Amenomori et al. 2008), the Pierre Auger Observatory (Schulz et al. 2013), and HiRes II (Abbasi et al. 2009).

## ~8% of mechanical power of SN --> CRs

# Contribution of (regular) SNR-CR to all-particle spectrum



**Fig. 2.** Contribution of SNR-CRs to the all-particle cosmic-ray spectrum. The thin lines represent spectra for the individual elements, and the thick-solid line represents the total contribution. The calculation assumes an exponential cut-off energy for protons at $E_c = 4.5 \times 10^6$ GeV. Other model parameters, and the low-energy data are the same as in Figure 1. Error bars are shown only for the proton and helium data. High-energy data: KASCADE (Antoni et al. 2005), IceTop (Aartsen et al. 2013), Tibet III (Amenomori et al. 2008), the Pierre Auger Observatory (Schulz et al. 2013), and HiRes II (Abbasi et al. 2009).

## ~8% of mechanical power of SN --> CRs

Combined fit of spectrum and composition data as measured by the Pierre Auger Observatory

extragalactic component

$A = 1$

$2 \leq A \leq 4$

$5 \leq A \leq 22$

$27 \leq A \leq 56$

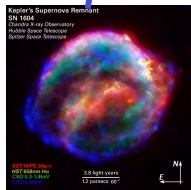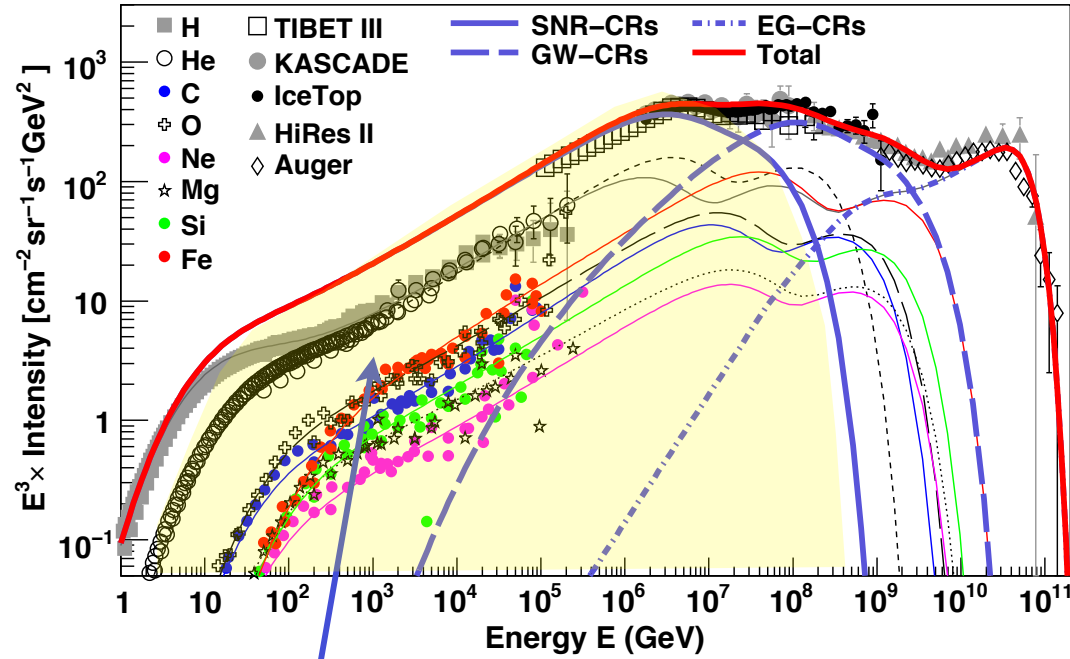Sub-EeV extra-gal. protons from interactions of heavier nuclei

see lecture on UHECR later

# all-particle spectra including 2<sup>nd</sup> galactic component
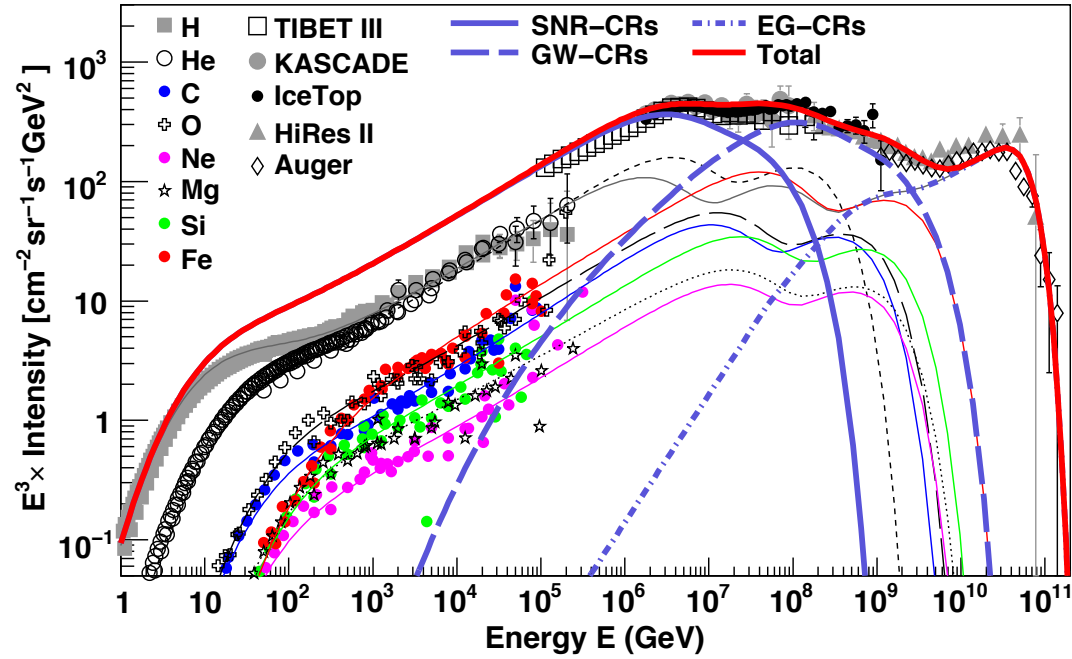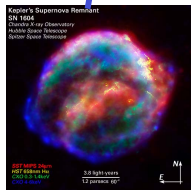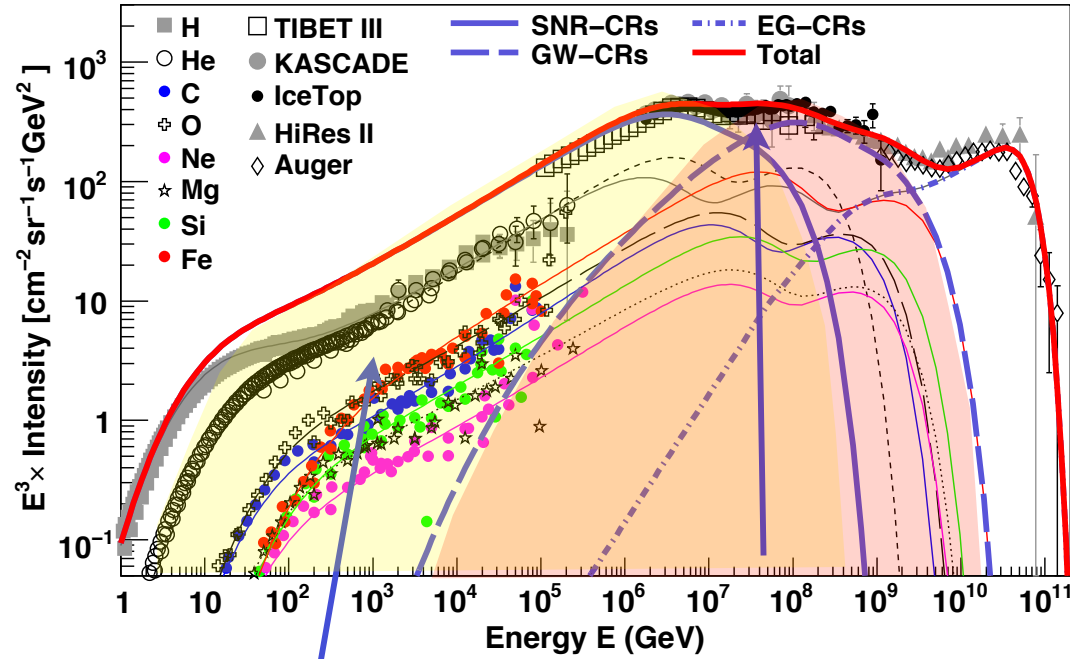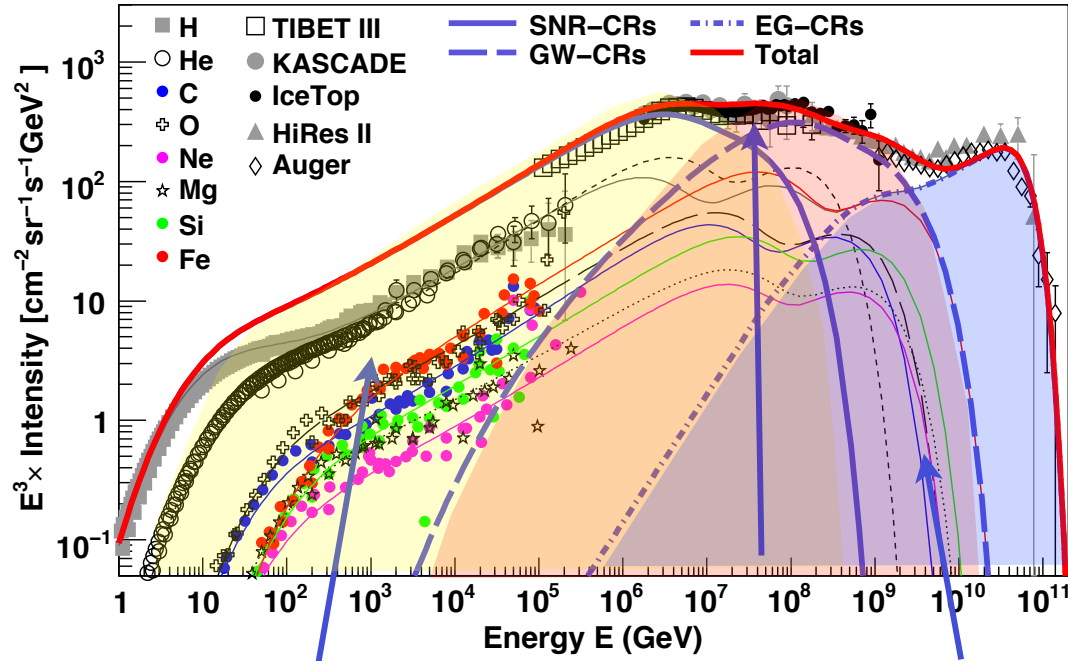
# all-particle spectra including 2nd galactic component

# all-particle spectra including 2ⁿᵈ galactic component

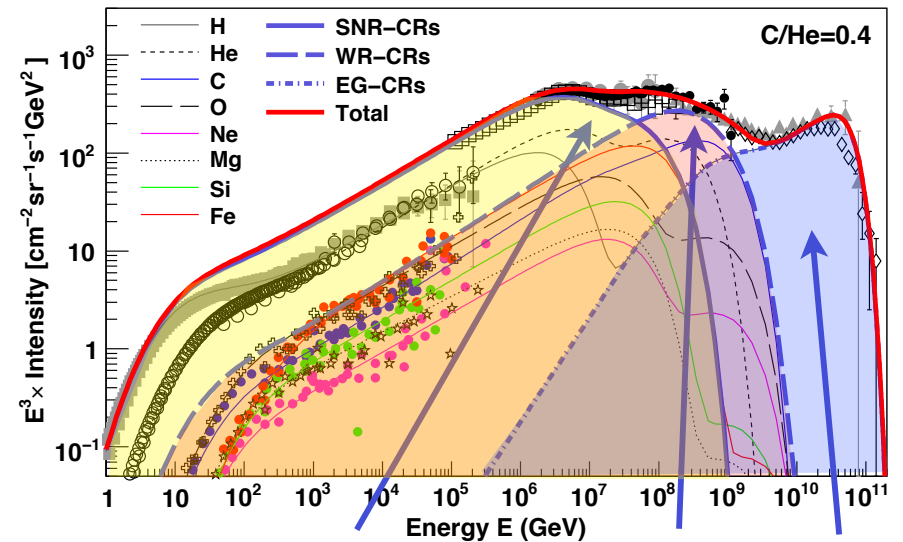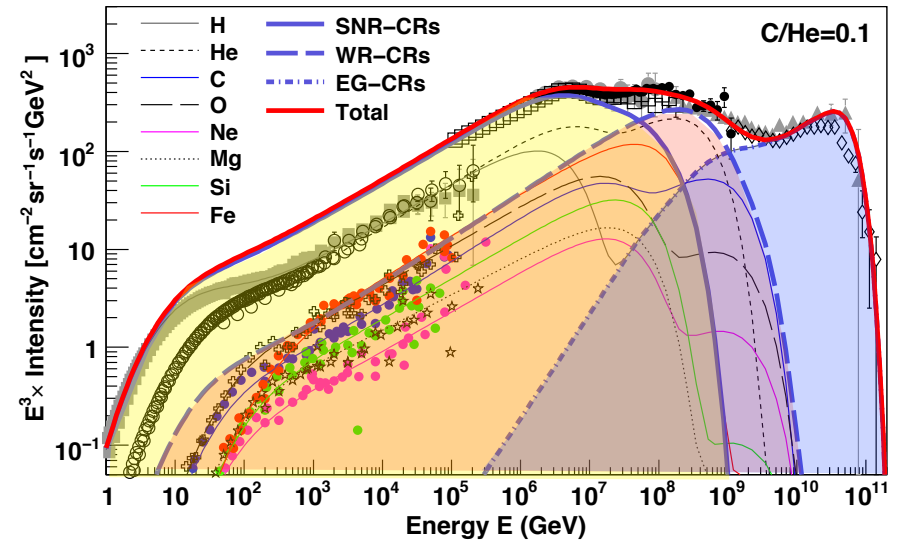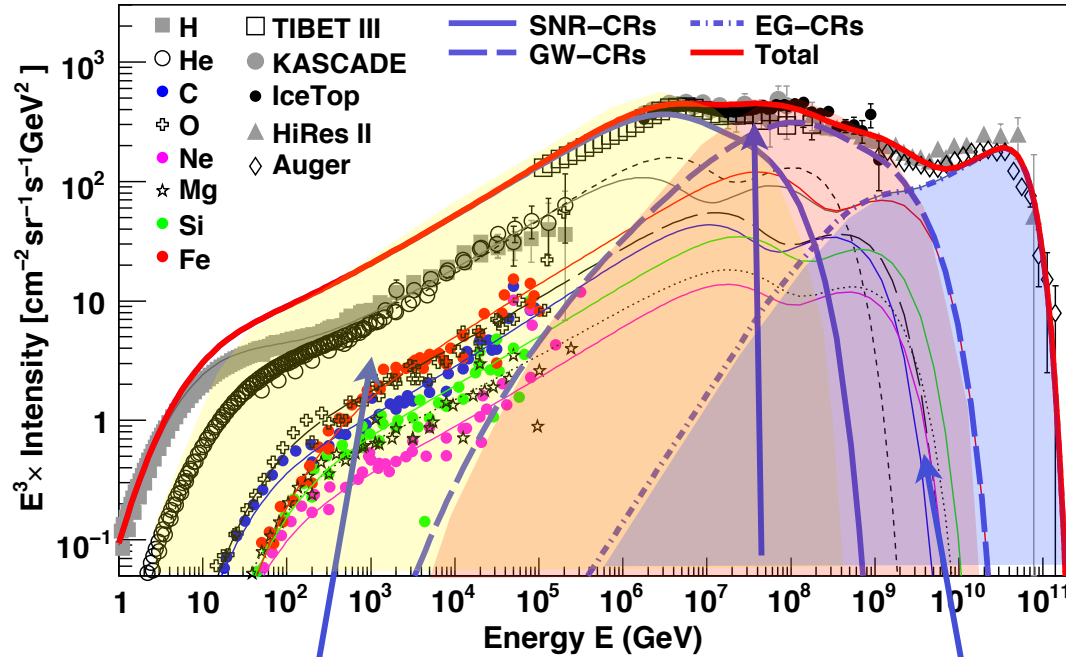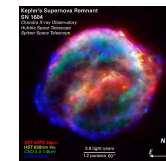# all-particle spectra including 2nd galactic component

**Table 3.** Injection energy of SNR-CRs used in the calculation of all-particle spectrum in the WR-CR model (Figure 6).

| Particle type | C/He = 0.1 $f(\times 10^{49}$ ergs$)$ | C/He = 0.4 $f(\times 10^{49}$ ergs$)$ |
|---|---|---|
| Proton | 8.11 | 8.11 |
| Helium | 0.67 | 0.78 |
| Carbon | $2.11 \times 10^{-2}$ | $0.73 \times 10^{-2}$ |
| Oxygen | $2.94 \times 10^{-2}$ | $2.94 \times 10^{-2}$ |
| Neon | $4.41 \times 10^{-3}$ | $4.41 \times 10^{-3}$ |
| Magnesium | $6.03 \times 10^{-3}$ | $6.03 \times 10^{-3}$ |
| Silicon | $5.84 \times 10^{-3}$ | $5.84 \times 10^{-3}$ |
| Iron | $5.77 \times 10^{-3}$ | $5.77 \times 10^{-3}$ |

S. Thoudam et al., A&A 595 (2016) A33

Legend (top-left plot):
- H (filled grey square)
- He (open circle)
- C (blue filled circle)
- O (cross)
- Ne (magenta filled circle)
- Mg (star)
- Si (green filled circle)
- Fe (red filled circle)
- TIBET III (open square)
- KASCADE (grey filled circle)
- IceTop (black filled circle)
- HiRes II (grey filled triangle)
- Auger (open diamond)
- SNR–CRs (solid blue line)
- GW–CRs (dashed blue line)
- EG–CRs (dash-dot blue line)
- Total (red line)

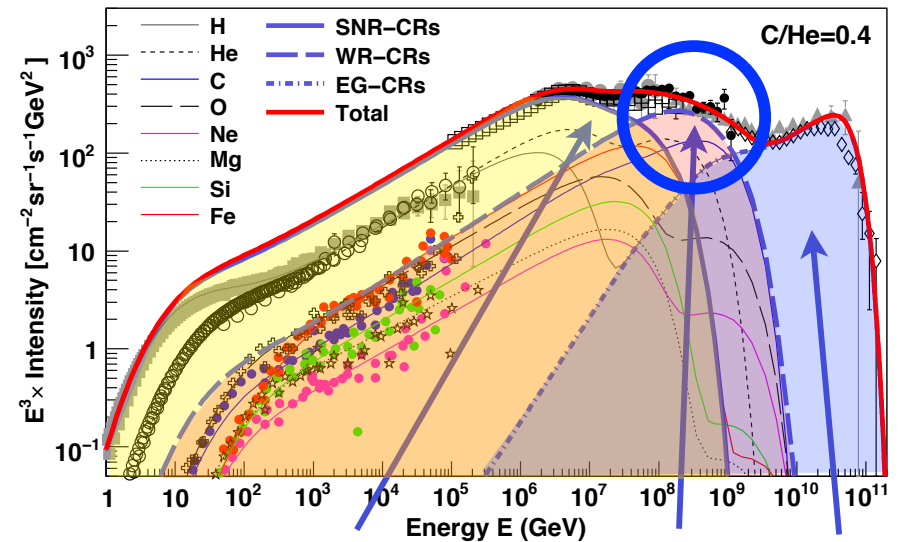Axes: $E^3 \times$ Intensity [cm$^{-2}$ sr$^{-1}$ s$^{-1}$ GeV$^2$] vs Energy E (GeV)
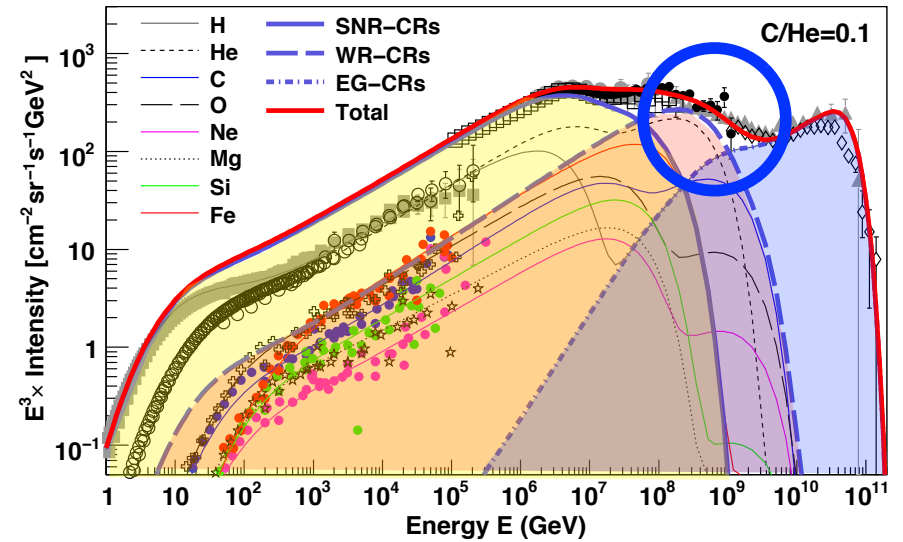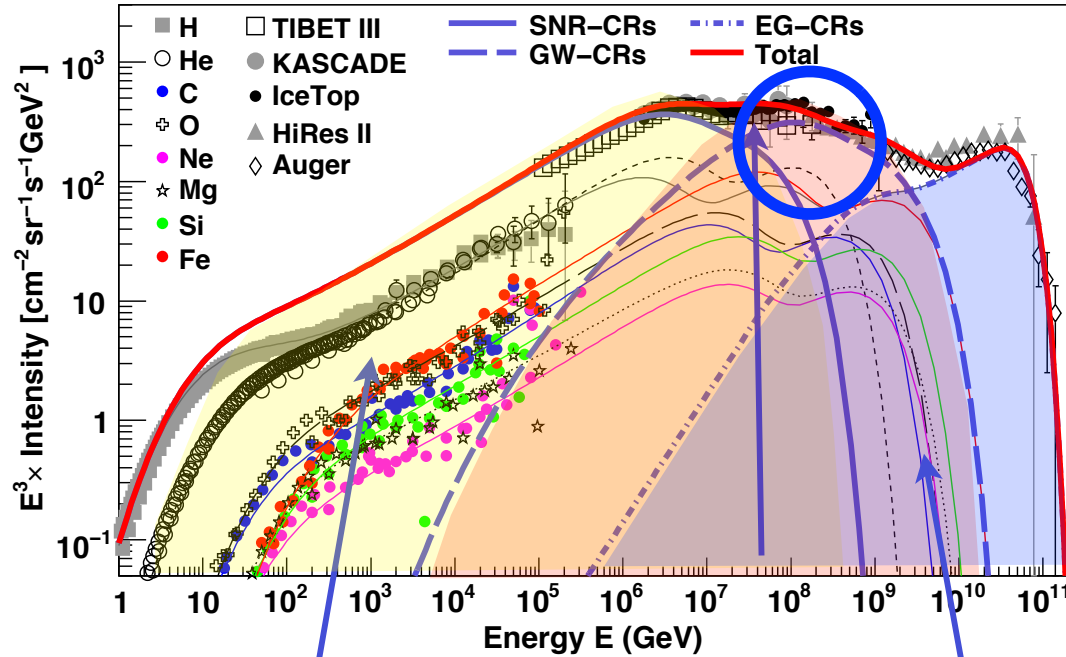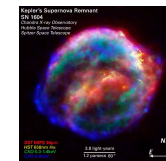
**Table 3.** Injection energy of SNR-CRs used in the calculation of all-particle spectrum in the WR-CR model (Figure 6).

| Particle type | C/He = 0.1 $f(\times10^{49}$ ergs) | C/He = 0.4 $f(\times10^{49}$ ergs) |
|---|---|---|
| Proton | 8.11 | 8.11 |
| Helium | 0.67 | 0.78 |
| Carbon | $2.11 \times 10^{-2}$ | $0.73 \times 10^{-2}$ |
| Oxygen | $2.94 \times 10^{-2}$ | $2.94 \times 10^{-2}$ |
| Neon | $4.41 \times 10^{-3}$ | $4.41 \times 10^{-3}$ |
| Magnesium | $6.03 \times 10^{-3}$ | $6.03 \times 10^{-3}$ |
| Silicon | $5.84 \times 10^{-3}$ | $5.84 \times 10^{-3}$ |
| Iron | $5.77 \times 10^{-3}$ | $5.77 \times 10^{-3}$ |

S. Thoudam et al., A&A 595 (2016) A33

# Mean logarithmic mass (lnA)
## WR-CR (C/He=0.4) + EG scenarios

$$\langle \ln A \rangle \equiv \sum_i r_i \ln A_i, \qquad \langle \ln A \rangle = \frac{X_{max}^{meas} - X_{max}^p}{X_{max}^{Fe} - X_{max}^p} \cdot \ln A_{Fe}.$$
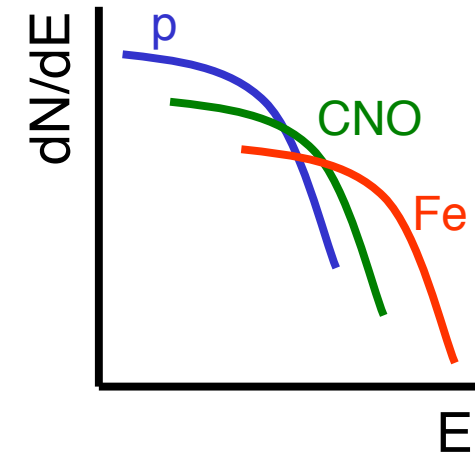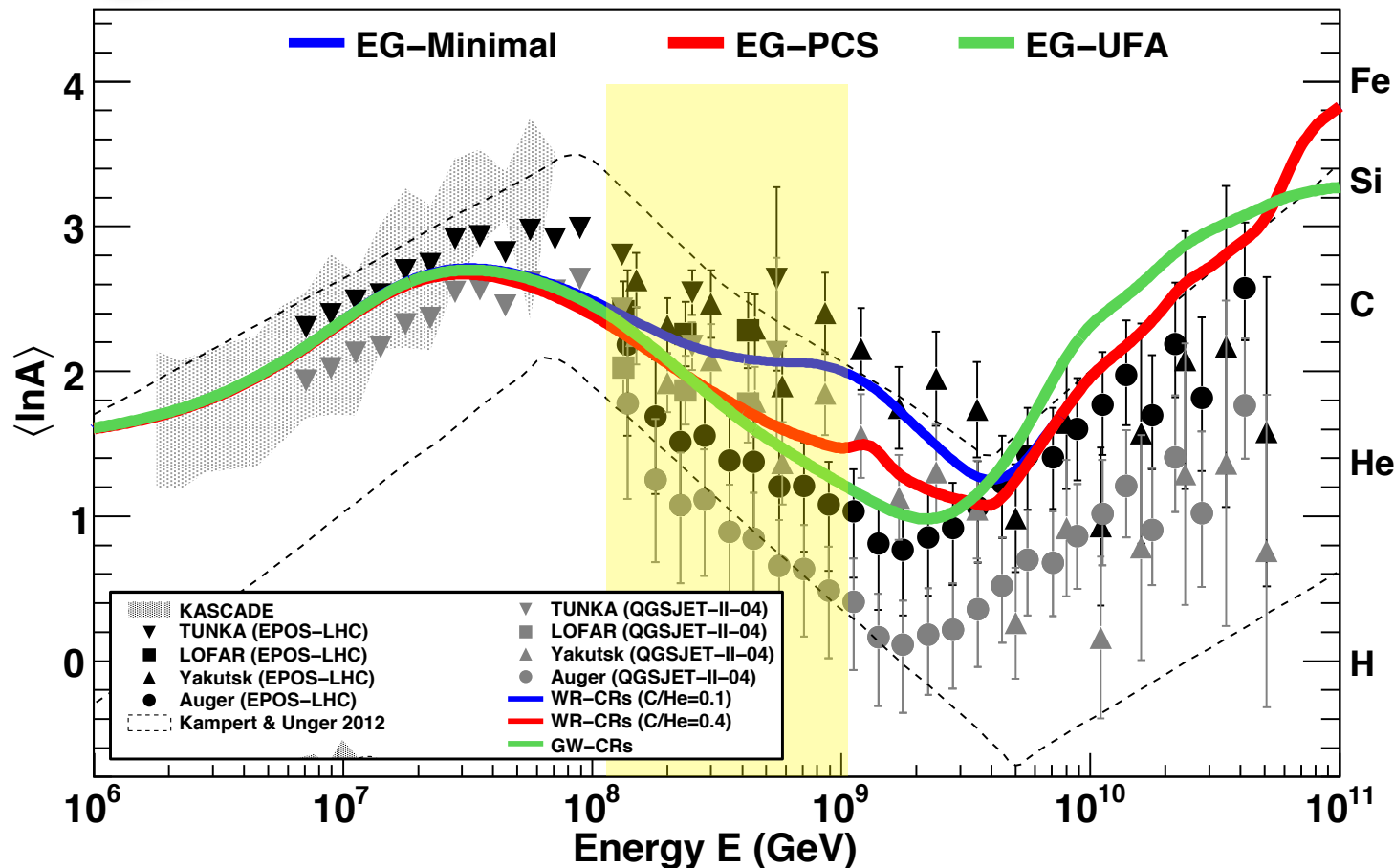


**Fig. 11.** Mean logarithmic mass for the three different EG-CR models combined with the WR-CR (C/He = 0.4) model. Data are the same as in Figure 8. Results obtained using WR-CR (C/He = 0.1) model are shown in Appendix B.

# Cosmic rays at the knee
## Results and implications

- knee in all-particle spectrum at ~4.5 PeV caused by fall-off of light elements (p, He)
- experimental (world) data indicate rigidity-dependent fall-off of individual elements
  (in particular unfolding by KASCADE[-Grande] and IceCube/Top)
- spectrum above knee is superposition of individual spectra (elemental knees)
  —> fine structure in all-particle spectrum
  —> end of galactic CR component
- astrophysical origin of knee:
  combination of maximum energy attained in sources (Supernovae) (Hillas criterion)
  and leakage from Galaxy

- 2nd galactic component at ~$10^{17}$ eV?
- extra-galactic origin >$10^{18}$ eV